DETECTING HAZARDOUS WEATHER POTENTIAL IN LOW SIGNAL-TO-NOISE RATIO SETTINGS: WEAKLY FORCED THUNDERSTORMS IN THE SOUTHEAST U.S.

by

PAUL WESLEY MILLER

(Under the Direction of Thomas L. Mote)

ABSTRACT

Weakly forced thunderstorms (WFT), convection forming in stagnant summer air masses, are a historical forecasting challenge for operational meteorologists. Pulse thunderstorms, defined by this dissertation as WFTs that produce severe weather, closely resemble their nonsevere counterparts, thwarting forecaster efforts to issue accurate severe weather warnings. This dissertation seeks to overcome the apparent similarities by developing a large, custom dataset of WFTs and applying machine learning techniques to accurately distinguish nonsevere WFTs from pulse thunderstorms as well as the convective environments that enhance WFT intensity. The WFT dataset (885,496 storms) is extracted from 15 years of warm season (May-September) composite reflectivity radar imagery from 30 collection sites in the Southeast, U.S., an active WFT region. Further, output from a high-resolution weather model, the Rapid Refresh, is used to characterize the convective environment of all WFTs between 2012–2015 (228,363 storms), and thirteen additional radar-derived and lightning-related parameters are recorded for WFTs during June and July of this subset (84,664 storms). Pulse thunderstorms, WFTs associated with *Storm Data* severe weather reports, constitute 0.60%, 0.65%, and 0.97% of each subset, respectively.

The results of this dissertation show that the spatial maximum in pulse thunderstorm activity, the Blue Ridge Mountains, is displaced from the overall WFT maximum in Florida and the Gulf Coast. Only two convective environmental parameters, vertical totals (VT) and total totals (TT), appreciably differentiate days with pulse thunderstorm activity from days with only nonsevere WFTs. When VTs (TTs) exceed 25.1°C (47.3°C), severe wind days are roughly 5x more likely. Meanwhile, severe hail days became roughly 10x more likely when VTs (TTs) exceed 26.0°C (49.2°C). A decision-tree-based machine learning algorithm, random forests, struggles to distinguish pulse thunderstorms from nonsevere WFTs in the broadest sample, but performs satisfactorily in a subset of the most active geographic regions and convective environments mentioned above. The critical success index (CSI) is 46.0%, which out-performs the U.S. National Weather Service CSI (34.8%) for severe thunderstorm warnings issued on pulse thunderstorms. Likely under-reporting of pulse thunderstorm-related severe weather is hypothesized to impede identification of clearer differences between pulse thunderstorm and nonsevere WFT environments and radar behavior.

INDEX WORDS: Severe Weather, Weakly Forced Thunderstorms, Disorganized Convection, Machine Learning, Southeast U.S.

DETECTING HAZARDOUS WEATHER POTENTIAL IN LOW

SIGNAL-TO-NOISE RATIO SETTINGS: WEAKLY FORCED THUNDERSTORMS

IN THE SOUTHEAST U.S.

by

PAUL WESLEY MILLER

B.S., Virginia Polytechnic Institute and State University, 2012

M.S., Virginia Polytechnic Institute and State University, 2014

A Dissertation Submitted to the Graduate Faculty of The University of Georgia in Partial

Fulfillment of the Requirements for the Degree

DOCTOR OF PHILOSOPHY

ATHENS, GEORGIA

2017

DETECTING HAZARDOUS WEATHER POTENTIAL IN LOW

SIGNAL-TO-NOISE RATIO SETTINGS: WEAKLY FORCED THUNDERSTORMS

IN THE SOUTHEAST U.S.

by

PAUL WESLEY MILLER

Major Professor:	Thomas L. Mote
Committee:	John A. Knox
	P. Lynne Seymour
	J. Marshall Shepherd

Electronic Version Approved:

Suzanne Barbour
Dean of the Graduate School
The University of Georgia
December 2017

ACKNOWLEDGEMENTS

The author acknowledges abundant support from his dissertation committee, particularly his major advisor Dr. Thomas Mote. Several scientists outside of the dissertation committee also provided helpful, constructive feedback that was incorporated into this document: Alan Stewart, Alan Black, and several anonymous reviewers. Further, the private industry partner Earth Networks supported this research through a generous donation of total lightning observations from its proprietary network.

TABLE OF CONTENTS

LIST OF TABLES

Page

LIST OF FIGURES

Page

CHAPTER 1

INTRODUCTION

1.1 Problem Statement

Despite the frequency with which "pulse," "air mass," "ordinary," and "single-cell" thunderstorms are referenced, there is little agreement among scholars and forecasters about what exactly constitutes this thunderstorm mode or similarly what, if anything differentiates them. These storms, broadly classified as disorganized convection, are agreed to develop in weakly sheared atmospheres characterized by moderate-to-high convective available potential energy (CAPE), occasionally capable of producing severe weather (winds $\geq$26 m s^{-1}, hail $\geq$2.54 cm, or a tornado). However, "weak shear" and "high instability" are subjective terms with no quantitative bounds. Consequently, studies investigating severe weather-storm mode relationships either neglect these storms altogether (e.g., Mazur et al. 2009), include them in broad "cellular" or "non-supercell" categories (e.g., Gallus et al. 2008; Duda and Gallus 2010; Smith et al. 2012), or apply widely varying and arbitrary identification criteria (e.g., Cerniglia and Snyder 2002; Fowle and Roebber 2003; Ashley and Gilson 2009). The congested and inconsistent nomenclature for disorganized convection to a serious impediment to scientific inquiry.

Consequently, research into the most basic aspects of disorganized convection has been wanting. Our modern-day assumptions regarding the most fundamental characteristics of these storms are informed by a 1940s research expedition conducted using World War II-era technology (Byers and Braham 1949) (Fig. 1.1). Despite an assumed occurrence maximum in the Southeast U.S., this has never been demonstrated through a formal climatology. The paucity of scholarly references to the seminal papers on disorganized thunderstorms further anecdotally illustrates the under-researched nature of pulse convection. For instance, Byers and Braham's (1948) article in the *Journal of Meteorology*, describing the results of a two-year landmark investigation into thunderstorm circulation and structure, has only been cited thirteen times between 2005 and 2015.

While many characteristics of disorganized thunderstorms are vague, one certainty is that forecasters experience exceptional difficulty anticipating their severity (Guillot et al. 2008) (Fig. 1.2). This results from a two-fold challenge. Not only are convective environments associated with severe disorganized storms poorly distinguished from their corresponding nonsevere environments (Doswell 1985), but within severe-supporting regimes, individual severe cells closely resemble nonsevere disorganized cells (Doswell 1985). Consequently, providing advanced warning for disorganized storm severity is a challenging process for National Weather Service (NWS) forecasters. False alarm rates (FAR) for severe thunderstorm warnings issued on these storms are greater than for any other storm mode, and the probability of detection (POD) is smaller than for supercells and line segments (Guillot et al. 2008). The disparities between NWS skill measures among different storm modes led Guillot et al. (2008) to even suggest that NWS warning performance measures should be corrected for the number of disorganized thunderstorms encountered by forecasters.

In order to more effectively warn the public of impending pulse severe weather, more focused research is needed for this convective mode. The purpose of this dissertation is to (1) develop a standard terminology for disorganized convection, particularly as it relates to severe weather, (2) create the first climatology of such thunderstorms for the Southeast U.S., (3) improve the operational understanding of convective environments supportive of severe disorganized storms, and (4) identify characteristic nowcasting features of severe disorganized cells.

1.2 Significance

As the primary mode of summertime convection in the Southeast U.S., disorganized thunderstorms are a perennial forecasting challenge and societal hazard. While disorganized thunderstorms pose a physical threat to people through severe weather, they are also responsible for deadly flash flooding, fatal lightning strikes, and aviation disaster. Smith et al. (2011) found that several of the most devastating flash floods ever recorded in the central Appalachians were produced by slow-moving, topographically driven thunderstorms occurring in weak flow regimes. Additionally, Ashley and Gilson (2009) determined that 84.4% of lightning fatalities between 1998 and 2009 could be attributed to these thunderstorms. The strong shear environments created by disorganized thunderstorm outflows can also lead to aviation crashes. The direct threat to human safety necessitates improved research and forecasting of these events.

While direct threats to human well-being are described above, disorganized convection also indirectly impact human health through their impacts on air quality. Disorganized thunderstorms are the primary lightning-producers during the summer months in the Southeast U.S., and lightning-produced nitrogen oxide compounds can be detrimental to the human respiratory system. The summertime disorganized thunderstorm maximum also coincides with the annual peak in surface ozone concentrations.

Disorganized-convection-enhanced NO_x can potentially contribute to increases in surface ozone concentrations and decreases in air quality. Additionally, interactions between thunderstorm rainfall, wind, and plant pollens have been associated with increases in emergency room visits for asthma attacks (Grundstein 2008, Taylor 2004). An improved ability to anticipate disorganized thunderstorm formation will enable health officials to better mitigate these threats.

Current climate models suggest that in a warming climate CAPE will generally increase and vertical wind shear will decrease, promoting more frequent severe disorganized thunderstorm environments across the eastern U.S. (Trapp et al. 2007; Brooks 2013; Diffenbaugh et al. 2013; Gensini et al. 2014a) (Fig. 1.3). Thus, humans will likely encounter the most challenging-to-forecast thunderstorms more frequently. Moreover, other studies have documented increases in thunderstorm initiation over or downwind of large urban areas (e.g., Mote et al. 2007; Bentley et al. 2010; Ashley et al. 2012; Haberlie et al. 2015; McLeod et al. 2017). This urban-induced precipitation is most common during the late afternoon on humid days characterized by synoptically benign conditions – which corresponds very well to disorganized thunderstorm regimes. Not only could disorganized environments begin occurring more frequently, but when present, the ever-expanding urban landscape will aid their formation more commonly.

Faced with a potentially greater frequency of disorganized thunderstorms, the challenges facing forecasters will only be exacerbated. It is imperative that meteorologists improve their understanding of the convective environments supporting severe disorganized storms as well as the individual storm characteristics indicative of disorganized severe weather. The results of this project will aid in the development of new nowcasting techniques, and hopefully, help improve NWS warning skill statistics for disorganized thunderstorms. In turn, human life and property will be better protected from the primary warm season severe weather threat facing residents of the Southeast U.S

1.3 Literature Review

1.3.1 Early disorganized thunderstorm research efforts

Following World War II, radar equipment and surplus fighter aircraft were utilized to perform the most thorough investigation of disorganized thunderstorms to-date. The "Thunderstorm Project" was conducted over two years and studied storms in both Florida and Ohio (Byers and Braham 1949). It was during this research program that the three-stage conceptual life cycle of a disorganized thunderstorm was posited along with other basic thunderstorm concepts that remain foundational to modern meteorology. The Thunderstorm Project also investigated thunderstorm rain, wind, and pressure fields; their spatial dimensions; spatial distributions; and vertical air currents.

In the sixty years following the Project, analyses of convective storms have grown tremendously in their scope and technological resources. However, the Thunderstorm Project remains the most thorough meteorological field campaign to explicitly investigate a large sample of disorganized thunderstorms. The observations collected during the Thunderstorm Project are still the most comprehensive available for disorganized thunderstorms despite their age and the antiquated technology that produced them. Though several other research efforts have revisited disorganized storms since the Thunderstorm Project (Browning et al. 1968; Lhermitte and Gilet 1975; Kropfli and Miller 1976; LeMone and Zipser 1980; Miller et al. 1983; Cunning et al. 1986), these studies were handicapped by the temporal and spatial coarseness to their observations, problems described by Kingsmill and Wakimoto (1991).

Unfortunately, despite its exceptional thoroughness and ground-breaking findings, the Thunderstorm Project was not overly concerned with storm severity (Byers and Braham 1949). The team did, however, document a “pressure nose” associated with a narrow swath of high winds along the outflow of a storm. This feature, later termed a “microburst” (Fujita 1981), would gain considerable attention from researchers due to the aviation risks it posed via dangerous wind shear. Ultimately, it was out of concern for the aviation industry that several microburst-related field campaigns were launched during the late 1970s and 1980s (Wilson and Wakimoto 2001). The Northern Illinois Meteorological Research on Downbursts (NIMROD), the Joint Airport Wind Shear (JAWS), and the Microburst and Severe Thunderstorm (MIST) projects investigated downburst-producing storms that included, but not limited to, disorganized thunderstorms. In one journal article resulting from MIST, Kingsmill and Wakimoto (1991) lament abundant research devoted toward strongly sheared storms to the detriment of microburst-producing disorganized thunderstorms.

1.3.2 What is a pulse thunderstorm?

Though there are some eight terms that are used to describe disorganized convection (see Section 2), one in particular holds a closer association with severe weather than the rest, “pulse.” While the Thunderstorm Project principally investigated what some meteorologists would term “pulse” thunderstorms, the project’s team members would not have recognized this word nor known its meaning. It would be thirty years later that the first documented reference to a “pulse thunderstorm” would occur (Wilk et al. 1979). Though the original Wilk et al. (1979) National Severe Storms Laboratory (NSSL) report has been lost to time, six years later the description was reproduced by Doswell (1985). According to Doswell’s definition, a pulse thunderstorm “closely resembles an ordinary non-severe thunderstorm cell,” but “possesses **briefly** [bold appearing in original] an intense updraft…during and immediately after which the storm produces a short episode of severe weather and then dissipates.” Consequently, “pulse” is used to describe the brief, temporal nature of the storm’s updraft intensification and subsequent period of severe weather.

At its root, Doswell’s definition is meant to distinguish the more intense, dangerous disorganized thunderstorms (i.e., pulse) from their nonsevere counterparts. However, this intentional distinction seems to have faded with time. It is relatively common for academic and operational sources to use “pulse” as a synonym for nonsevere disorganized thunderstorms (e.g., Fowle and Roebber 2003; Beasley et al. 2008; Ashley and Gilson 2009; Frugis and Wasula 2011; Bluestein 2013) – a duality was conveyed by Brotak (2009) in a layman-directed aviation article. Perhaps due the confusion stated above, a second term, “pulse severe,” has arisen to firmly associate the pulse storm with severe weather. However, the existence and need for this second, severe-specific form casts further doubt on whether “pulse” alone is intended to convey storm severity.

Regardless of whether termed “pulse” or “pulse severe,” defining a storm mode based on its association with severe weather has posed a challenge for researchers. Since the primary severe weather database in the U.S., *Storm Data*, is fraught with well-documented errors (e.g., Witt et al. 1998b; Witt et al. 1998a; Williams et al. 1999; Trapp et al. 2006; Miller et al. 2016), allowing the quality of severe weather reports to influence the classification of storm mode is problematic. Not only is the classification dependent on the number and quality of reports, but this also precludes real-time radar-based categorizations that may be possible for other storm modes. Studies have attempted to define "severity" using more consistent radar-derived measures (e.g., Smith et al. 2004; Lakshmanan and Smith 2009; Hobson et al. 2012; Lack and Fox 2012). However, this approach fundamentally compromises any comparisons of radar attributes between severe and nonsevere disorganized thunderstorms.

For the remainder of Section 1, "pulse thunderstorms" will reference the subset of disorganized storms associated with severe weather.

1.3.3 Pulse thunderstorm environments

Studies dealing with the prediction of disorganized thunderstorm severity do so according to one of two general approaches. The first involves detecting convective environments supportive of its greatest severe weather threats: severe hail and downburst winds. This technique can sometimes also be referred to as an "ingredients-based" approach as outlined by Doswell et al. (1996). The second seeks to identify storm-scale features that help distinguish potential pulse storms from nonsevere disorganized storms. Most studies employing ingredients-based approaches have focused on near-storm environments of tornadic thunderstorms (e.g., Thompson et al. 2003; Thompson et al. 2007), with disorganized convection addressed in a generic "non-supercell" category. Whenever pulse environments are more directly investigated, it is typically in the context of wet microbursts, one of the chief pulse thunderstorm hazards in the Southeast U.S.

Studies have found that severe wet microbursts generally occur in atmospheres characterized by a deep moist layer extending from the surface to 4–5 km above ground level (Johns and Doswell 1992). Above the moist layer lies a mid-level dry layer with smaller equivalent potential temperature values (θ_e). In wet microburst environments, the difference between the maxmimum θ_e observed just above the surface and the minimum θ_e aloft exceeded 20 K whereas non-microbust-producing thunderstorm days exhibited differences less than 13 K (Roberts and Wilson 1989; Atkins and Wakimoto 1991; Stewart 1991; Wheeler and Spratt 1995). Building on this result, McCann (1994) developed a microburst-predicting "wind index" (WINDEX) to be used in the forecasting of wet downburst potential. McCann's index was calculated using environmental variables from regional soundings such as the height of the freezing level, the environmental lapse rate, the near surface mixing ratio, and the mixing ratio at the freezing level. WINDEX proved more skillful in predicting wet microburst formation than traditional stability indices (McCann 1994).

As a result of successful environmental investigations, efforts have been made to incorporate WINDEX and vertical θ_e profiles into NWS forecaster computer displays (Ellrod et al. 2000). Whereas the initiative above would encompass all NWS offices, some local forecasting offices have used convective parameters to develop their own pulse thunderstorm warning protocols (Falk et al. 1998; Funk 2006). Additionally, microburst climatologies can help forecasters better anticipate the time of day, season, and locations favorable for microburst, but such climatologies have only been attempted for a limited number of locations (Falk et al. 1998; Sanger 1999).

Many of the studies referenced above share a similar shortcoming. Though microbursts are a primary hazard of pulse convection, they are also commonly associated with more organized thunderstorm modes such as quasi-linear convective systems (QLCS) and supercells (e.g., Kuchera and Parker 2006). These ingredients-based studies might be skewed towards more organized thunderstorm environments beyond the weakly sheared pulse regime. Only one of the preceding studies (Falk et al. 1998) explicitly considered downbursts resulting from disorganized thunderstorms. Additionally, these studies consider relatively small sample sizes in which the proportion of microburst environments is over-represented. Recent research suggests that this approach artificially bolsters the signal-to-noise ratio (Murphy 2017), yielding results that do not effectively transfer to an operational setting.

1.3.4 Identification of individual pulse cells

The advancement of radar systems during the 1970s catalyzed the development of severe thunderstorm warning protocols using remotely sensed storm features. While these efforts have primarily focused on more organized convective modes, researchers have identified several radar signatures useful for detecting pulse-thunderstorm-related severe weather. Wilk et al. (1979) observed that pulse storms were characterized by the appearance of the initial radar echo between 7–9 km AGL whereas echoes for nonsevere storms generally formed between 3–6 km. Subsequent studies have also tied echo heights to pulse storm severity (Falk et al. 1998; Cerniglia and Snyder 2002; Donavon and Jungbluth 2007), and there is a physical logic to this finding. The presence of a suspended precipitation core suspended high in the atmosphere represents a large amount of potential energy that can translate into severe wind gusts upon the updraft's collapse.

Other analyses have identified vertically integrated liquid (VIL) density (VIL divided by echo top; e.g., Stewart 1991; Amburn and Wolf 1997; Cerniglia and Snyder 2002) and the rate of increase in the maximum echo height (Paxton and Shepherd 1993) to be useful indicators of impending severity. In addition to VIL density and echo height, Cerniglia and Snyder (2002) determined that the probability of hail (POH) and probability of severe hail (POSH) algorithms (Witt et al. 1998b) were also reliable signals of severe wind and hail. This study, conducted by NWS forecasters and concerned only with pulse thunderstorms, offers a clear template of operationally desirable outcomes. However, Cerniglia and Snyder (2002) conducted their study on a sample containing >70% pulse thunderstorms, the ramification of which was described in Section 1.3.3.

The radar identification of potential wet microbursts, commonly associated with pulse convection, received a great deal of attention during the 1980-1990s. In what "may be the most complete study of a single disorganized thunderstorm since Byers and Braham (1949)," Wakimoto and Bringi (1988) identified a small hail shaft (width <1 km) within the microburst. On dual-polarization radar, this hail shaft was characterized by a "Z_{DR} trough," an area of near-zero Z_{DR} surrounded by larger values. Because Z_{DR} represents the difference between the horizontally and vertically polarized radar returns, areas of high Z_{DR} correspond large rain drops, which typically possess an oblate shape. Meanwhile, hail, which tends to tumble as it falls, produces a near-zero Z_{DR}. Thus, the Z_{DR} trough is useful for discerning areas of hail surrounded by large rain drops within the downdraft. The latent heat consumption of the melting hail can lead to downdraft cool and acceleration.

However, due to the scarcity of dual-polarization radars until 2012, this microburst feature has received little additional attention until recent years (e.g., Kuster et al. 2016; Mahale et al. 2016). WSR-88D velocity scans have also suggested that microbursts are preceded by mid-level convergence (Roberts and Wilson 1989; Atkins and Wakimoto 1991; Falk et al. 1998), indicative of the entrainment of unsaturated air. This convergence signature plays a key role in the Damaging Downburst Prediction and Detection algorithm (Eilts et al. 1996; Smith et al. 2004) now available to NWS forecasters via the Warning Decision Support System (Wilson and Wakimoto 2001). Despite the promising results of these previous studies, researchers have yet to test their transferability to a much larger sample containing a realistic ratio of severe-to-nonsevere thunderstorms, much less in weakly sheared environments.

The rapid development of new, emerging technologies presents an unexplored frontier for pulse thunderstorm research. Recent dual-polarization upgrades to WSR-88Ds nationwide now permit investigations of additional pulse weather signals (such as the Z_{DR} trough). Furthermore, the launch of the Geostationary Lightning Mapper (GLM) aboard the GOES-16 satellite (Goodman et al. 2013) will facilitate the application of total-lightning-based features [i.e., the lightning jump (Schultz et al. 2009, 2011)] to pulse thunderstorm forecasting. One recent approach to severe thunderstorm warning issuance showed promise by combining radar- and lightning-based metrics to determine potential severity (Rudlosky and Fuelberg 2013). However, before these techniques can be transferred to weakly sheared environments, research efforts focusing on pulse convection using a realistic ratio of severe-to-nonsevere storms will be required; thus far, these efforts have been few (Miller et al. 2015a).

1.4 Research Objectives

This dissertation will consist of four primary research tasks listed below. A section of the dissertation will be devoted to each task.

Task 1 research question: What is meant by the term "pulse" as a thunderstorm mode descriptor in operational and academic contexts? Is there a consensus in its application, and if so, is it appropriate? (Section 2)

Task 2 research question: When and where do disorganized (and pulse) thunderstorms occur most frequently in the Southeast U.S.? (Section 3)

Task 3 research question: What model-derived convective parameters (and values of them) best distinguish between pulse environments and nonsevere disorganized thunderstorm environments? (Section 4)

Task 4 research question: What radar and total lightning characteristics of pulse thunderstorms, when contextualized by environmental variables, can be used to diagnose severity? (Section 5)

This dissertation will focus on pulse thunderstorms forming over the Southeast U.S. Moist, humid air masses inhabit this region for much of the warm season, promoting the frequent formation of disorganized thunderstorms. Thunderstorm climatologies (though not restricted to pulse thunderstorms) identify the Southeast U.S. as a relative maximum for convective activity (e.g., Changnon 2001; Zipser et al. 2006). Thus, this region will provide the largest sample of pulse thunderstorms compared to other regions of the U.S. The definition of the Southeast used here is similar to that of Rickenbach et al. (2015) who recently conducted an analysis of precipitation structures in the same region. Figure 1.5 shows the WSR-88D sites that provide coverage of the Southeast U.S.

1.5 Conclusion

Disorganized thunderstorms are the primary summer forecasting challenge for meteorologists within the Southeast U.S. These storms, while small and short-lived, can nonetheless produce severe hail and wind on occasion. Though given devoted attention in the late 1940s and again in the 1980s (e.g., Byers and Braham 1949; Kingsmill and Wakimoto 1991), they continue to pose a significant impediment for the meteorologists tasked with diagnosing their severity. Researchers have shed some light on microbursts, the primary pulse thunderstorm hazard; however, there still much to be discovered about this class of thunderstorms.

Despite posing a smaller severe weather threat on a per storm basis, pulse thunderstorms are a clear detriment to NWS warning skill statistics. The POD and FAR for warnings issued on pulse storms reflect a poorer performance than those issued on other storm modes (Guillot et al. 2008). However, efforts to adapt new forecasting technologies to pulse thunderstorm prediction are sparse (Miller et al. 2015a). The paucity of contemporary pulse thunderstorm forecasting research is especially troubling since climate modeling studies suggest pulse thunderstorms will become more frequent in the future.

In order to meet the growing needs of current and future meteorologists, this dissertation proposes a four-stage research project. Task 1 involves scouring operational text products, peer-reviewed journal articles, government reports, and educational meteorology texts to inform a standard definition of "pulse" that will be applied in all later stages (Section 2). The second task will combine radar and severe weather observations collected across the Southeast U.S. to develop the first known climatology of disorganized thunderstorms in this region (Section 3). Task 3 builds upon the results of Task 2 by comparing the convective environments that support pulse thunderstorms versus nonsevere disorganized thunderstorms (Section 4). Lastly, Task 4 will identify characteristic radar and lightning features of pulse thunderstorms (Section 5).

The purpose of this dissertation is to enable forecasters to more effectively anticipate pulse thunderstorms by realistically representing the ratio of pulse storms to nonsevere storms. The research tasks outlined herein will contribute to this goal in two key ways: 1) better differentiating pulse from nonsevere environments and 2) better distinguishing individual pulse cells from nonsevere disorganized storms within those environments. Additionally, the creation of the first disorganized thunderstorm climatology will allow forecasters to better assess their relative exposure to pulse convection. While Section 2 will provide a valuable academic contribution, Sections 3, 4, and 5 will provide long overdue operational insight toward pulse thunderstorm forecasting.

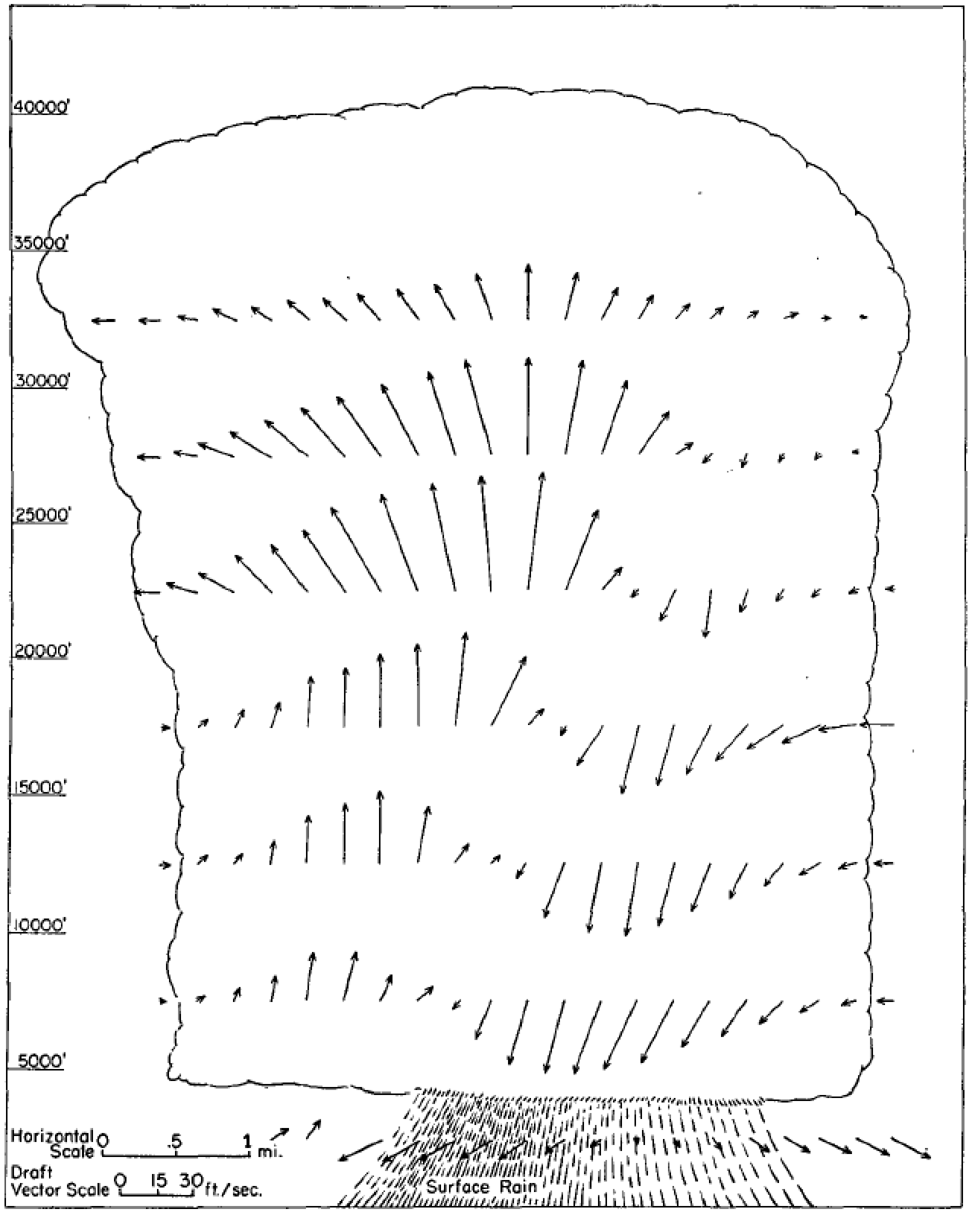

Figure 1.1. The circulation within a mature disorganized thunderstorm. Taken from Byers and Braham (1948).

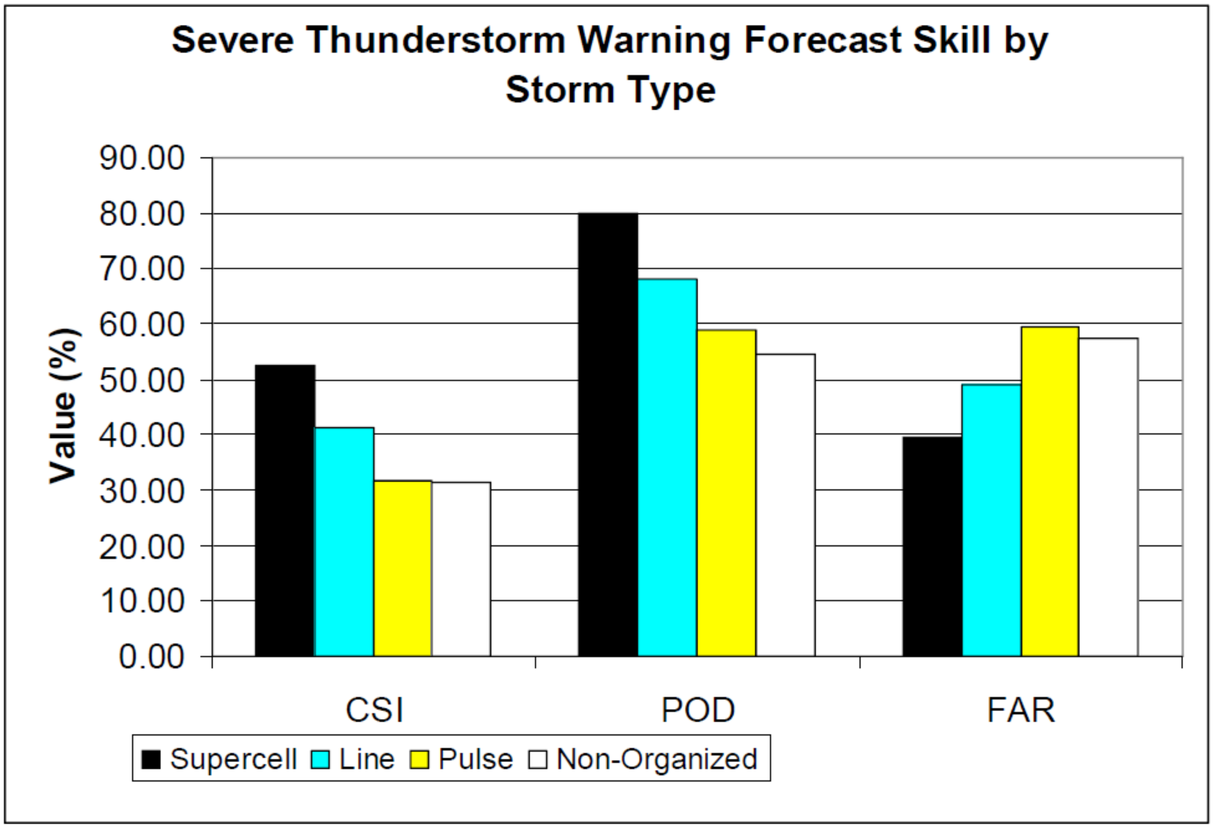

Figure 1.2. NWS severe thunderstorm warning skill as a function of storm mode. The critical success index (CSI) for pulse thunderstorms is lower than for both supercells and thunderstorm lines. The poorer warning skill of pulse convection is also reflected in a smaller POD and a larger FAR. Taken from Guillot (2008).

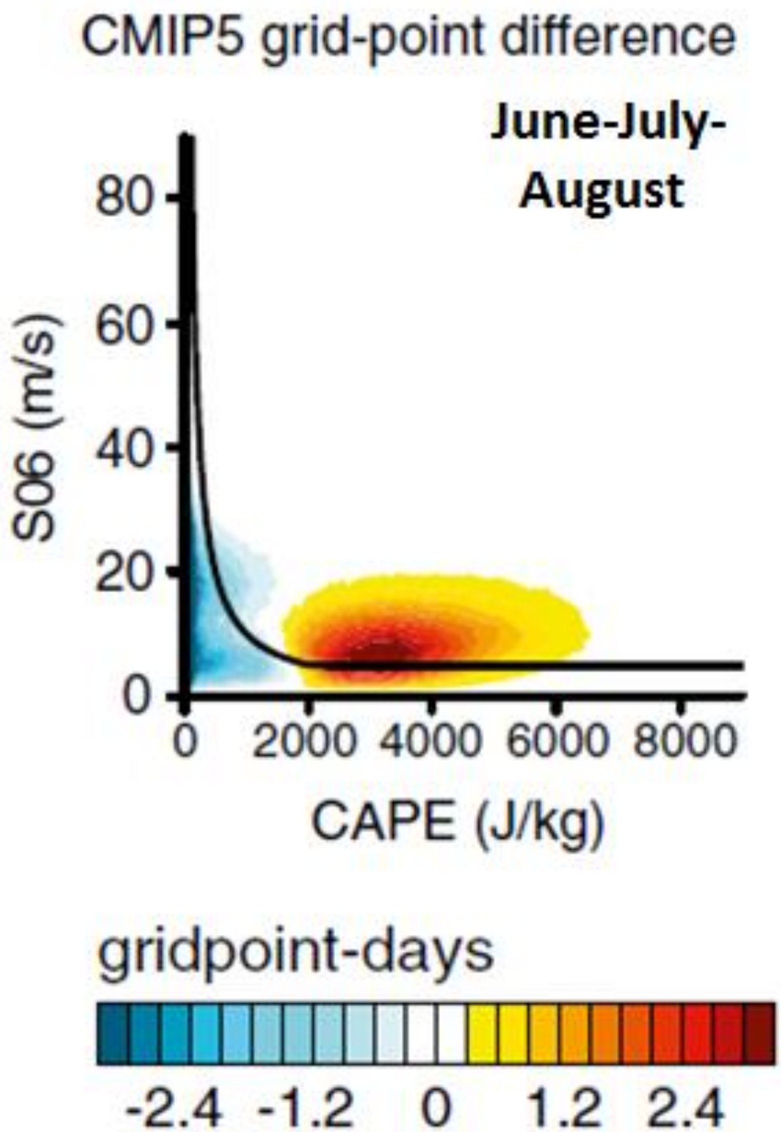

Figure 1.3. Image adapted from Diffenbaugh et al. (2013) depicting the results of a severe weather climate modeling study. The number of days supporting severe convection [defined as combinations of CAPE and 0–6-km shear (S06) lying above or to the right of the solid black line] was found to increase under anthropogenic climate change scenarios. The greatest increase occurs in environments with less than 10 m s^{-1} S06, suggesting an increase in pulse thunderstorms.

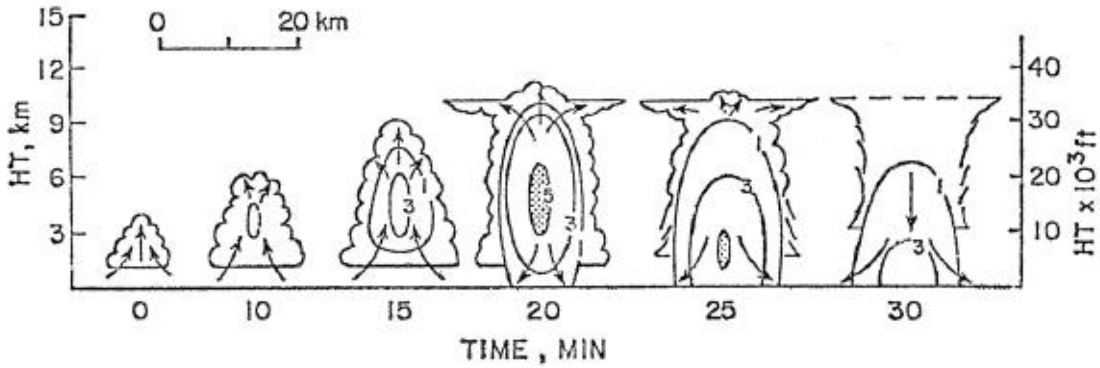

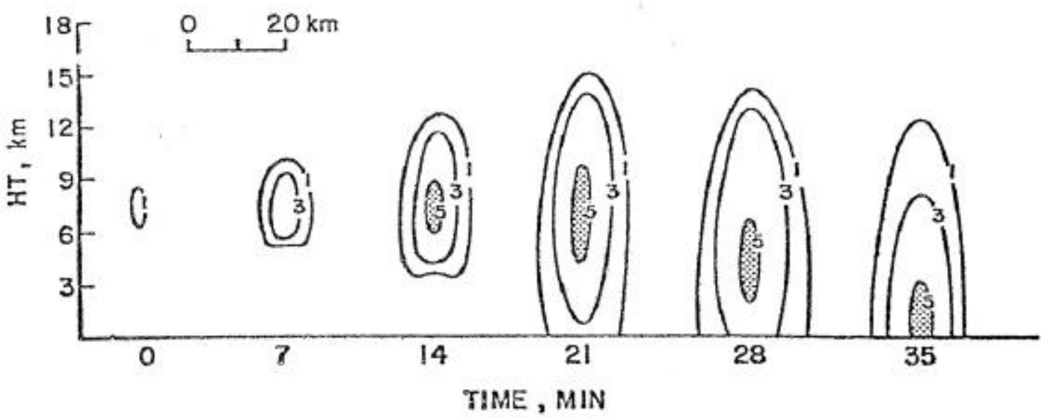

Figure 1.4. Comparison of the life cycles of a nonsevere disorganized thunderstorm (top) and a pulse storm (bottom). Note the height of the first echo with a pulse storm forms between 7–9 km as compared to 3–6 km for a nonsevere storm. Taken from Doswell (1985).

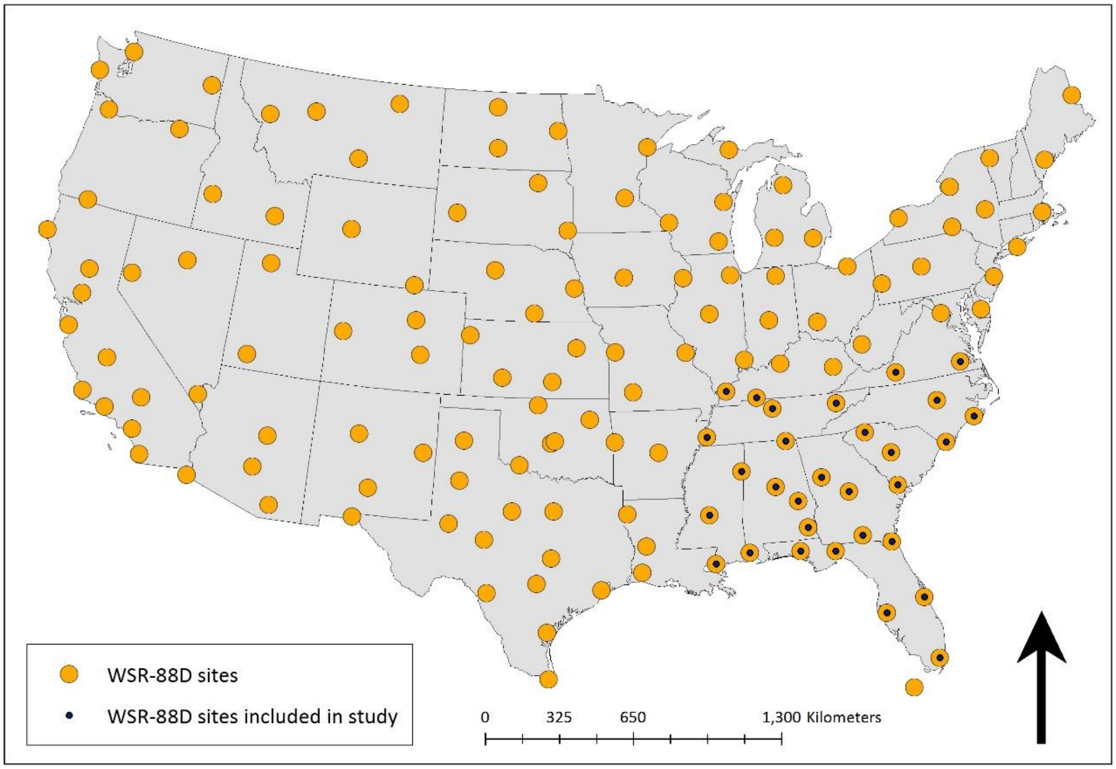

Figure 1.5. Map of WSR-88D sites in the continental U.S. (orange dots). Sites that fall within, or provide coverage of, the Southeast U.S. are denoted by a smaller concentric black dot. Black arrow indicates due north.

CHAPTER 2

STANDARDIZING THE DEFINITION OF A "PULSE" THUNDERSTORM[1]

[1] Miller, P. W., and T. L. Mote, 2017: Standardizing the definition of a "pulse" thunderstorm. *Bull. Amer. Meteor. Soc.*, **98,** 905–913, doi:http://dx.doi.org/10.1175/BAMS-D-16-0064.1. Reprinted here with permission of the publisher.

Abstract

Isolated, short-lived thunderstorms forming in weakly forced environments are referenced through a surplus of terminology. Further, the language used to describe the strongest, severe-weather-producing subset of these storms is applied inconsistently, posing a communication hurdle for the effective dissemination of hazardous weather risks. The term "pulse thunderstorm" was originally coined to describe an anomalously strong air-mass thunderstorm often associated with a larger convective complex. However, recent applications of "pulse" have evolved to also describe nonsevere, single-cell storms, and both uses can currently be observed within research, operational, and educational texts. This paper reviews the history of "pulse," performs a content analysis on nearly 1500 pulse-referencing Storm Prediction Center (SPC) convective outlooks (CO) and mesoscale discussions (MD), and summarizes the deficiencies with the contemporary disorganized convection nomenclature. The larger CO sample (n=997) establishes that temporal trends in "pulse" references model traditional expectations whereas the detailed MDs (n=458) showcase examples of pulse-related terminology. The MD content analysis reveals that (1) the term "pulse" frequently appears in conjunction with severe-weather-related language and (2) that pulse-related words (e.g., brief, isolated) are equally represented in multicell-referencing MDs. In the interest of effective communication and reproducible research, the definition of "pulse" is proposed to be standardized according to the term's original (i.e., severe, multicellular) meaning. Further, thunderstorms forming within synoptically homogeneous air masses in the absence of large-scale dynamical lift are suggested to be termed "weakly forced thunderstorms." By corollary, pulse storms represent the subset of weakly forced thunderstorms associated with severe weather.

2.1 Introduction

"Pulse thunderstorm" is a widely recognized term within the meteorological lexicon. Though its applications vary, contemporary uses of "pulse" *broadly* reference a small, short-lived, and isolated updraft forming in a weakly sheared environment. Aside from "pulse" (and its sister term "pulse-type"), the weather nomenclature also contains several other words to describe disorganized convection (see http://www.spc.noaa.gov/faq/#4.4 for a description of "organized" versus "disorganized" thunderstorms). "Air-mass," "ordinary," "garden-variety," and "single-cell" are all commonly used to indicate unicellular, non-supercellular convection. Meanwhile, broadcast meteorologists frequently opt for the phrase "pop-up" or "popcorn" thunderstorm to communicate this convective mode to their audiences.

These storms are a staple feature of the summer climate across the central and eastern United States. Fueled by the diurnal instability, short-lived, isolated convection generally forms during the afternoon in hot, humid, summertime air masses. Typically lasting between 30 minutes and one hour, each cell consists of a three-stage life cycle (i.e., the cumulus, mature, and dissipating stages) first described by Byers and Braham (1949) during the Thunderstorm Project. They are almost a daily feature of the southeastern U.S. sky during the warm season.

While most disorganized thunderstorms cause relatively little human inconvenience, the strongest cells can produce surface conditions exceeding severe weather warning criteria. Pulse thunderstorms are generally not tornado-producers (relative to supercell thunderstorms), but their associated large hail and high wind threats can be particularly troublesome to diagnose. Consequently, meteorologists experience considerable difficulty issuing accurate severe weather warnings for pulse thunderstorms. False alarm ratios (FAR) are larger and probabilities of detection (POD) are smaller for warnings issued on pulse thunderstorms than for other storm modes (Guillot et al. 2008). However, perhaps their greatest impact on human activity occurs in the absence of severe weather. Even when their outflow winds remain below severe criteria, the dangerous shear conditions created by pulse-storm microbursts can lead to aviation tragedy (e.g., NTSB 1986). Further, more individuals are killed by lightning strikes from pulse storms than any other convective mode (Ashley and Gilson 2009).

Though many meteorologists are familiar with the term “pulse,” its applications in meteorological literature suggest it has multiple connotations within the field. “Pulse” was originally intended to reference a briefly severe member of a multicell thunderstorm complex, typically forming in a weakly sheared environment (personal communication, Les Lemon, former NSSL research scientist, 2015). However, in recent decades the application of this term has broadened to also describe nonsevere storms while simultaneously narrowing to exclude multicellular structures. As the meteorological community focuses more attention on clearly and effectively communicating weather hazards to the public, the array of terminology used to describe disorganized convection is a self-inflicted handicap. This is a timely discussion given that general circulation models suggest that unstable, weakly sheared atmospheres will become increasingly frequent in future climate scenarios (Diffenbaugh et al. 2013; Gensini and Mote 2015), and references to pulse storms may become more common as a result. In order to facilitate new research into these difficult-to-forecast storms as well as effectively communicate their potential hazards, a standard nomenclature for disorganized convection is needed.

The purpose of this paper is to propose a common definition for a pulse thunderstorm. However, in doing so the nomenclature of all disorganized convection must also be addressed. In subsequent sections, this paper (1) summarizes the historical development of the term “pulse” and its use in academic and educational contexts, (2) performs a content analysis of Storm Prediction Center (SPC) text products to infer “pulse” applications in an operational setting, and (3) describes the deficiencies with the current terminology. We conclude by suggesting a consolidated nomenclature for disorganized convection, including a standard application for pulse thunderstorm.

2.2 A brief history of the term “pulse”

“Pulse” was first coined as a thunderstorm mode descriptor by Wilk et al. (1979)[2]. This document, created for a Federal Aviation Administration (FAA) training program, was prepared by researchers at the National Severe Storms Laboratory (NSSL). According to one of the coauthors, “pulse” was intended to describe “a multicellular storm that is largely non-severe. However, occasionally one cell within the multicellular complex will briefly become severe.” The authors selected “pulse” to reference a “local surge of the updraft portion of the cell” that was structured as a discrete bubble rather than a current (personal communication, Les Lemon, 2015). The “pulse” was seen as the mechanism responsible for the subsequent severe weather.

This original meaning was essentially preserved in both educational and research texts for the first 20 years of the term’s existence, as indicated by a chronology of such resources in Table 2.1. However, the application of the term broadened following the new

[2] Wilk et al. (1979) is no longer accessible, but readers seeking more information can reference Burgess and Lemon (1990) for a similar definition.

millennium. Cerniglia and Snyder (2002) are the first to make an explicit reference to "nonsevere pulse storms," indicating that all cases of short-lived, isolated convection may be termed "pulse." In the ensuing decades, this interpretation has become increasingly frequent. Nine of the 18 textbooks, web tutorials, and research papers in Table 2.1 produced after 2000 appear to either apply "pulse" as a synonym for all isolated ordinary-cell convection or abstain from including a severe-weather criterion in their definition. As the meaning of "pulse" expanded to include nonsevere thunderstorms, a new variation gained traction within the severe-weather lexicon: "pulse severe" (e.g., Cerniglia and Snyder 2002; Miller and Petrolito 2008). The need for an explicitly severe variation of the term further illustrates the evolved meaning of "pulse" proper. "Pulse" also appears in many other journal articles and internet resources, but the reference is too brief to confidently infer the authors' concept of this storm mode.

The definitions provided by the current NWS and AMS glossaries Table 2.2 presumably offer credible standards for disorganized convection terminology. Though the NWS glossary (NWS 2016a) defines more of the current lexicon than the AMS *Glossary of Meteorology* (AMS 2016), its definitions demonstrate the same evolution evident in research texts. Separate entries are given to "pulse" and "pulse severe," and these definitions are not similar. The NWS "pulse severe" definition requires that the storm be a single-cell, but "pulse" does not. According to the NWS glossary, a convective line segment or a supercell could qualify as a pulse storm if the period of severe weather were sufficiently brief. Although the NWS definition is clear that severe weather is to be associated with this storm mode, the requirement that a "pulse severe" storm adhere to single-cell expectations is inconsistent with Wilk et al. (1979). Despite the AMS's formal procedure for fielding and reviewing user-suggested definitions, the online open-access *Glossary of Meteorology* largely reflects definitions published in the original (Huschke 1959) and revised (Glickman 2000) hardcopy editions. Consequently, neither "pulse" nor any of its variant forms are defined; only the definition for "ordinary cell" is explicitly provided[3]. Entries for "air-mass thunderstorm" and "convective cell" redirect to "air-mass shower" and "cell," respectively, creating confusion over whether the redirected term is synonymous with the first.

2.3 The use of "pulse" in SPC text products

This section surveys hundreds of SPC convective outlooks (CO) and mesoscale discussions (MD) (SPC 2015) to gauge operational applications of "pulse" in addition to its research and educational uses described above. While fewer than 30 research articles and textbooks were identified that use "pulse" with enough detail to discern the authors' concept of the storm mode (Table 2.1), operational products provide hundreds of accessible examples.

2.3.1 Data and methods

A content analysis (Krippendorff 2012) was performed using the publicly available web archive of SPC COs (http://www.spc.noaa.gov/products/outlook/) and MDs (http://www.spc.noaa.gov/products/md/) issued between 2003, the first year that the modern-format archive is available, and 2014. Any CO or MD that contained the term

---

[3] We intend to submit new definitions for the disorganized convection terminology discussed herein following the appearance of this article in printed form.

"pulse" was considered "pulse-referencing" and became a candidate for the content analysis. The 12-yr archive yielded a pulse-referencing database of 997 COs and 458 MDs.

Put simply, content analysis is the quantitative analysis of qualitative data, a technique that has been previously applied to the atmospheric sciences (Harrison 1982; Stewart et al. 2016). The analysis was conducted in two stages. The first stage seeks to establish the credibility of "pulse" references in SPC operational products as a relevant commentary on storm mode through a word frequency analysis. Though less detailed than MDs, the larger sample of COs can be used to track instances of "pulse" in COs through time and compare the temporal trends against traditional expectations.

The second stage of the analysis leverages the descriptive format of MDs to identify the vocabulary commonly used by forecasters in conjunction with "pulse." With single words serving as the unit of analysis, an inductive dictionary of pulse-related terms was developed following the five-step process recommended by Short et al. (2009) to optimize content validity. All words within the body of pulse-referencing MDs were considered candidates for the dictionary. This inductive technique differs from a deductive approach by forming the dictionary from *observed* recurring words rather than conceptually associated words that theoretically *should* recur.

The five-step process used in stage two is as follows: (1) Computer-aided text analysis software (McKenny et al. 2012) searched the archive of pulse-referencing MDs for recurring words. (2) The NWS glossary entry[4] for "pulse severe thunderstorm" was selected as the working definition. (3) Two doctoral students identified a subset of terms from the list developed in (1) associated with the definition selected in (2). Each rater

[4] Because the NWS definition for "pulse severe thunderstorm" references a "single-cell thunderstorm," the raters were instructed to select terms related to either definition.

independently reviewed the entire set of recurring words. (4) The inter-rater reliability score (Holsti 1969), a value between 0–1 with higher scores indicating stronger rater agreement, was calculated to be 0.76, with an alternative measure, Krippendorff's α statistic (Krippendorff 2012), yielding 0.72. (5) The raters compared their results, conferred over the discrepancies in their subsets, and mutually agreed upon the final 62-term dictionary that is shown in Table 2.3.

This inductive technique is meant to provide a broad overview of pulse-related word choice patterns and will only partially consider word context through a collocation (recurring expressions of two or more words) analysis using the Natural Language Toolkit (Bird et al. 2009). Thirty-one different forecasters and 86 different co-author combinations authored the 458 pulse-referencing MDs.

2.3.2 Results

The results of the first stage, shown in Fig. 2.1, confirm that the operational usage of "pulse" in SPC COs adheres to the undisputed expectations of the term. Eighty-eight percent of "pulse" references appear between May and August (Fig. 2.1a) with usage also peaking in the late afternoon/early evening (1630 UTC and 2000 UTC) on the day of concern (Fig. 2.1b). Figure 2.1c provides additional context by comparing the percent change in storm mode references as the outlook approaches the period of concern. Instances of "pulse" increase rapidly into Day 1 with a 29.6% increase between the 1300 UTC and 1630 UTC updates, roughly coincident with the onset of peak daytime heating. "Pulse" references then plummet dramatically following the loss of solar radiation. By comparison, references to "supercell" show less variation between each CO update period.

The second stage of the content analysis, performed on SPC MDs, yielded a 62-member pulse-term dictionary (Table 2.3) with the most frequently used dictionary words shown in Fig. 2.2. Three of the six dictionary words appearing in at least 60% of pulse-referencing MDs express well-acknowledged components of pulse thunderstorm descriptions ("storms," "weak," "shear"). Meanwhile, the other three terms ("severe," "wind," "hail") are closely tied to the NWS severe-weather warning criteria. Table 2.4 explores the context of these words by identifying any recurring neighboring terms, and sheds greater light on how SPC forecasters often apply pulse-related terminology in their text. Many of the rater-identified terms in Table 2.3 are also quantitatively identified as members of these recurring phrases. Again, the association with weak vertical wind shear, large instability, and severe weather is clear. The collocations also indicate that the isolated severe threat posed by pulse thunderstorms, though worthy of an MD issuance, frequently fails to satisfy weather watch criteria.

We acknowledge that because the purpose of SPC MDs is to communicate severe weather potential, frequent severe weather language is expected. However, when referencing potentially severe storms in weakly sheared environments, "pulse" is the overwhelming word-of-choice in SPC MDs. Table 2.5 shows that "pulse" references account for 58.6% of disorganized convection terminology. If variant forms (i.e., pulse-type) are included, then the proportion rises to 97.5%.

Although Table 2.3 was developed by examining pulse-referencing MDs, these words may simply be generic to all convection. If the terms in Table 2.3 are generic descriptors of all thunderstorms, then they would be expected to occur equally frequently across all convective MDs. If they are not generic descriptors, then they would be expected to occur less frequently in non-pulse-referencing MDs. Figure 2.3 supports the latter scenario by calculating the number of times a Table-2.3 term appeared in an MD's text and stratifying the results by storm mode. Indeed, the mean score for pulse-referencing MDs (24.0) significantly exceeds that for supercell-referencing MDs (17.5; Student's *t*-test yields $p<0.001$). This suggests that supercell-referencing MDs are characterized by a different set of vocabulary than the pulse-related terms identified by the raters, and by extension, Table 2.3 does not contain common language for all thunderstorms. However, the mean score for multicell-referencing MDs is statistically indistinguishable from pulse-referencing MDs (Fig. 2.3). The 62 pulse-related words in Table 2.3 are used equally frequently in MDs referencing multicell storms.

Combining the results in Figs. 2.2 and 2.3 and Table 2.3, the language contained in SPC pulse-referencing MDs resembles the traditional Wilk et al. (1979) description more than the nonsevere, single-celled, contemporary application. The frequent inclusion of severe-weather-related language and the equal representation of pulse-related terms in multicell-referencing MDs supports a severe, multicellular nature to pulse thunderstorms. Because MDs are only a sample of operational language, this result cannot be generalized across the whole operational community. Nevertheless, this analysis provides valuable insight toward how the SPC's broad professional and lay-person readership (SPC 2015) are exposed to applications of "pulse."

2.4 The motivation for standardization

The inconsistent and variable terminology for disorganized convection may seem inconsequential on the surface, but it poses a real problem for effective communication.

This section enumerates four major shortcomings of the current terminology that motivates the proposed standardization in the concluding section.

2.4.1 Redundancy

If the common phrase “pulse severe” is read with the Wilk et al. (1979) definition in mind, then the use of “severe” is redundant. More specifically, it is a form of linguistic error called “pleonasm.” Lehmann (2005) suggests that authors may sometimes choose to include redundant information in order to underscore a particular aspect of a word’s meaning. In other situations, the inclusion of repeated information may be due to uncertainty about whether the predicate term already contains that information. For instance, an author might choose the phrase “pulse severe storm” to emphasize that a pulse storm is severe. Alternatively, confused by the discrepancies in pulse thunderstorm definitions, the author might be unsure what the term actually means. The accompanying adjective “severe” is then intended to clarify elements of the word that may be in doubt. Pleonasm, as with all redundancy, weakens the language that contains it (Grice 1975). “Pulse severe,” though unambiguous in its association with severe weather, creates ambiguity by casting uncertainty on whether “pulse” alone implies severity. For comparison, pleonasm is less common for storm modes with a well-established, objective criterion. Few supercell-referencing MDs contain “mesocyclone” (0.7%), “rotating” (4.2%), or “rotation” (6.7%), the defining element of a supercell thunderstorm. Until the pulse thunderstorm’s definition is standardized, redundant phrasing will continue to confuse readers.

2.4.2 The pulse thunderstorm as a severe single-cell

As the meaning of "pulse" has evolved, some sources now reference a pulse thunderstorm as a single-cell thunderstorm that produces severe weather (e.g., Bluestein 2013; NWS 2016a). However, despite its ubiquity across the meteorological literature, there is relatively little precedent for a true single-cell thunderstorm. Though successfully simulated within a three-dimensional numerical cloud model by Weisman and Klemp (1982), a legitimate one-celled thunderstorm has proved elusive in field campaigns. Horace Byers, Project Director for the famed Thunderstorm Project, summarizes his field observations by saying, "While every storm must be one-celled at the beginning, the simple unicellular type was found to be rare because its period as a solitary cell lasts only a few minutes after it has reached rainy, thundery conditions. Thus, the textbook diagram of a thunderstorm, always unicelIular, is misleading" (Byers 1949). Byers' conclusion was informed by 1,363 aircraft penetrations of 179 thunderstorms in two different regions at five vertical levels yielding 4,218 minutes (2.93 days) of flight recordings. Even the "most complete study of a single air-mass storm since Byers and Braham" (Kingsmill and Wakimoto 1991) consisted of two small updrafts (Wakimoto and Bringi 1988). The concept of a single-cell thunderstorm, while valuable as a conceptual model, is disconnected from thorough field observations. If true single-cell thunderstorms occur so rarely, how can a pulse thunderstorm be a severe single-cell?

2.4.3 A congested vocabulary

As mentioned previously, the meteorological lexicon contains a wealth of terms referring to short-lived, isolated, summertime thunderstorms. The modifiers "air-mass," "ordinary," "single-cell," "pop-up," "popcorn," "garden-variety," "pulse," and "pulse-type" are each commonly employed by meteorologists. Summing all these words yields a total of *eight* terms describing the same basic concept. At best, the "pulse" family references a severe subset of air-mass/ordinary/single-cell/pop-up/popcorn/garden-variety thunderstorms. Otherwise, all eight words essentially share the same meaning.

The congested vocabulary of disorganized convection is a significant barrier to research and public communication. If these terms are truly synonyms, then they should be consolidated for more effective communication. If they represent truly distinct phenomena, then they need to be clearly defined as such. In *Eloquent Science*: *A Practical Guide to Becoming a Better Writer, Speaker, & Atmospheric Scientist*, David Schultz writes on the subject of redundant jargon: "Sometimes multiple terms have arisen to describe the same thing… Part of good scholarship is not to create any more unnecessary terms, but to identify and clarify any discrepancies or confusion with existing terms. If multiple terms exist, consistency is key to communicating with your audience… Even terms we think we may be familiar with, we may misuse" (2013, p. 91).

2.4.4 Inconsistent technical identification

Perhaps in response to the ambiguities stated above, researchers seeking to identify pulse thunderstorms employ widely varying criteria. Environmental thermodynamic and/or kinematic parameters, radar reflectivity factor, areal extent, temporal longevity, proximity to other convection, and (possibly) severe weather reports are often considered in their identification. Simultaneously, dynamical features, such as a radar-indicated mesocyclone, may be used to exclude a storm from being categorized as "pulse." Though the variables included in the classification process may be similar, the combination of variables and choice of thresholds regularly differ. Several other attempts to identify pulse convection essentially treat the category as a "catch-all" for storms failing to fit any other category (e.g., Cerniglia and Snyder 2002; Guillot et al. 2008; Ashley and Gilson 2009). While identification techniques are expected to differ between analyses, the variable categorization schemes can capture storms much different than the one envisioned by Wilk et al. (1979). Further, the variety of identification strategies inhibits reproducibility and comparisons of pulse-storm-related studies.

2.5 Conclusions

The revision of storm mode definitions is ongoing in other areas of mesoscale meteorology. Corfidi et al. (2016) have sought to initiate a similar conversation regarding the formal definition of a derecho. As the authors explain, "While questions of this sort may be dismissed as academic, they are not considering that meteorological terms increasingly are becoming part of the everyday lexicon, and that the use of concise, readily understood vocabulary is essential in communicating information to the general public." This same rationale is equally, if not more, applicable to pulse thunderstorms given their frequency during the summer.

Although an objective dynamical criterion (similar to that for a supercell) is most desirable, the paucity of pulse thunderstorm research precludes the suggestion of an appropriate feature at this time. Candidates for requisite dynamical signatures include radar-sensed divergence at the cloud top and base (Burgess and Lemon 1990) or the constriction feature described by Kingsmill and Wakimoto (1991). However, in the interim, the meteorological community would benefit by conceptually standardizing the definition of “pulse” and deciding what, if anything, differentiates it from other disorganized convection. With this goal in mind, a restructuring of the disorganized convection nomenclature is suggested below.

1) The basic conceptual model for a convective cell as outlined by Byers and Braham (1949) and simulated by Weisman and Klemp (1982) should be retained, but only for educational purposes. Often called a “single-cell” thunderstorm, this term is misleading given the frequent multicellular nature to disorganized convection (Byers 1949). This idealized thunderstorm could instead called a “Byers-Braham cell,” a name introduced by Doswell (1985, p. 48), and the use of “single-cell” thunderstorm should be avoided.

2) When referring to the operational equivalent of the Byers-Braham cell, it should be acknowledged that nearly all disorganized convection is at least weakly multicellular. At risk of further congesting the lexicon, our initial thought was to retain “air-mass thunderstorm” for this purpose because it is the only current option that communicates any information about the storm environment. However, a dialogue between the authors, reviewers, and editor concluded that by ignoring the role of mesoscale boundaries in convection initiation this term is also undesirable. We therefore recommend an essentially new, yet not unprecedented, alternative, which was also suggested during the review process: “weakly forced thunderstorm” (Rose et al. 2008; Bentley et al. 2012b). Environments favorable for this storm mode are characterized by the instability and moisture necessary for convection. However, a synoptic lifting mechanism and its attendant shear regime are absent,

imposing temporal and spatial limitations on any convection. Within the synoptically homogeneous air mass, weakly forced thunderstorm formation is routinely aided by both strong and subtle mesoscale variations in air temperature, moisture, and wind direction. Thus, weakly forced thunderstorms should be understood to reference *synoptically* weakly forced thunderstorms.

3) The subset of severe-weather-producing weakly forced thunderstorms could simply be called “severe weakly forced thunderstorms” without relying on any additional terminology. Such language perhaps even more directly communicates the anticipated hazards than “pulse thunderstorm.” However, given the predominance of “pulse” in the meteorological lexicon, standardizing future applications of “pulse” to reference severe-weather-producing weakly forced thunderstorms is more practical than eliminating it altogether. This proposed definition has a historical precedent stemming from Wilk et al. (1979) and a contemporary precedent in SPC MDs. Because storm severity is included by this definition, pulse storms should not be described as severe.

As the meteorological lexicon expands and matures, it is only prudent to critically re-evaluate our own vocabulary with the goal of optimizing clear and consistent communication. The abundance of terminology referencing brief, summertime convection impedes the clear, effective dissemination of severe-weather hazards, and retards scientific research directed at these storms. This paper offers a prototype for future re-evaluations of meteorogical language while serving as an immediate call to thin and standardize the congested vocabulary of disorganized convection.

2.6 Acknowledgements

The authors thank Dr. Alan Stewart for his helpful comments on an earlier draft of this essay. Exchanges between the authors, the reviewers, and the editor also greatly improved this essay as well as the quality of its recommendations.

2.7 References

AMS, 2016: Glossary of Meteorology. Accessed 18 January 2016. [Available online at http://glossary.ametsoc.org/.]

Ashley, W. S., and C. W. Gilson, 2009: A reassessment of U.S. lightning mortality. *Bull. Amer. Meteor. Soc.*, **90,** 1501–1518, doi:10.1175/2009BAMS2765.1.

Beasley, W. H., D. E. Williams, and P. T. Hyland, 2008: Analysis of surface electric-field contours in relation to cloud-to-ground lightning flashes in air-mass thunderstorms at the Kennedy Space Center. *20th International Lightning Detection Conference*, Tucson, Arizona, Vaisala. [Available online at http://es.vaisala.com/Vaisala %20Documents/Scientific%20papers/Analysis_of_surface_electric-field_ contours.pdf.]

Bentley, M. L., J. A. Stallins, and W. S. Ashley, 2012: Synoptic environments favourable for urban convection in Atlanta, Georgia. *Int. J. Climatol.*, **32,** 1287–1294, doi:10.1002/joc.2344.

Bird, S., E. Loper, and E. Klein, 2009: *Natural Language Processing with Python.* O'Reilly Media Inc.

Bluestein, H. B., 2013: *Severe Convective Storms and Tornadoes: Observations and Dynamics.* Springer, 456 pp.

Burgess, D. W., and L. R. Lemon, 1990: Severe thunderstorm detection by radar. *Radar in Meteorology*, D. Atlas, Ed., Springer, 619–647.

Byers, H. R., 1949: Structure and dynamics of the thunderstorm. *Science*, **110,** 291-294, doi:10.1126/science.110.2856.291.

Byers, H. R., and R. R. Braham, 1949: *The Thunderstorm: Report of the Thunderstorm Project.* US Government Printing Office, 287 pp.

Cerniglia, C. S., and W. R. Snyder, 2002: Development of warning criteria for severe pulse thunderstorms in the Northeastern United States using the WSR-88D. National Weather Service. Eastern Region Technical Attachment No. 2002-03, 14 pp.

[Available online at http://docs.lib.noaa.gov/noaa_documents/NWS/NWS_ER/Eastern_Region_Tech_Attachment/TA_2002-03.pdf.]

Corfidi, S. F., M. C. Coniglio, A. E. Cohen, and C. M. Mead, 2016: A proposed revision to the definition of “Derecho”. *Bull. Amer. Meteor. Soc.*, **97,** 935–949, doi:10.1175/bams-d-14-00254.1.

Cover, T. M., and J. A. Thomas, 1991: Information theory and statistics. *Elements of Information Theory*, 1 ed., John Wiley & Sons, 279–335.

Diffenbaugh, N. S., M. Scherer, and R. J. Trapp, 2013: Robust increases in severe thunderstorm environments in response to greenhouse forcing. *Proc. Natl. Acad. Sci.*, **110,** 16361–16366, doi:10.1073/pnas.1307758110.

Doswell, C. A. I., 1985: The operational meteorology of convective weather. Volume II: Storm scale analysis. NOAA. Technical Memorandum ERL ESG-15, 240 pp. [Available online at http://docs.lib.noaa.gov/noaa_documents/OAR/ERL_ESG/TM_ERL_ESG_15.pdf.]

Fowle, M. A., and P. J. Roebber, 2003: Short-range (0–48 h) numerical prediction of convective occurrence, mode, and location. *Wea. Forecasting*, **18,** 782–794, doi:10.1175/1520-0434(2003)018<0782:SHNPOC>2.0.CO;2.

Frugis, B., and T. Wasula, 2011: Development of warning thresholds for one inch or greater hail in the Albany, New York, county warning area. National Weather Service. Eastern Region Technical Attachment No. 2011-05, 24 pp. [Available online at http://docs.lib.noaa.gov/noaa_documents/NWS/NWS_ER/Eastern_Region_Tech_Attachment/TA_2011-05.pdf.]

Gensini, V. A., and T. L. Mote, 2015: Downscaled estimates of late 21st century severe weather from CCSM3. *Climatic Change*, **129,** 307–321, doi:10.1007/s10584-014-1320-z.

Glickman, T., Ed., 2000: *Glossary of Meteorology*. 2nd ed. Amer. Meteor. Soc., 855 pp.

Grice, H. P., 1975: Logic and conversation. *Syntax and Semantics III - Speech Acts*, P. Cole, and J. L. Morgan, Eds., Academic Press, 41–58.

Guillot, E. M., T. M. Smith, V. Lakshmanan, K. L. Elmore, D. W. Burgess, and G. J. Stumpf, 2008: Tornado and severe thunderstorm warning forecast skill and its relationship to storm type. *24th Int. Conf. Interactive Information Processing Systems for Meteor., Oceanogr., and Hydrol.*, New Orleans, LA, American Meteorological Society. [Available online at http://ams.confex.com/ams/pdfpapers/132244.pdf.]

Harrison, M. R., 1982: The media and public perceptions of climatic change. *Bull. Amer. Meteor. Soc.*, **63,** 730–730, doi:10.1175/1520-0477(1982)063<0730:TMAPPO>2.0.CO;2.

Holsti, O. R., 1969: *Content Analysis for the Social Sciences and Humanities.* Addison-Wesley, 235 pp.

Howard, K. W., J. J. Gourley, and R. A. Maddox, 1997: Uncertainties in WSR-88D measurements and their impacts on monitoring life cycles. *Wea. Forecasting*, **12,** 166–174, doi:10.1175/1520-0434(1997)012<0166:uiwmat>2.0.co;2.

Huschke, R. E., Ed., 1959: *Glossary of Meteorology*. 1st ed. Amer. Meteor. Soc., 638 pp.

Kingsmill, D. E., and R. M. Wakimoto, 1991: Kinematic, dynamic, and thermodynamic analysis of a weakly sheared severe thunderstorm over northern Alabama. *Mon. Wea. Rev.*, **119,** 262–297, doi:10.1175/1520-0493(1991)119<0262:KDATAO>2.0.CO;2.

Krippendorff, K., 2012: *Content Analysis: An Introduction to Its Methodology.* Sage, 456 pp.

Lack, S. A., and N. I. Fox, 2012: Development of an automated approach for identifying convective storm type using reflectivity-derived and near-storm environment data. *Atmos. Res.*, **116,** 67–81, doi:10.1016/j.atmosres.2012.02.009.

Lakshmanan, V., and T. Smith, 2009: Data mining storm attributes from spatial grids. *J. Atmos. Oceanic Technol.*, **26,** 2353–2365, doi:10.1175/2009jtecha1257.1.

Lehmann, C., 2005: Pleonasm and hypercharacterisation. *Yearbook of Morphology 2005*, G. Booij, and J. Van Marle, Eds., Springer Netherlands, 119–154.

Markowski, P., and Y. Richardson, 2010: *Mesoscale Meteorology in Midlatitudes.* 1 ed. Wiley-Blackwell, 407 pp.

McKenny, A. F., J. C. Short, and S. M. Newman, 2012: CAT Scanner. Version 1.0. [Available online at http://www.amckenny.com/CATScanner/.]

Miller, D., and A. Petrolito, 2008: Anticipating pulse severe thunderstorms using the WSR-88D all-tilts display. National Weather Service. Eastern Region Technical Attachment No. 2008-02, 11 pp. [Available online at http://docs.lib.noaa.gov/noaa_documents/NWS/NWS_ER/Eastern_Region_Tech_Attachment/TA_2008-02.pdf.]

Miller, P. W., A. Ellis, and S. Keighton, 2015: A preliminary assessment of using spatiotemporal lightning patterns for a binary classification of thunderstorm mode. *Wea. Forecasting*, **30,** 38–56, doi:10.1175/WAF-D-14-00024.1.

NTSB, 1986: Aircraft Accident Report: Delta Air Lines Inc., Lockheed L-1011-385-1, N726DA. Dallas/Fort Worth - International Airport, Texas, August 2,1985. NTSB/AAR-86/05, 164 pp. [Available online at http://www.ntsb.gov/investigations/AccidentReports/Reports/AAR8605.pdf.]

NWS, 2016a: National Weather Service Glossary. Accessed 21 January 2016. [Available online at http://w1.weather.gov/glossary/.]

——, 2016b: JetStream - Online school for weather. Accessed 21 January 2016. [Available online at http://www.srh.noaa.gov/jetstream/tstorms/tstrmtypes.html.]

Rose, L. S., J. A. Stallins, and M. L. Bentley, 2008: Concurrent Cloud-to-Ground Lightning and Precipitation Enhancement in the Atlanta, Georgia (United States), Urban Region. *Earth Interact.*, **12,** 1–30, doi:10.1175/2008EI265.1.

Schultz, D., 2013: *Eloquent Science: A Practical Guide to Becoming a Better Writer, Speaker, and Atmospheric Scientist.* Springer Science & Business Media, 412 pp.

Short, J. C., J. C. Broberg, C. C. Cogliser, and K. C. Brigham, 2009: Construct validation using computer-aided text analysis (CATA): An illustration using entrepreneurial orientation. *Organizational Research Methods***,** 1–28, doi:10.1177/1094428109335949.

Smith, T. M., K. L. Elmore, and S. A. Dulin, 2004: A damaging downburst prediction and detection algorithm for the WSR-88D. *Wea. Forecasting*, **19,** 240–250, doi:10.1175/1520-0434(2004)019<0240:ADDPAD>2.0.CO;2.

SPC, 2015: SPC product descriptions. Accessed 11 November 2015. [Available online at http://www.spc.noaa.gov/misc/about.html.]

Stewart, A. E., C. A. Williams, M. D. Phan, A. L. Horst, E. D. Knox, and J. A. Knox, 2016: Through the eyes of the experts: Meteorologists' perceptions of the probability of precipitation. *Wea. Forecasting*, **31,** 5–17, doi:10.1175/WAF-D-15-0058.1.

Stewart, S. R., 1991: The prediction of pulse-type thunderstorm gusts using vertically integrated liquid water content (VIL) and the cloud top penetrative downdraft mechanism. NOAA. Technical Memorandum NWS SR-136, 20 pp. [Available online at http://docs.lib.noaa.gov/noaa_documents/NWS/NWS_SR/TM_NWS_SR_136.pdf.]

Stull, R., 2015: *Practical Meteorology: An Algebra-based Survey of Atmospheric Science* University of British Columbia, 938 pp.

UCAR, 2010: Radar signatures for severe convective weather. Accessed 21 January 2016. [Available online at http://www.meted.ucar.edu/radar/severe_signatures/.]

——, 2012: Tropical severe local storms. Accessed 21 January 2016. [Available online at http://www.meted.ucar.edu/tropical/synoptic/local_storms/.]

——, 2013: A convective storm matrix: Buoyancy/shear dependencies. Accessed 21 January 2016. [Available online at http://www.meted.ucar.edu/convectn/csmatrix/index.htm.]

Wakimoto, R. M., and V. Bringi, 1988: Dual-polarization observations of microbursts associated with intense convection: The 20 July storm during the MIST project. *Mon. Wea. Rev.*, **116,** 1521–1539, doi:10.1175/1520-0493(1988)116<1521:DPOOMA>2.0.CO;2.

Weisman, M. L., and J. B. Klemp, 1982: The dependence of numerically simulated convective storms on vertical wind shear and buoyancy. *Mon. Wea. Rev.*, **110,** 504–520, doi:10.1175/1520-0493(1982)110<0504:tdonsc>2.0.co;2.

Wilk, K. E., L. R. Lemon, and D. W. Burgess, 1979: Interpretation of radar echoes from severe thunderstorms: a series of illustrations with extended captions. National Severe Storms Laboratory. Prepared for FAA ARTCC coordinator training.]

Table 2.1. Survey of pulse-referencing research and educational documents published between 1979 and 2015. Although more texts reference pulse thunderstorms than those shown here, they do not include enough descriptive detail to yield useful insight.

#	Source	Type of source	Purpose	Excerpt
1	Wilk et al. (1979)	FAA training document	Radar detection of thunderstorm	No longer available, but similar to Burgess and Lemon (1990) definition (personal communication, Les Lemon, 2015).
2	Doswell III (1985)	NOAA technical memorandum	Severe thunderstorm identification	"Perhaps the most common severe weather producer among the secondary classes is the so-called pulse storm. Such a storm…closely resembles an ordinary non-severe thunderstorm cell in many respects...In essence, it is a cell which, for some reason, possesses **briefly** an intense updraft. This strong updraft lasts only a short time, during and immediately after which the storm produces a short episode of severe weather and then dissipates (hence, its name)."
3	Burgess and Lemon (1990)	Textbook	General meteorological education	"It closely resembles the ordinary thunderstorm with a few notable exceptions. In many cases, the thunderstorm cell that becomes severe is a member of an ordinary cell complex although it can exist in isolation. The intense updraft is relatively short-lived, taking the form of a single bubble or pulse. Thus, the first-echo height (6–9 km) is higher than for the ordinary cell. The area of more intense reflectivities (50+ dBZ) is also much higher, persistent, and maintains continuity with descent to the ground. As the core descends to the ground, high winds (often classic downbursts) and brief large hail may occur. The duration of severe weather and the total storm lifetime are short. Succeeding storm cells in the pulse storm are ordinary...The pulse storm environment is frequently characterized by low shear, relatively deep moisture, and high instability."
4	Stewart (1991)	NOAA technical memorandum	Severe thunderstorm identification	"…a technique has been proposed to assist operational meteorologists in forecasting the gust potential of air-mass (pulse-type) thunderstorms in near real-time situations."
5	Howard et al. (1997)	Journal article	Radar performance	"The idealized reflectivity structure we used depicts the life cycle of a 'pulse'-type, single-cell thunderstorm (Doswell 1985). Pulse-

				type storms are common in moderately unstable, weakly sheared environments and have short-lived, strong updrafts. We focus primarily on this type of storm due to their frequency in central Arizona and because they often produce severe, short-lived downburst winds…”
6	Cerniglia and Snyder (2002)	NWS technical attachment	Severe thunderstorm identification	“The [radar] data were sorted into storm types to extract severe and non-severe pulse storms. All events that were organized along a line, squall line, front, bow echo, or that were tornadic, were eliminated. Storms that contained a mesocyclone, whether algorithm or user defined, at any point prior to the severe report were also eliminated.”
7	Fowle and Roebber (2003)	Journal article	Model verification	“The second stage was the verification of convective mode. Observed storms were categorized as linear, multicellular, or isolated (pulse storms)…The isolated storm mode was defined by a reflectivity area greater than 40 dBZ that had a spatial coverage of less than 500 km^2.”
8	Smith et al. (2004)	Journal article	Severe thunderstorm identification	“This makes severe outflows from these ‘pulse’ thunderstorms difficult for weather forecasters to issue warnings for…”
9	Beasley et al. (2008)	Conference paper	Lightning/electric field analysis	“Because isolated, air-mass, or ‘pulse’ thunderstorms are the most likely type to develop…”
10	Guillot et al. (2008)	Conference paper	Storm mode classification	“…‘pulse storms’, defined for this study as any thunderstorm that is strong or severe but does not possess a mesocyclone and rotating updraft.”
11	Miller and Petrolito (2008)	NWS technical attachment	Severe thunderstorm identification	“This paper illustrates how the WSR-88D All-Tilts Display was used to make a Severe Thunderstorm Warning (SVR) decision for a pulse thunderstorm…” and “A pulse severe thunderstorm developed rapidly over central Edgefield County, South Carolina…”

12	Ashley and Gilson (2009)	Journal article	Lightning fatality analysis	"Unorganized, pulse-style convection includes storms that do not fit the above MCS or supercell definitions and subjectively appear to lack any spatial or temporal organization in reflectivity data."
13	Lakshmanan and Smith (2009)	Journal article	Storm cell identification	"…difficult to issue tornado warnings when the tornadoes are associated with short-lived pulse storms…"
14	Radar Signatures for Severe Convective Weather (UCAR 2010)	COMET MetEd	General meteorological education	"Multicellular pulse thunderstorms: in weaker deep layer shear environments storms tend to be multicellular in nature with several collocated updrafts in different stages of development. At any one scan it may seem as though one of the pulse storms is a single cell with one dominant reflectivity signature, but it may merely be one or more short-lived cells developing and dissipating within a scan or two (~20 minutes)."
15	Markowski and Richardson (2010)	Textbook	General meteorological education	"Thus, single-cell convection tends to occur near and shortly after the time of maximum daytime heating (when CIN is smallest and CAPE is largest) and tends to dissipate quickly after sunset. It only occasionally produces hail or wind gusts that could be characterized as severe. When severe weather is produced, it is generally of the pulse variety—short lived, usually marginal (e.g., a brief wind gust above 25 ms^{-1}), and difficult to issue warnings for."
16	JetStream – Online school for weather (NWS 2016b)	Online tutorial	General meteorological education	"Also called a 'pulse' thunderstorm, the ordinary cell consists of a one-time updraft and one-time downdraft."
17	Frugis and Wasula (2011)	NWS technical attachment	Severe thunderstorm identification	"Storms were classified as pulse (ordinary), multicell or supercell."
18	Lack and Fox (2012)	Journal article	Storm mode classification	"An important distinction is made between air mass thunderstorms and pulse thunderstorms. Although similar in structure, the pulse thunderstorm has characteristics that allow for the rapid formation of hail and/or the possibility for a severe downburst."

19	Tropical Severe Local Storms (UCAR 2012)	COMET MetEd	General meteorological education	"The single cell or ordinary pulse thunderstorm evolution can be described by three stages: *cumulus*, *mature*, and *dissipating*."
20	Bluestein (2013)	Textbook	General meteorological education	"Storms that behave like ordinary cells and consist of only one cell are sometimes referred to as 'pulse'-type, single-cell convective storms."
21	A Convective Storm Matrix: Buoyancy/Shear Dependencies (UCAR 2013)	COMET MetEd	General meteorological education	"Ordinary cells that produce these bursts of severe weather are often referred to as pulse storms."
22	Miller et al. (2015c)	Journal article	Storm mode classification	"…single-cell thunderstorms capable of producing severe weather, also termed pulse storms…"
23	Stull (2015)	Textbook	General meteorological education	"Air-mass thunderstorms that produce short duration severe weather (heavy precipitation, strong winds, lightning, etc.) during the mature stage are called pulse storms."

Table 2.2. Entries for common disorganized convection terms taken from the NWS (2016a) and AMS (2016) glossaries.

#	Source	Term	Definition
1	AMS Glossary	Ordinary cell	"The most basic component of a convective storm, consisting of a single main updraft that is usually quickly replaced by a downdraft once precipitation begins. Ordinary cells are especially observed in environments with weak vertical wind shear, and typically have lifetimes of 30–50 minutes. Ordinary cells are the primary component of multicell storms."
2	NWS Glossary	Single-cell thunderstorm	"This type of thunderstorm develops in weak vertical wind shear environments. On a hodograph, this would appear as a closely grouped set of random dots around the center of the graph. They are characterized by a single updraft core and a single downdraft that descends into the same area as the updraft. The downdraft and its outflow boundary then cut off the thunderstorm inflow. This causes the updraft and the thunderstorm to dissipate. Single cell thunderstorms are short-lived. They only last about 1/2 hour to an hour. These thunderstorms will occasionally become severe (3/4[5] inch hail, wind gusts in the excess of 58 miles an hour, or a tornado), but only briefly. In this case, they are called Pulse Severe Thunderstorms."
3	NWS Glossary	Air-mass thunderstorm	"Generally, a thunderstorm not associated with a front or other type of synoptic-scale forcing mechanism. Air mass thunderstorms typically are associated with warm, humid air in the summer months; they develop during the afternoon in response to insolation, and dissipate rather quickly after sunset. They generally are less likely to be severe than other types of thunderstorms, but they still are capable of producing downbursts, brief heavy rain, and (in extreme cases) hail over 3/4[1] inch in diameter. Since all thunderstorms are associated with some type of forcing mechanism, synoptic-scale or otherwise, the existence of true air-mass thunderstorms is debatable."
4	NWS Glossary	Pulse storm	"A thunderstorm within which a brief period (pulse) of strong updraft occurs, during and immediately after which the storm produces a short episode of severe weather. These storms generally are not tornado producers, but often produce large hail and/or damaging winds…"
5	NWS Glossary	Pulse severe thunderstorms	"Single cell thunderstorms which produce brief periods of severe weather (3/4[1] inch hail, wind gusts in the excess of 58 miles an hour, or a tornado)."

[5] Since the establishment of its glossary, the NWS increased the severe hail criterion from 0.75 in to 1.0 in.

Table 2.3. Dictionary of 62 inductively identified words frequently used by SPC forecasters in association with "pulse." The fraction of pulse-referencing MDs containing each term are shown. Full versions of words are provided in italics beneath any abbreviations.

Term	Fraction	Term	Fraction
STORMS	0.729	TSTM	0.188
WIND	0.664	[*THUNDERSTORM*]	
SEVERE	0.662	MARGINAL	0.183
WEAK	0.657	ASCENT	0.181
SHEAR	0.651	DMGG	0.179
HAIL	0.638	[*DAMAGING*]	
ISOLATED	0.592	MOISTURE	0.172
AFTERNOON	0.572	LOCALLY	0.164
STRONG	0.537	WEATHER	0.153
BOUNDARY	0.507	CLUSTERS	0.146
LAPSE	0.441	BOUNDARIES	0.140
GUSTS	0.428	HEAVY	0.138
WINDS	0.410	CELLS	0.135
INSTABILITY	0.393	INTENSITY	0.118
CONVECTION	0.382	BRIEF	0.114
DAMAGING	0.360	RAINFALL	0.107
UNSTABLE	0.360	ISOLD	0.103
CONVECTIVE	0.338	[*ISOLATED*]	
HEATING	0.334	INTENSE	0.094
OUTFLOW	0.317	STATIONARY	0.087
STORM	0.308	SMALL	0.085
TSTMS	0.299	DOWNBURST	0.083
[*THUNDERSTORMS*]		DAMAGE	0.081
COVERAGE	0.297	GUSTY	0.076
STRONGER	0.295	NUMEROUS	0.072
EVENING	0.277	CLOUD	0.070
THUNDERSTORMS	0.245	SPORADIC	0.055
MARGINALLY	0.234	RAIN	0.050
AIRMASS	0.214	AFTN	0.033
THUNDERSTORM	0.210	[*AFTERNOON*]	
DEWPOINTS	0.207	UPDRAFT	0.033
CONVERGENCE	0.205	STG	0.017
SVR	0.205	[*STRONG*]	
[*SEVERE*]		DEWPTS	0.007
ORGANIZATION	0.190	[*DEWPOINTS*]	

Table 2.4. Bigrams and trigrams (collocations of length two and three, respectively) found within pulse-referencing MDs. Phrases were identified by determining their pointwise mutual information (PMI; Cover and Thomas 1991), a measure of how much one word reduces the uncertainty that a second word appears within a five-word window. Bigrams and trigrams were required to appear in at least 25% of pulse-referencing MDs to be listed to filter out strongly associated, yet infrequent, collocations.

Top 25 Bigrams		**Top Three Trigrams**
AIR MASS	DAMAGING GUSTS	STEEP LAPSE RATES
STEEP LAPSE	WATCH ANTICIPATED	WEATHER WATCH NOT
LAPSE RATES	WEATHER NOT	DAMAGING WINDS GUSTS
NEXT HOURS	WATCH NOT	
STEEP RATES	WINDS GUSTS	
NOT ANTICIPATED	DAMAGING WINDS	
MLCAPE J/KG	BOUNDARY LAYER	
DEEP LAYER	MARGINALLY SEVERE	
LOW LEVEL	WEAK SHEAR	
VALUES J/KG	SEVERE THREAT	
WEATHER WATCH	SEVERE HAIL	
OUTFLOW BOUNDARY	STRONG WINDS	
LARGE HAIL		

Table 2.5. Counts of terms used to describe disorganized convection as they appear in SPC MDs between 2003 and 2014.

Term	Count
Air mass	7
Garden-variety	0
Ordinary	0
Pop-up	0
Popcorn	0
Pulse multicell	29
Pulse	323
Pulse severe	31
Pulse-like	28
Pulse-type	109
Pulse-type severe	17
Single-cell	7

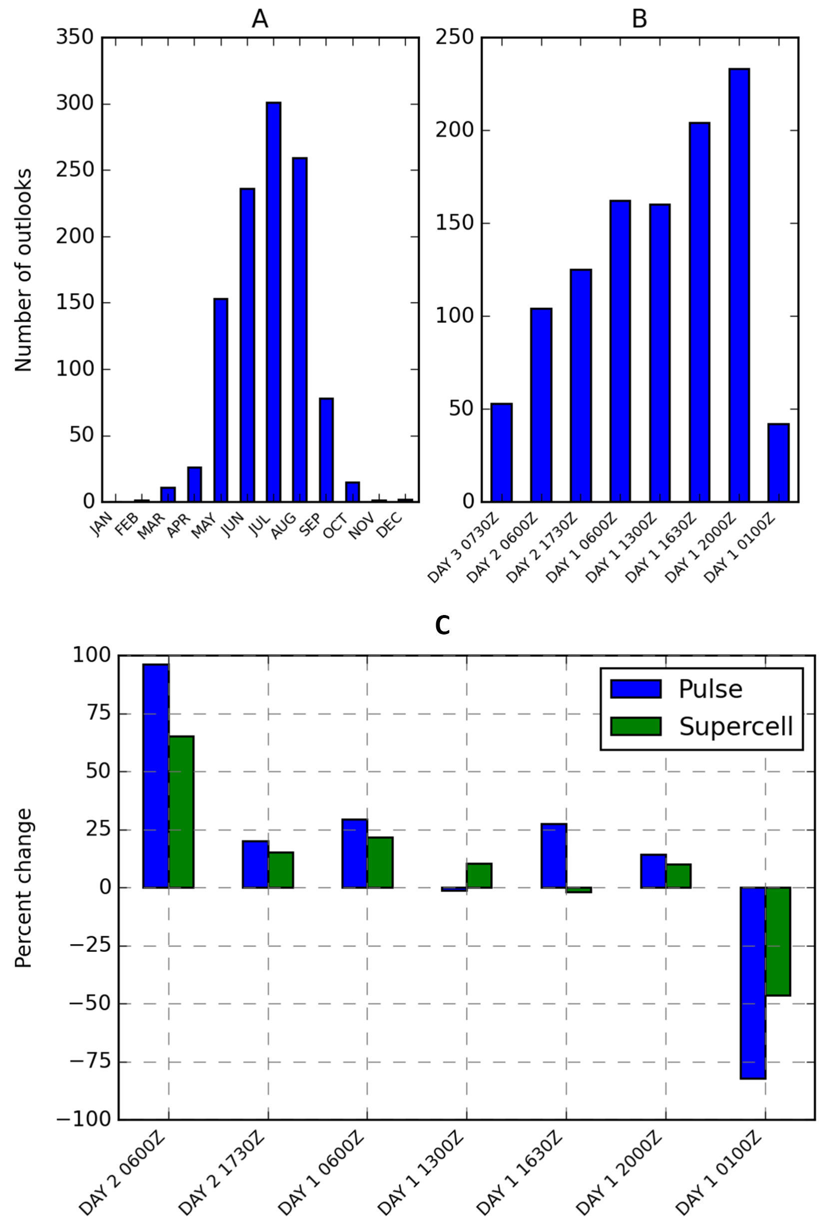

Figure 2.1. Distribution of "pulse" appearances in SPC COs (A) by month and (B) by outlook issuance. (C) Percent change in the number of references to "supercell" and "pulse" compared to the immediately preceding outlook period. There is a sharp increase in "pulse" uses during the Day 1 1630Z outlook accompanied by an 80% decrease following the loss of diurnal heating.

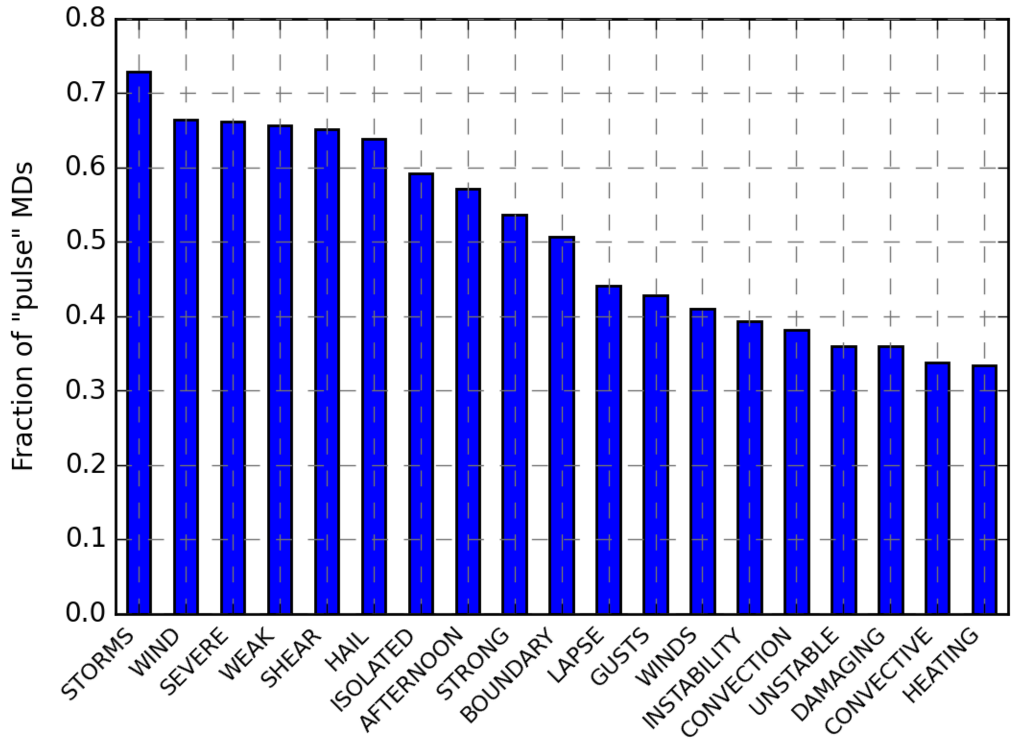

Figure 2.2. Fraction of pulse-referencing MDs containing the terms from Table 2.1. Only terms appearing in at least than one third of pulse MDs are compared.

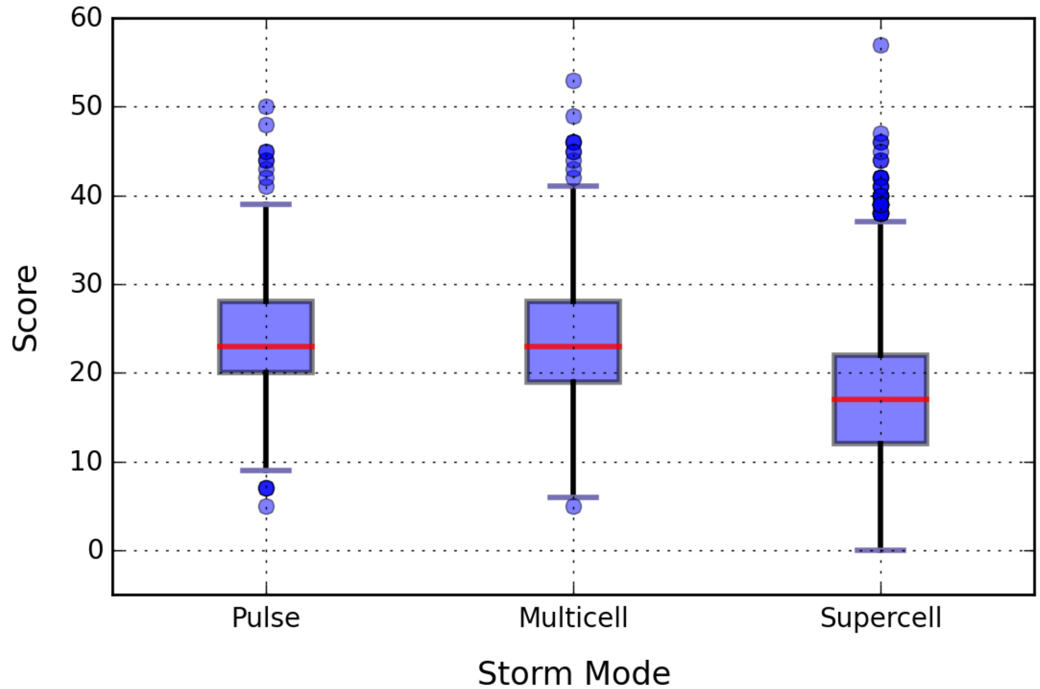

Figure 2.3. Boxplots of Table 2.1 word scores for pulse-, multicell-, and supercell-referencing MDs. Median scores are indicated by red lines, and the shaded blue boxes demarcate the middle 50% of the scores (i.e., the interquartile range). Outliers are depicted by blue circles placed beneath (above) the 25th (75th) percentile minus (plus) the interquartile range.

CHAPTER 3

A CLIMATOLOGY OF WEAKLY FORCED AND PULSE THUNDERSTORMS IN THE SOUTHEAST UNITED STATES [6]

[6] Miller, P., and T. Mote, 2017: A climatology of weakly forced and pulse thunderstorms in the Southeast United States. *J. Appl. Meteor. Climatol.***,** In press. Reprinted here with permission of the publisher.

Abstract

Weakly forced thunderstorms (WFTs), convection forming in the absence of a synoptic forcing mechanism and its associated shear regime, are the dominant convective mode during the warm season in the Southeast United States. This study uses 15 years (2001–2015) of warm season (May-September) composite reflectivity images from 30 WSR-88D sites in the Southeastern United States to detect WFTs and pulse thunderstorms, defined as WFTs associated with a severe weather event. Thunderstorms were identified as regions of contiguous reflectivities greater than or equal to 40 dBZ using connected neighborhoods labeling. Ward's clustering was then performed upon the duration, size, strength, initiation time, and solidity of the approximately 1.9 million resulting thunderstorms. Of the 10 clusters of morphologically similar storms, five groups, containing 885,496 thunderstorms, were designated as WFTs.

In line with previous work, WFT development mirrors landscape features, such as the Appalachian Mountains and Mississippi Delta. However, the large sample size also reveals more subtle nuances to the spatial distribution, such as decreases over river valleys and increases along the Atlantic fall line. The most active pulse thunderstorm region, the Blue Ridge mountains, was displaced from the overall WFT maximum: the Florida peninsula and Gulf Coast. Most pulse thunderstorms were associated with larger moisture values, particularly in the mid-levels, which supported larger and longer-lasting WFT complexes. Synoptically, two distinct modes of variability yielded WFT-favorable environments: the intrusion of the Bermuda High from the east and the expansion of high pressure over the Southern Plains from the west.

3.1 Introduction

Weakly forced convection, thunderstorms forming without the support of synoptic-scale lift and shear, constitute the majority of thunderstorms world-wide. As jet stream dynamics shift poleward during the summer months, weakly forced thunderstorms (WFTs) become increasingly common producers of mid-latitude precipitation, especially in the Southeastern United States. Without the support of large-scale forcing, WFTs rely upon mesoscale boundaries or preferential heating along orographic features for development. While some of these boundaries are regular and predictable, others are more difficult to detect. Consequently, several recent attempts have been made to identify heterogeneities in land cover (e.g., Haberlie et al. 2015), soil moisture (e.g., Frye and Mote 2009; Ford et al. 2015), terrain (e.g., Miller et al. 2015b), and humidity (e.g., Fabry 2006; Lee et al. 2016) that may influence convection under synoptically quiescent conditions in the southern and eastern U.S.

Despite the prevalence of this storm mode in the Southeast U.S., attempts to explicitly identify WFTs have been limited and challenging (Miller and Mote 2017b). Though forecasting textbooks emphasize the role of climatology in formulating a weather forecast (e.g., Lackmann 2011, p. 311), such a tool is unavailable for this already difficult-to-forecast thunderstorm type. In addition to forecasting implications, the absence of a WFT climatology impedes the establishment of broader connections between disorganized convection and the global climate system. Illustrating this potential, studies have discussed the important fraction of convective rainfall and latent heat release contributed by isolated, shallow convection in tropical regions (Schumacher and Houze 2003) as well as the role of lower-topped cumulus clouds in controlling radiative inputs and conditioning the atmosphere for subsequent deep convection (e.g., Johnson et al. 1999; de Szoeke et al. 2014). Though the precipitation climatology (Ingram et al. 2013) and regional lightning patterns (Murphy and Konrad 2005) in the Southeast U.S. maintain a summertime signal consistent with WFTs, there has been no attempt to create an explicit WFT climatology for this, or any other, region of the world.

Further, the accurate prediction of pulse thunderstorms, defined as severe WFTs [See Miller and Mote (2017b) for a detailed description of the disorganized convection nomenclature employed here.], remains a challenge for contemporary forecasters (Guillot et al. 2008). For instance, a recent study found that National Weather Service (NWS) accuracy statistics during severe thunderstorm warning outbreaks, typically occurring in modest-instability, weak-shear environments, were poorer than the national average (Bruick and Karstens 2017). Climate models suggest that these pulse thunderstorm-supporting environments will become increasingly frequent in future climate regimes (Diffenbaugh et al. 2013) with recent studies already documenting a shift toward these conditions (Senkbeil et al. 2017; Ye et al. 2017). Within quiescent, WFT-favorable regimes, ever-growing urban areas are also known to promote convection (Shepherd 2005; Mote et al. 2007). As extreme examples of landscape change, urbanization poses a propensity to modify thunderstorm initiation patterns (Niyogi et al. 2010; Ashley et al. 2012). Given the disproportionate concentration of cultural and economic output in these areas, a more thorough understanding of their influence on regional thunderstorm climatologies, as well as the thunderstorms they produce, is essential. Though posing a weaker severe wind and hail threat than supercells and derechos on a per-storm basis, WFT-associated lightning kills more people (Ashley and Gilson 2009) and threatens to suspend sporting events and airport ground operations for many more days each year.

As the climatic conditions conducive to their formation and the human-induced landscape change aiding their initiation both advance, so should our understanding of WFTs and pulse thunderstorms. This study seeks to investigate foundational, yet under-examined, questions of WFT activity through 15 years of radar observations in the Southeastern U.S. (Fig. 3.1), including their frequency, favored areas of development, the synoptic conditions enhancing their formation, and their tendency to produce severe weather.

3.2 Data and methods

The goal of the methodology is to develop a dataset of WFTs, defined here as storms forming in the absence of synoptic-scale lift and shear, which in turn yields generally small, short-lived, diurnally-driven convection. This relationship between storm environment and storm morphology was demonstrated by Weisman and Klemp (1982) and has been incorporated into meteorological curricula during the intervening decades (e.g., Markowski and Richardson 2010; Bluestein 2013). However, storms in weakly forced environments can sometimes violate the morphology suggested by Weisman and Klemp (1982) by growing into groups of cells that do not propagate "in any systematic, predictable way" (Markowski and Richardson 2010, p. 203). Because these storms are nonetheless weakly forced, the methodology must also retain the flexibility to include such events when they are detected. Pulse thunderstorms, a key consideration of this work, often occur in the latter arrangement (Burgess and Lemon 1990; Miller and Mote 2017b).

Based on the work referenced above, the following methodology operates on the hypothesis that storms with similar radar-inferred morphologies form, on average, in similar convective environments. Section 3.2.1 describes how the storms and their radar-inferred morphologies are detected, whereas Section 3.2.2 details how the storm morphologies are related to the convective environment. Because thunderstorm morphology is observed at a much greater spatial and temporal resolution via radar than convective environments are observed via radiosondes, it is more feasible to designate WFTs based on their morphologies once their composite convective environment is known. Essentially, this approach establishes relationships between morphologically similar storms and their host environment, so that WFTs can be identified in the absence of proximate sounding data.

3.2.1 Deriving thunderstorms from radar imagery

Thunderstorms are identified using 15 years (2001–2015) of Weather Surveillance Radar - 1988 Doppler (WSR-88D) level-III composite reflectivities for 30 sites in the Southeastern U.S. (Fig. 3.1) during the warm season (May-September), totaling approximately 10 million radar scans. Consistent data was not available for two WSR-88Ds, KHTX and KDGX, until 2002 and 2003, respectively. The composite reflectivity product, commonly used to identify areas of convection, is a 1-km resolution gridded image extending 230 km from the radar site that indicates the strongest reflectivity detected at any altitude above each grid cell. Composite reflectivity is also advantageous in its ability to mitigate challenges associated with beam blockage in the Southern Appalachian Mountains; however, it also introduces several limitations, which are discussed in Section

3.2.3. Between 2005–2006 all WSR-88Ds received a signal processing upgrade that allowed the radar to detect reflectivity with greater precision. The effect of this upgrade on any temporal trends will be discussed in Section 3.3. Radar images for each site, generally available at ~5-min intervals when convection is present, were ordered chronologically and divided into consecutive 24-hr periods from 1200 UTC 1 May to 1200 UTC 1 October of each year.

Connected neighborhoods labeling was applied to grid cells with reflectivities of 40 dBZ or greater, a common reflectivity threshold for convection (e.g., Haberlie et al. 2015; Fabry et al. 2017), across all scans for each day. If gaps in radar coverage persisted for longer than 30 min, then the day was subdivided upon the coverage gap, and the labeling procedure was performed separately on each subdivision. In connected neighborhoods labeling, each convective grid cell (≥40 dBZ) is examined in three dimensions (x, y, t) to determine if any other cell in a 26-member neighborhood (a perfect 3x3x3 cube minus the center cell-of-interest) is also convective. The labeling technique extracts storms by expanding each group of spatiotemporally contiguous convective grid cells in all dimensions until no additional convective cells can be identified. Figure 3.2a-c illustrates a hypothetical example of the labeling process. For any redundant storms in regions of overlapping radar coverage, only the storm detected by the nearest radar, as shown by the polygons in Fig. 3.1, was retained.

For each storm, the time of first detection (measured in hours after 1200 UTC; TFD), duration (min; DUR), maximum reflectivity (dBZ; MAX REF), maximum size in a single image (number of grid cells; MAX SIZE), and solidity (SOL) were recorded. The solidity measure, a unitless ratio between 0–1, compares a storm's average size in each image to its maximum size in any single image, MAX SIZE. This ratio helps distinguish storms that were morphologically uniform across their entire lifetime (large solidity) from those that exhibited considerable inter-image changes in their spatial footprint (small solidity). These variables were recorded given their role in traditional storm mode definitions, and the use of similar measures in previous storm mode classification studies (e.g., Lakshmanan and Smith 2009; Miller et al. 2015c). The latitude and longitude of the storm's centroid in its first-detected radar scan was also recorded for use in constructing the spatial climatology.

A quality assurance and control procedure was implemented to improve the likelihood that each group of convective pixels represented a whole, legitimate convective event (i.e., remove ground clutter and partially detected events). "Storms" were removed from the dataset if one of the following five conditions applied: The storm (1) was ongoing at the beginning or end of a 24-hr period (or an intra-24-hr subdivision); (2) abutted the edge of a radar's spatial coverage domain; (3) persisted fewer than 30 min, a routine duration requirement (e.g., Lock and Houston 2013; Burghardt et al. 2014); (4) was first detected within a 10x10-grid-cell square centered on the radar site; or (5) was initially detected at a recurring first-detection location (first-detection centroid repeated ≥5 times) and never exceeded eight grid cells in MAX SIZE. Conditions 1 and 2 were designed to eliminate storms for which only partial data existed whereas conditions 3, 4, and 5 were meant to reduce the amount of suspected ground clutter in the dataset. In eliminating partially detected storms, many large, organized convective systems that spanned multiple WSR-88D coverage domains were discarded by condition 2. However, because the goal of this study is to document WFTs, relatively stationary storms, the removal of spatially expansive convective systems was desirable.

Condition 5 was based on the idea that the landscape features responsible for ground clutter are fixed and will recur within the dataset. Of the unique first-detection initiation centroids, 89.5% were never repeated and 0.2% repeated five or more times. Given that first-detection centroids of any repetition were uncommon within the dataset, first-detection centroids recurring ≥5 times were viewed with even greater skepticism. The distribution of MAX SIZEs for storms originating from these highly active first-detection points (Fig. 3.3) were disproportionately skewed towards small values, consistent with the appearance of ground clutter on radar. Condition 5 affected relatively few events, but was necessary to produce accurate graphic representations of the spatial climatology. The stipulations above yielded approximately 1.9 million viable storms.

Severe weather events (winds ≥ 26 m s^{-1}, hail ≥ 2.56 cm in diameter, or a tornado) from NCEI's *Storm Data* publication were paired with storms if the report's latitude and longitude coincided with any of a storm's constituent grid cells and the report occurred after its TFD and before its time of last detection. Though several studies have documented data quality concerns within *Storm Data*'s severe weather reports (e.g., Weiss et al. 2002; Trapp et al. 2006; Miller et al. 2016), these discrepancies were judged unlikely to influence the broad distinction between hazardous and non-hazardous WFTs. For instance, by only requiring that the report occur after first detection and before last detection, the influence of the report's uncertain timestamp (Williams et al. 1999) was minimized. However, spatial errors in *Storm Data* reports and/or unreported severe weather events may cause truly pulse thunderstorms to be classified as benign WFTs within the dataset. Overall, 91.0% (82,777 out of 90,955) of *Storm Data* reports were successfully paired with a convective reflectivity.

3.2.2 Designating weakly forced thunderstorms

Ward's clustering (Ward 1963) was applied to identify natural groupings of the five storm morphology metrics listed above among all of the thunderstorms in the dataset, and then assess the composite convective environments of each morphological grouping. Storms belonging to clusters with small, short-lived, diurnally driven characteristics which also formed in weakly sheared, unstable environments will be considered WFTs. Ward's clustering was selected because, unlike other hierarchical, agglomerative clustering techniques, it avoids the use of Euclidean distance to determine clusters. Instead, distance is expressed via the standardized total within-cluster error, which is proportional to the sum of the differences between each member of a cluster and the cluster's mean. The process begins with all storms as separate clusters, and iteratively combines the two groups whose merge will yield the new group with the smallest total within-cluster error of all the possible merges. Merging continues until a desired number of clusters is reached. Figure 3.2d-f depicts a simplified 2-d example (MAX SIZE and TFD only) using a small hypothetical dataset distributed similarly to the real dataset. Figure 3.2d shows each "storm" is plotted as its own cluster at the beginning of the procedure, and Fig. 3.2e depicts how Ward's method would have grouped the storms after several hundred iterations. Figure 3.2f illustrates a single step in the hypothetical clustering process from five to four groups. Ward's method merged the purple and green clusters from Fig. 3.2e because the new resulting cluster contains less total error than if, for instance, the green and blue clusters had been merged.

Given the dissimilar units of the spatial and temporal metrics, this Ward's method was conceptually more appropriate, and it yielded the most interpretable results among other methods tested. See Gong and Richman (1995) for a comparison of various clustering procedures and their application in climate science. The cluster analysis was performed until 10 clusters remained. Using fewer than 10 clusters overgeneralized some clusters while using more than 10 clusters yielded no appreciable insight toward intra-cluster variability. Hereafter, the ten Ward's clusters will be referenced as "storm types" and abbreviated "T1…T10" following the values shown in the "Type" column of Table 3.1[7].

The results of the cluster analysis (Table 3.1) indicate that Ward's clustering capably segregates the storms according to their spatial and temporal traits. However, because the definition of a WFT is intimately related to the storm environment, composite 1200 UTC soundings were generated at three approximately collocated radiosonde (http://esrl.noaa.gov/raobs/) and radar data collection sites (KBNA/KOHX, KFFC, and KTBW) along a diagonal transect through the center of the study area (Fig. 3.1) using the SHARPpy software package (Blumberg et al. 2017). Days at each site were stratified according to the thunderstorm type that contributed the largest total number of grid cells at that site on a given day (Table 3.2).

Figure 3.4 depicts composite wind profiles; Figs. 3.5–3.7 show full skewT-logP diagrams; and Tables 3.3–3.4 present kinematic and thermodynamic variables at each site, respectively. The parameters in Tables 3.3–3.4 were either selected due to their traditional

[7] The sequencing of the storm types was modified from its original output to improve the interpretability of the results.

association with storm organization [0–6-km shear, mixed-layer CAPE (MLCAPE), forecast surface-based CAPE (SBCAPE), low-level θ_e], or they were chosen to represent elements of the composite wind fields and storm morphology metrics that may not be captured by the other variables (0–8-km shear, 0–12-km max wind, 0–12-km mean wind, TPW).

When compared to the composite sounding metrics, seemingly minor differences between storm types correspond to appreciable variations in the convective environment. For instance, T7 is differentiated only by small decreases in MAX REF and MAX SIZE from T3, but formed in more stable, directionally sheared environments, and stronger flow environments at KBNA and KFFC. This comparison illustrates the proficiency of Ward's clustering to separate morphologically similar storms whose small, short-lived characteristics were likely related to weaker instability on days with stronger forcing rather than the stronger instability on days with weaker forcing. We do not expect that each storm type corresponds to a specific forcing mechanism, only that types with/without synoptic lifting mechanisms can be differentiated through their shear environments.

Based on guidance from Tables 3.1–3.4 and Fig. 3.4, T3, T4, and T5 were judged to best holistically represent WFTs in the Southeast U.S. due to their mostly short-lived, small, morphologically uniform, and diurnally driven storms in generally weak-shear, high-instability environments at the three transect points. Though T1 and T2 represent larger, stronger storms than the stereotypical WFT, upscale growth likely occurred in a relatively disorganized fashion without the aid of appreciable vertical wind shear. (See Fig. 3.8 for an example.) These storms, referenced at the beginning of Section 3.2, are consistent with the often multicell nature of WFTs (Miller and Mote 2017b). For the sake of simplicity and by necessity, the WFT categorizations above are generalized across the entire Southeast U.S. because only a handful of WSR-88Ds are collocated with radiosonde launch points. In total, 885,496 storms were classified as WFTs.

The synoptic patterns associated with WFT activity at KFFC, selected for its location in the center of the domain, were represented using the Earth Systems Research Laboratory's (ESRL) North American Regional Reanalysis (Mesinger et al. 2006) daily compositing tool (http://www.esrl.noaa.gov/psd/cgi-bin/data/narr/plotday.pl/). For each storm type, synoptic composites of 500-hPa vector wind, 850-hPa geopotential height, and total precipitable water (TPW) were generated. The first two fields will help establish the presence (or absence) of any synoptic-scale forcing whereas the third will indicate the moisture content of the atmosphere. These same variables have been previously used to discern disorganized thunderstorm environments (Miller et al. 2015c).

3.2.3 Limitations

In some cases, confident WFT/non-WFT classifications at one transect site might be less clear elsewhere in the domain; however, these cases represent a minority of the categorizations. For instance, T5 at KBNA (3.9% of all KBNA days) could be argued to represent a more organized kinematic environment whereas T8 at KTBW is debatably representative of a weak-shear, high-CAPE regime (<1% of KTBW days). More importantly, the most frequent storm types at each site are among the most stereotypical WFT environments. All three composite soundings for T2, T3, and T4, collectively comprising 64.6% of all thunderstorm days along the transect, depict stereotypical weak-shear, high-instability regimes. Further, the relative frequencies of the storm-type days, also obey regional climatological expectations. The kinematically active T6 days occur most frequently at the northernmost site along the transect and gradually decrease with southward extent. Similarly, the higher-moisture T1 and T2 days are most frequent at the KTBW coastal site, and decrease with northward extent toward the interior of the Southeast U.S.

This method of WFT identification was also complicated by the presence of storms with 40-dBZ composite reflectivities that appeared small, short-lived, diurnally driven, but were actually associated with a different process. For instance, bright-banding within areas of non-weakly forced precipitation, especially at greater distances from the radar, may have presented a similar morphological signature to a WFT. This is one reason that all 30 WSR-88D sites in the Southeast were included and that storms were tracked using observations from the nearest radar. Another safeguard was the exclusion of storms that ventured too close to edge of the radar's coverage domain. Figure 3.9a shows that nearly 100% of storms that qualified as WFTs possessed MAX REFs meeting or exceeding 50 dBZ. Even if bright banding did, in some cases, artificially bolster nonconvective reflectivities above the 40-dBZ limit, the storms appearing in the final WFT dataset almost certainly represented areas of convection according to most reflectivity-based definitions. [See Haberlie et al. (2015) for a thorough summary of such convection identification definitions.] However, when inspected via composite reflectivity, a WFT-like signature would have been noted. Because we did not individually inspect all >800,000 WFTs, nonconvective bright-banding-related echoes, elevated convection, and stratiform echo maxima may have infiltrated the dataset in some cases.

Similarly, areas of sporadic 40-dBZ reflectivity within a more organized and strongly forced mesoscale convective system might mimic the expected WFT morphology. Despite the measures taken to eliminate storm morphologies whose composite environments were too strongly forced (as inferred from vertical wind shear), some strongly forced convective structures may have circumvented the methodology. For instance, Fig. 3.9b shows the distribution of all 0–6-km wind shear values used to create the composite soundings at KFFC. Whereas the bulk of the distributions for the WFT clusters are similar to the composite wind fields, a few outliers are present. Figure 3.9c shows a radar image for one of the 0–6-km shear outliers from the T3 distribution (4 May 2002; 17.5 m s^{-1} 0–6-km shear). In this case, small areas of convection in a non-weakly forced complex mimicked the morphology of a WFT, and deceived the methodology. However, this situation is an outlier (Fig. 3.9b). Figure 3.9d shows an example radar image from the middle of the same T3 distribution (12 June 2010; 4.1 m s^{-1} 0–6-km shear) where the methodology capably captures WFTs. Future efforts might seek to improve upon these aspects of the classification methodology, particularly the "false positives" resulting from the use of composite reflectivity.

3.3 Results and discussion

3.3.1 Spatial and temporal distribution of WFT activity

Though the role of terrain in storm development is ultimately secondary to atmospheric processes, the following discussion leverages the large WFT sample size to identity underlying terrain influences on WFT first-detection patterns that become apparent when large-scale forcing is weak. (Section 3.3.2 will consider the synoptic-scale environments in more detail.) The general influence of landforms and terrain features in weakly forced regimes is well known, and the broad pattern of WFT activity shown in Fig. 3.10 is consistent with these features. Larger WFT first-detection densities sharply outline the Southeast U.S. coast, especially south of KMHX, reflecting the role of the heated land surface in building parcel instability and/or the efficiency of the sea breeze in initiating convection. WFTs are frequent over the Florida peninsula, coastal areas, and southern Appalachian Mountains where the mesoscale sea breeze circulation (e.g., Pielke 1974) or preferential orographic heating (e.g., Hallenbeck 1922) can trigger convection in the absence of large-scale dynamical support. WFT frequency also diminishes in the northern tier of the domain where jet stream dynamics would support organized convection more frequently.

Beyond these general patterns, Fig. 3.10a shows that the regional WFT climatology is more nuanced that what might be assumed. For instance, there is a slight reduction in WFT frequency within a transition region between higher frequencies along the coast and likewise high frequencies along the dotted line in Fig. 3.10b (marked “A”). Previous work, noting similar signatures with a Southeastern U.S. lightning climatology, attributes the increase in convection to preferential heating along the Atlantic fall line (Bentley and Stallins 2005), a geologic transition from the Piedmont region to the low-lying coastal plain. This southwest-to-northeast oriented topographic relief would favor surface heating by creating a more orthogonal angle of incidence for incoming radiation beginning as soon as the sun rises above the horizon. Previous research has found this type of topography to favor convection in weakly sheared environments (Miller et al. 2015b). Similarly, Sims and Raman (2016) show that differential heating along accompanying soil-type boundaries in this zone support thermal circulations that also aid convection. The slight reduction of WFT activity on the fringe of the fall line transition region may also be related to surface divergence resulting from gradual upslope flow toward the fall line, a result that can be partially observed in the simulations of surface convergence by Kirshbaum et al. (2015). This recent modeling study showed that even the near-negligible relief surrounding the interior Mississippi Valley was still responsible for a nearly 50% decrease in the incidence of convection over the Valley.

However, even within areas of generally increased frequency, the WFT climatology captures small, subtle minima. For instance, reduced WFT activity is noted over Lake Okeechobee, FL, and Lake Pontchartrain, LA, (marked “B” and “C” respectively) likely related to the stabilizing effect of the relatively cool water in comparison to the land surface temperature and/or surface divergence resulting from the lake breeze (Frank et al. 1967). On an even smaller scale, the French Broad River valley in western North Carolina (marked “D”), the Tennessee River valley in East Tennessee (marked “E”), and the Hiwassee and Notteley River valleys along the North Carolina-Georgia state line (marked “F”) are also coincident with a decrease in WFT activity. Such patterns were also noted in a high-resolution study of convective cloud formation in satellite imagery with their cause attributed to divergent flow at the surface resulting from the upslope component of the mountain-valley circulation (Gibson and Vonder Haar 1990). Other features of the WFT climatology support recent work that documents a decrease in radar echoes over the Mississippi Delta (marked “G”) (Kirshbaum et al. 2015) and a relative maximum in unorganized precipitation offshore of the North Carolina coast (marked “H”) (Rickenbach et al. 2015).

Two additional large relative minima are also apparent in the climatology which are not readily explained: east-central Mississippi and west-central Alabama (marked “I”) and the broad corridor from northeast Georgia (marked “J”) stretching northeast to central North Carolina. The first relative void is discernible in Gibson and Vonder Haar’s (1990) analysis of both shallow and deep satellite-derived convective cloud frequency. They assert that the feature is not a result of random vertical motions, but seeing no viable terrain features that might contribute to the signature, they only loosely speculate that this minimum is tied to land use/land cover patterns. The same minima is also clearly noted in a similar, but more recent, study of convective cloud activity by Gambill and Mecikalski (2011). Though the purpose of their work was to investigate ties between convective clouds and land cover type, the analysis is conducted on an aggregate level over the whole Southeast U.S., and does not consider this minimum specifically.

Similarly, the relative void roughly paralleling the Southern Appalachians from northeast Georgia to central North Carolina possesses no obvious terrain or land cover heterogeneities. Yet, the same minima can be observed in radar analyses of convective frequency by both Outlaw and Murphy (2000) and Fabry et al. (2017). Rickenbach et al. (2015) also document this feature; however, they note that convection tends to fill the void later in the day compared to its surroundings, rather than be altogether absent. The steep relief posed by the Appalachian Mountains, though likely suppressing convection in the immediately surrounding flat terrain through surface divergence associated with the valley-mountain circulation, would seem unlikely to suppress WFT activity >100 km to the south. One initial hypothesis is that the slightly larger proportion of cropland in this region, a land cover type associated with decreases in convective cloud percentage by Gambill and

Mecikalski (2011), may discourage WFT activity. Alternatively, stabilized air formed by convection within the active WFT regions on either side may lead to weak subsidence over the minimum. Further research is required to more directly establish which, if either, of these processes contribute to the first-detection minima.

Consistent with expectations, Fig. 3.11a shows that WFTs are most common in July and August with smaller frequencies in May and September. Straddling the core of the warm season, these months represent transition periods from spring to summer and summer to fall when mid-latitude westerly flow strengthens into the cold season and instability is weaker. Clear interannual variability in the number of WFTs is also been observed over the past 15 years (Fig. 3.11b) with annual deviations near 20% in some years (max negative anomaly, -19.8% in 2002; max positive anomaly, 20.7% in 2007). The visual trend in the number of WFTs suggests a possible shift toward more numerous WFTs since 2006. However, the WFT-frequency transition seemingly corresponds to a WSR-88D processing upgrade (Patel and Macemon 2004). The increased data precision available post-2006 would allow for more precise detection of 40-dBZ echoes, leading previously non-qualifying cells to perhaps satisfy the convective reflectivity threshold. The possible post-2006 shift in WFT activity should be treated with skepticism until future research can examine the effects of data quality improvements in greater detail.

3.3.2 Synoptic patterns associated with WFT activity

Figure 3.12 characterizes the 500-hPa winds, 850-hPa geopotential heights, and TPWs for the same dates used to compute the KFFC composite soundings in Section 3.2.2. Figures 3.13–3.14 depict the 25th and 75th percentiles for the two scalar fields, 850-hPa height and TPW.) Note that these days may not have been conducive for WFTs over the whole Southeast; rather, they were tied to WFT-favorable conditions in the polygon containing KFFC in Fig. 3.1. The composites reveal two modes of variability that favor WFT activity near the center of the study domain: (1) the expansion of anticyclonic flow related to the Bermuda High from the east and (2) the intrusion of high pressure over the Southern Plains from the west. T1, T2, and T3 are representative of the first mode with an anticyclonic circulation over the Bahamas expanding across the southern tier of the Southeast. Meanwhile, T4 and T5 correspond to the second mode with mid-level ridging over the Central U.S. placing KFFC in a region of northwesterly 500-hPa flow.

Closer to the surface, the influence of the Bermuda High is more apparent. The 850-hPa geopotential heights show that all five WFT clusters are characterized by the intrusion of the Bermuda High into the southeastern U.S. Similar 850-hPa height patterns have been found on days characterized by lightning-inferred WFT activity in southwest Virginia (Miller et al. 2015c) as well as days associated with urban-initiated convection in Atlanta, GA (Bentley et al. 2012a). On T3 days, the westward expansion of the Bermuda High is similar to the other WFT clusters (Fig. 3.12); however, its strength is weaker over the Southeast, with the 1564-m contour situated entirely over the western Atlantic. A similar regime to T3, the largest WFT cluster by number of storms (Table 3.1), was identified by Diem (2013) as being conducive to a disproportionate number of rainfall days in the Atlanta metropolitan area. On larger time scales, the position of the Bermuda High may exercise a control on the frequency of disorganized convection in the Southeast and contribute to the interannual variability seen in Fig. 3.11b. The 850-hPa height composites (Fig. 3.12) may represent a middle ground whereby disorganized convection dominates. If the Bermuda High advances too far westward all convection is suppressed, and if it drifts too far eastward, meridional flow develops and larger, more productive precipitation systems forms (Stahle and Cleaveland 1992).

Within each synoptic mode of variability, moisture availability appears to exercise an additional influence on WFT frequency and size. When high pressure from the western Atlantic dominated (mode 1), storms grew larger and were longer-lived on the most moist subset of these days (T1 and T2). In contrast, when TPW values were smaller yet the circulation pattern remained unchanged (T3), storms were more numerous, but remained smaller and shorter-lived. The same is true when high pressure from the Southern Plains encroached over the Southeast (mode 2). T4 days, with higher TPW than T5 days, were associated with fewer, but larger and longer-lived, storms.

Interactions between moisture and convection are complex, and readers interested in a more comprehensive account of the relationship are directed toward Sherwood et al. (2010) and James and Markowski (2010). However, there are some basic, intuitive relationships that may help explain the formation of the larger storms in the higher-TPW environments. When present at the surface, higher humidity promotes convection by increasing CAPE, and when moisture extends above the surface, it can mitigate the stabilizing effect of entrainment (e.g., Jorgensen and LeMone 1988). Table 3.4 shows evidence of the former in that KFFC's composite sounding CAPE calculations mirror the relative increases/decreases of TPW. However, the differences in MAX SIZE and DUR between T2 and T3, both demonstrated to form in similar synoptic regimes, are very large, whereas the difference in forecast SBCAPE is only roughly 50 J kg^{-1}. Such a relatively minor difference in instability is unlikely to affect such a dramatic shift in storm morphology.

In both the lower and mid-troposphere, higher humidity has been tied to increased waterloading in thunderstorms by reducing evaporation due to entrainment (Wissmeier and Goler 2009) though this relationship is also dependent on CAPE (James and Markowski 2010). Because radar reflectivity is proportional to the size and number of hydrometeors, larger or more abundant hydrometeors would favor thunderstorms reaching the 40-dBZ threshold used to define areas of convection in Section 3.2.1, driving increases in MAX SIZE and possibly DUR. Table 3.5 shows that this is indeed the case for the KFFC composite soundings. On T1 and T2 days, associated with the largest and longest-lived WFTs, mean mixing ratios between 1000–850 hPa are only roughly 3% larger than on T3, T4, and T5 days. However, in the low-to-mid troposphere (850–500 hPa) the difference in mean mixing ratio increases to 21%. This result is consistent with James and Markowski (2010) who found that in their 1500-J kg^{-1} CAPE simulations, the duration of convection was extremely sensitive to mid-level RH with lower RHs suppressing convective intensity and duration.

3.3.3 Characteristics of pulse thunderstorms

Constituting just 0.6% of all WFTs, pulse thunderstorms represented a very small fraction of the dataset. However, this small subset is disproportionately concentrated among the two least frequent storm types. Though T1 and T2 only account for 2% of all WFTs, 66% all pulse thunderstorms are associated with these two groups (Table 3.1). In contrast, only 0.03% of pulse thunderstorms are associated with T3, the most frequent WFT type. Table 3.6 compares the relative spatial and temporal storm metrics of pulse thunderstorms and all WFTs. Pulse storms are considerably larger and longer-lived suggesting that most WFT severe weather episodes occur with cells that are members of a larger disorganized group. This finding is consistent with previous accounts of pulse thunderstorm morphologies described at the beginning of Section 3.2.

Figure 3.15 shows the first-detection locations of all pulse thunderstorms during the 15-yr study period. The patterns shown in this image must be interpreted with caution given that previous research has tied the frequency of severe weather reports to population density and National Weather Service severe weather warning issuance (Weiss et al. 2002). Nonetheless, when compared to the annual first-detection density of all WFTs (Fig. 3.10a), the spatial distribution of pulse thunderstorms shows clear departures from the broader set of all WFTs. The Florida peninsula and Gulf Coast, maxima of WFT first-detection density, are relatively inactive areas of pulse thunderstorm activity. Alternatively, the regions of greatest pulse thunderstorm first-detection density are displaced further north in the domain, namely the western Carolinas and western Virginia along the Blue Ridge mountains. This region was also identified by Harrison and Karstens (2016) as a local maximum of NWS severe weather products that also referenced slower storms speeds than their neighboring regions. The reason for the concentration of pulse thunderstorm first-detections in this region is not immediately apparent. Variations in the thermodynamic storm environment, such as the height of the freezing level, may favor severe convection further north in the domain.

As discussed in Section 3.3.2, T1 and T2 days demonstrate similar in 850-hPa heights to the other WFT days, but are generally differentiated by greater forecast SBCAPE

(Table 3.4) and increased moisture (Fig. 3.12). Though the concentration of pulse thunderstorms in these two clusters may be reflexively attributed to instability, the SBCAPE differences in the composite soundings do not appear large enough to account for the concentration of pulse thunderstorms in T1 and T2 versus T3, T4, and T5. Once again, the more pronounced variations in moisture, particularly in the mid-levels, could offer an alternative explanation. Field observations during the Cirrus Regional Study of Tropical Anvils and Cirrus Layers-Florida Area Cirrus Experiment (CRYSTAL-FACE) found that a 20% increase in mean mixing ratio between 750 and 500 hPa corresponded to a 1-km increase in cloud top penetration even when CAPE remained unchanged (Sherwood et al. 2004). This increase is nearly identical to the 21% greater T1 and T2 mid-level mixing ratios found in Section 3.3.2. Cloud top heights often serve as a proxy for convective intensity (e.g., Adler and Negri 1988; Bedka 2011). Thus, the association of pulse thunderstorms with higher-TPW clusters may be partially explained by greater mid-level moisture favoring higher cloud tops and, by extension, stronger updrafts.

3.4 Conclusion

Fifteen years of radar observations between 2001–2015 in the Southeast U.S. were mined for instances of spatiotemporally contiguous convective echoes, of which 885,496 were deemed to represent WFTs. Pronounced spatial variations in WFT and pulse thunderstorm first-detection density were evident even in a region where WFTs are generally described as ubiquitous. However, the spatial focus of pulse thunderstorms, the Blue Ridge mountains, was significantly displaced from the areas of greatest all-inclusive WFT activity: the Florida peninsula and Gulf Coast.

WFT environments near the center of the domain formed via two distinct modes of variability. Both modes were characterized by two centers of anticyclonic flow in the mid-levels but differed in the direction from which the dominant high-pressure encroached upon the Southeast. With the first mode, the Bermuda High circulation expands westward over the Florida Peninsula whereas with the second, anticyclonic 500-hPa winds shift east from the Southern Plains region placing the Southeast in a region of weak, northwest flow. In both modes, greater moisture availability, rather than instability, was associated with larger, longer-lasting WFTs, which were also responsible for the majority of severe weather reports.

Combining the spatial pattern of WFT development with the links to larger-scale features, forecasts of both the location and severity of WFTs may be improved. With a 15-yr WFT dataset and its derived climatology now available, operational forecasters can begin to better recognize the moisture and circulation patterns most conducive to WFTs, particularly pulse thunderstorms. Forecasters may begin considering whether to tailor the probability of precipitation in weakly forced environments based on the local, presumably landscape-driven, effects depicted in Fig. 3.10. This is also a valuable result for city planners tasked with siting infrastructure that may be adversely impacted by thunderstorm activity (e.g., an airport, sports stadium), or alternatively, may desire preferential storm activity (e.g., a reservoir). Future research needs to examine the near-storm environment of WFTs, especially pulse thunderstorms, in a much more comprehensive and statistically robust manner. In this paper, the parameters presented were derived from a composite sounding rather than a distribution of many model-derived proxy soundings, an approach future researchers might consider.

3.5 Acknowledgments

The authors thank Dr. Mace Bentley and three anonymous reviewers for their helpful comments on earlier versions of this manuscript.

3.6 References

Adler, R. F., and A. J. Negri, 1988: A satellite infrared technique to estimate tropical convective and stratiform rainfall. *J. Appl. Meteor.*, **27,** 30–51, doi:10.1175/1520-0450(1988)027<0030:ASITTE>2.0.CO;2.

Ashley, W. S., and C. W. Gilson, 2009: A reassessment of U.S. lightning mortality. *Bull. Amer. Meteor. Soc.*, **90,** 1501–1518, doi:10.1175/2009BAMS2765.1.

Ashley, W. S., M. L. Bentley, and J. A. Stallins, 2012: Urban-induced thunderstorm modification in the Southeast United States. *Climatic Change*, **113,** 481-498, doi:10.1007/s10584-011-0324-1.

Bedka, K. M., 2011: Overshooting cloud top detections using MSG SEVIRI Infrared brightness temperatures and their relationship to severe weather over Europe. *Atmos. Res.*, **99,** 175–189, doi:http://dx.doi.org/10.1016/j.atmosres.2010.10.001.

Bentley, M. L., and J. A. Stallins, 2005: Climatology of cloud-to-ground lightning in Georgia, USA, 1992–2003. *Int. J. Climatol.*, **25,** 1979–1996, doi:10.1002/joc.1227.

Bentley, M. L., J. A. Stallins, and W. S. Ashley, 2012: Synoptic environments favourable for urban convection in Atlanta, Georgia. *Int. J. Climatol.*, **32,** 1287-1294, doi:10.1002/joc.2344.

Bluestein, H. B., 2013: *Severe Convective Storms and Tornadoes: Observations and Dynamics.* Springer, 456 pp.

Blumberg, W. G., K. T. Halbert, T. A. Supinie, P. T. Marsh, R. L. Thompson, and J. A. Hart, 2017: SHARPpy: An open source sounding analysis toolkit for the atmospheric sciences. *Bull. Amer. Meteor. Soc.*, **98,** 1625–1636, doi:10.1175/BAMS-D-15-00309.1.

Bruick, Z. S., and C. D. Karstens, 2017: An investigation of local and national NWS warning outbreaks for severe convective events. *J. Operational Meteor.*, **5,** 14-25, doi:http://dx.doi.org/10.15191/nwajom.2017.0502.

Burgess, D. W., and L. R. Lemon, 1990: Severe thunderstorm detection by radar. *Radar in Meteorology*, D. Atlas, Ed., Springer, 619–647.

Burghardt, B. J., C. Evans, and P. J. Roebber, 2014: Assessing the predictability of convection initiation in the High Plains using an object-based approach. *Wea. Forecasting*, **29,** 403–418, doi:10.1175/WAF-D-13-00089.1.

de Szoeke, S. P., J. B. Edson, J. R. Marion, C. W. Fairall, and L. Bariteau, 2014: The MJO and air–sea interaction in TOGA COARE and DYNAMO. *J. Climate*, **28,** 597-622, doi:10.1175/JCLI-D-14-00477.1.

Diem, J. E., 2013: Influences of the Bermuda High and atmospheric moistening on changes in summer rainfall in the Atlanta, Georgia region, USA. *Int. J. Climatol.*, **33,** 160–172, doi:10.1002/joc.3421.

Diffenbaugh, N. S., M. Scherer, and R. J. Trapp, 2013: Robust increases in severe thunderstorm environments in response to greenhouse forcing. *Proc. Natl. Acad. Sci.*, **110,** 16361–16366, doi:10.1073/pnas.1307758110.

Fabry, F., 2006: The spatial variability of moisture in the boundary layer and its effect on convection initiation: Project-long characterization. *Mon. Wea. Rev.*, **134,** 79–91, doi:10.1175/MWR3055.1.

Fabry, F., V. Meunier, B. Puigdomènech Treserras, A. Cournoyer, and B. Nelson, 2017: On the climatological use of radar data mosaics: Possibilities and challenges. *Bull. Amer. Meteor. Soc.*, **In press**, doi:10.1175/BAMS-D-15-00256.1.

Ford, T. W., S. M. Quiring, O. W. Frauenfeld, and A. D. Rapp, 2015: Synoptic conditions related to soil moisture-atmosphere interactions and unorganized convection in Oklahoma. *J. Geophys. Res.: Atmos.*, **120,** 11519–11535, doi:10.1002/2015JD023975.

Frank, N. L., P. L. Moore, and G. E. Fisher, 1967: Summer shower distribution over the Florida Peninsula as deduced from digitized radar data. *J. Appl. Meteor.*, **6,** 309–316, doi:10.1175/1520-0450(1967)006<0309:SSDOTF>2.0.CO;2.

Frye, J. D., and T. L. Mote, 2009: Convection initiation along soil moisture boundaries in the southern Great Plains. *Mon. Wea. Rev.*, **138,** 1140–1151, doi:10.1175/2009MWR2865.1.

Gambill, L. D., and J. R. Mecikalski, 2011: A satellite-based summer convective cloud frequency analysis over the southeastern United States. *J. Appl. Meteor. Climatol.*, **50,** 1756–1769.

Gibson, H. M., and T. H. Vonder Haar, 1990: Cloud and convection frequencies over the southeast United States as related to small-scale geographic features. *Mon. Wea. Rev.*, **118,** 2215–2227.

Gong, X., and M. B. Richman, 1995: On the application of cluster analysis to growing season precipitation data in North America east of the Rockies. *J. Climate*, **8,** 897–931.

Guillot, E. M., T. M. Smith, V. Lakshmanan, K. L. Elmore, D. W. Burgess, and G. J. Stumpf, 2008: Tornado and severe thunderstorm warning forecast skill and its relationship to storm type. *24th Int. Conf. Interactive Information Processing Systems for Meteor., Oceanogr., and Hydrol.*, New Orleans, LA, American Meteorological Society. [Available online at http://ams.confex.com/ams/pdfpapers/132244.pdf.]

Haberlie, A. M., W. S. Ashley, and T. J. Pingel, 2015: The effect of urbanisation on the climatology of thunderstorm initiation. *Quart. J. Roy. Meteorol. Soc.*, **141,** 663–675.

Hallenbeck, C., 1922: The topographic thunderstorm. *Mon. Wea. Rev.*, **50,** 284–287.

Harrison, D. R., and C. D. Karstens, 2016: A climatology of operational storm-based warnings: A geospatial analysis. *Wea. Forecasting*, **32,** 47–60, doi:10.1175/WAF-D-15-0146.1.

Ingram, K. T., K. Dow, L. Carter, and J. Anderson, Eds., 2013: *Climate of the Southeast United States: Variability, Change, Impacts, and Vulnerability*. Island Press.

James, R. P., and P. M. Markowski, 2010: A numerical investigation of the effects of dry air aloft on deep convection. *Mon. Wea. Rev.*, **138,** 140–161, doi:10.1175/2009MWR3018.1.

Johnson, R. H., T. M. Rickenbach, S. A. Rutledge, P. E. Ciesielski, and W. H. Schubert, 1999: Trimodal characteristics of tropical convection. *J. Climate*, **12,** 2397–2418, doi:10.1175/1520-0442(1999)012<2397:TCOTC>2.0.CO;2.

Jorgensen, D. P., and M. A. LeMone, 1988: Vertical velocity characteristics of oceanic convection. *J. Atmos. Sci.*, **46,** 621–640, doi:10.1175/1520-0469(1989)046<0621:VVCOOC>2.0.CO;2.

Kirshbaum, D. J., F. Fabry, and Q. Cazenave, 2015: The Mississippi Valley convection minimum on summer afternoons: Observations and numerical simulations. *Mon. Wea. Rev.*, **144,** 263–272, doi:10.1175/MWR-D-15-0238.1.

Lackmann, G., 2011: *Midlatitude Synoptic Meteorology*. 1 ed. American Meteorological Society, 345 pp.

Lakshmanan, V., and T. Smith, 2009: Data mining storm attributes from spatial grids. *J. Atmos. Oceanic Technol.*, **26,** 2353–2365, doi:10.1175/2009jtecha1257.1.

Lee, T., and Coauthors, 2016: An observational Study of convection initiation under quiescent conditions in the Southeastern United States. Preprints. *Annual Meeting of the American Meteorological Society*, New Orleans, LA, American Meteorological Society, 6A3. [Available online at https://ams.confex.com/ams/96Annual/webprogram/Paper282669.html.]

Lock, N. A., and A. L. Houston, 2013: Empirical examination of the factors regulating thunderstorm initiation. *Mon. Wea. Rev.*, **142,** 240–258, doi:10.1175/MWR-D-13-00082.1.

Markowski, P., and Y. Richardson, 2010: *Mesoscale Meteorology in Midlatitudes.* 1 ed. Wiley-Blackwell, 407 pp.

Mesinger, F., and Coauthors, 2006: North American regional reanalysis. *Bull. Amer. Meteor. Soc.*, **87,** 343–360, doi:10.1175/bams-87-3-343.

Miller, P. W., and T. L. Mote, 2017: Standardizing the definition of a "pulse" thunderstorm. *Bull. Amer. Meteor. Soc.*, **98,** 905–913, doi:http://dx.doi.org/10.1175/BAMS-D-16-0064.1.

Miller, P. W., A. Ellis, and S. Keighton, 2015a: Spatial distribution of lightning associated with low-shear thunderstorm environments in the central Appalachians region. *Phys. Geography*, **36,** 127–141, doi:http://dx.doi.org/10.1080/02723646.2015.1011257.

——, 2015b: A preliminary assessment of using spatiotemporal lightning patterns for a binary classification of thunderstorm mode. *Wea. Forecasting*, **30,** 38–56, doi:10.1175/WAF-D-14-00024.1.

Miller, P. W., A. W. Black, C. A. Williams, and J. A. Knox, 2016: Quantitative assessment of human wind speed overestimation. *J. Appl. Meteor. Climatol.*, **55,** 1009–1020, doi:10.1175/JAMC-D-15-0259.1.

Mote, T. L., M. C. Lacke, and J. M. Shepherd, 2007: Radar signatures of the urban effect on precipitation distribution: a case study for Atlanta, Georgia. *Geophys. Res. Lett.*, **34,** 1–4, doi:10.1029/2007GL031903.

Murphy, M. S., and C. E. Konrad, 2005: Spatial and temporal patterns of thunderstorm events that produce cloud-to-ground lightning in the interior southeastern United States. *Mon. Wea. Rev.*, **133,** 1417–1430.

Niyogi, D., and Coauthors, 2010: Urban modification of thunderstorms: An observational storm climatology and model sase study for the Indianapolis urban region. *J. Appl. Meteor. Climatol.*, **50,** 1129–1144, doi:10.1175/2010JAMC1836.1.

Outlaw, D. E., and M. P. Murphy, 2000: A radar-based climatology of July convective initiation in Georgia and surrounding area. NWS. Eastern Region Technical Attachment No. 2000-04, 24 pp. [Available online at http://www.weather.gov/media/erh/ta2000-04.pdf.]

Patel, N., and R. W. Macemon, 2004: NEXRAD Open Radar Data Acquisition (ORDA) signal processing & signal path. Preprints. *20th International Conference on Interactive Information and Processing Systems (IIPS) for Meteorology*, *Oceanography, and Hydrology*, Seattle, WA, Amer. Meteor. Soc., 5.4. [Available online at https://ams.confex.com/ams/pdfpapers/70926.pdf.]

Pielke, R. A., 1974: A three-dimensional numerical model of the sea breezes over South Florida. *Mon. Wea. Rev.*, **102,** 115–139, doi:10.1175/1520-0493(1974)102<0115:ATDNMO>2.0.CO;2.

Rickenbach, T. M., R. Nieto-Ferreira, C. Zarzar, and B. Nelson, 2015: A seasonal and diurnal climatology of precipitation organization in the southeastern United States. *Quart. J. Roy. Meteorol. Soc.*, **141,** 1938–1956, doi:10.1002/qj.2500.

Schumacher, C., and R. A. Houze, 2003: The TRMM precipitation radar's view of shallow, isolated rain. *J. Appl. Meteor.*, **42,** 1519–1524, doi:10.1175/1520-0450(2003)042<1519:TTPRVO>2.0.CO;2.

Senkbeil, J. C., M. E. Saunders, and B. Taylor, 2017: Changes in summer weather type frequency in Eastern North America. *Annals of the American Association of Geographers*, 1–17, doi:10.1080/24694452.2017.1295839.

Shepherd, J. M., 2005: A review of current investigations of urban-induced rainfall and recommendations for the future. *Earth Interact.*, **9,** 1–27, doi:10.1175/EI156.1.

Sherwood, S. C., P. Minnis, and M. McGill, 2004: Deep convective cloud-top heights and their thermodynamic control during CRYSTAL-FACE. *Journal of Geophysical Research: Atmospheres (1984–2012)*, **109,** 1–11, doi:10.1029/2004JD004811.

Sherwood, S. C., R. Roca, T. M. Weckwerth, and N. G. Andronova, 2010: Tropospheric water vapor, convection, and climate. *Reviews of Geophysics*, **48,** 1–29, doi:10.1029/2009RG000301.

Sims, A. P., and S. Raman, 2016: Interaction between two distinct mesoscale circulations during summer in the coastal region of eastern USA. *Boundary-Layer Meteorology*, **160,** 113–132, doi:10.1007/s10546-015-0125-6.

Stahle, D. W., and M. K. Cleaveland, 1992: Reconstruction and analysis of spring rainfall over the Southeastern U.S. for the past 1000 years. *Bull. Amer. Meteor. Soc.*, **73,** 1947-1961, doi:10.1175/1520-0477(1992)073<1947:RAAOSR>2.0.CO;2.

Trapp, R. J., D. M. Wheatley, N. T. Atkins, R. W. Przybylinski, and R. Wolf, 2006: Buyer beware: Some words of caution on the use of severe wind reports in postevent assessment and research. *Wea. Forecasting*, **21,** 408–415, doi:http://dx.doi.org/10.1175/WAF925.1.

Ward, J. H., 1963: Hierarchical grouping to optimize an objective function. *Journal of the American Statistical Association*, **58,** 236–244, doi:10.1080/01621459.1963.10500845.

Weisman, M. L., and J. B. Klemp, 1982: The dependence of numerically simulated convective storms on vertical wind shear and buoyancy. *Mon. Wea. Rev.*, **110,** 504–520, doi:10.1175/1520-0493(1982)110<0504:tdonsc>2.0.co;2.

Weiss, S. J., J. Hart, and P. Janish, 2002: An examination of severe thunderstorm wind report climatology: 1970–1999. Preprints. *21st Conf. Severe Local Storms*, San Antonio, TX, American Meteorological Society, 11B.2. [Available online at https://ams.confex.com/ams/SLS_WAF_NWP/techprogram/paper_47494.htm.]

Williams, E., and Coauthors, 1999: The behavior of total lightning activity in severe Florida thunderstorms. *Atmos. Res.*, **51,** 245–265, doi:10.1016/s0169-8095(99)00011-3.

Wissmeier, U., and R. Goler, 2009: A comparison of tropical and midlatitude thunderstorm evolution in response to wind shear. *J. Atmos. Sci.*, **66,** 2385–2401, doi:10.1175/2009JAS2963.1.

Ye, H., E. J. Fetzer, S. Wong, and B. H. Lambrigtsen, 2017: Rapid decadal convective precipitation increase over Eurasia during the last three decades of the 20th century. *Science Advances*, **3**, doi:10.1126/sciadv.1600944.

Table 3.1. Counts of total and severe storms grouped into each of the 10 types and medians of the radar-derived metrics used to categorize them (TFD: time of first-detection in hours after 1200 UTC; DUR: duration in min; MAX REF: maximum composite reflectivity in dBZ; MAX SIZE: largest number of grid cells in any single image; SOL: solidity, a unitless measure of morphological consistency). When applicable, the interquartile range is shown in parenthesis. WFT types are bolded.

Type	Storms	Severe storms	TFD	DUR	MAX REF*	MAX SIZE	SOL
1	**2,456**	**652**	**6.86 (5.09)**	**392 (162)**	**65 (5)**	**1811 (822)**	**0.43 (0.09)**
2	**35,972**	**2,907**	**7.86 (5.64)**	**248 (126)**	**60 (5)**	**496 (312)**	**0.45 (0.09)**
3	**591,647**	**190**	**7.67 (5.29)**	**60 (44)**	**50 (5)**	**40 (40)**	**0.51 (0.08)**
4	**86,938**	**1,400**	**8.55 (4.11)**	**88 (55)**	**60 (0)**	**88 (85)**	**0.52 (0.08)**
5	**168,483**	**229**	**8.09 (3.65)**	**47 (21)**	**55 (0)**	**34 (26)**	**0.63 (0.07)**
6	71,382	1,064	9.34 (9.27)	178 (63)	55 (5)	188 (141)	0.48 (0.10)
7	260,762	50	7.66 (6.68)	41 (19)	45 (0)	25 (31)	0.52 (0.11)
8	269,382	14	5.80 (4.61)	41 (17)	50 (0)	22 (18)	0.63 (0.08)
9	177,578	6	19.22 (4.27)	53 (39)	50 (5)	33 (37)	0.49 (0.08)
10	212,454	5	18.98 (4.53)	45 (24)	50 (5)	25 (23)	0.62 (0.09)

*Given the limited precision of the composite reflectivity product, MAX REFs often congregated around discrete values yielding a narrow interquantile range.

Table 3.2. Number of 1200 UTC soundings categorized by prevalent storm type for KBNA, KFFC, and KTBW. WFT types are bolded.

Type	KBNA	KFFC	KTBW
All	2,275	2,275	2,279
1	**36**	**56**	**160**
2	**343**	**423**	**790**
3	**372**	**387**	**556**
4	**158**	**173**	**97**
5	**58**	**56**	**21**
6	241	249	322
7	99	81	53
8	38	29	16
9	85	85	17
10	65	65	46
No storm	780	743	201

Table 3.3. Kinematic parameters (m s^{-1}) of KBNA, KFFC, and KTBW 1200 UTC composite soundings for each storm type. WFT types are bolded. In several cases, an appreciable increase in the strength of the mid-latitude westerlies occurred just above the 6-km level traditionally used to calculate bulk wind shear. Consequently, shear was calculated over the 0–8-km layer which can also help infer the organization of deep moist convection (Markowski and Richardson 2010, p. 201).

	KBNA				KFFC				KTBW			
Type	0–6-km Shear	0–8-km Shear	0–12-km Max Wind	0–12-km Mean Wind	0–6-km Shear	0–8-km Shear	0–12-km Max Wind	0–12-km Mean Wind	0–6-km Shear	0–8-km Shear	0–12-km Max Wind	0–12-km Mean Wind
1	**6.1**	**6.2**	**7.9**	**5.0**	**4.3**	**5.1**	**7.2**	**3.0**	**2.1**	**2.6**	**4.6**	**1.2**
2	**7.2**	**8.7**	**12.8**	**6.1**	**4.3**	**5.1**	**8.8**	**3.6**	**2.4**	**3.1**	**4.8**	**1.3**
3	**7**	**8.7**	**12.8**	**5.8**	**4.7**	**6.2**	**9.4**	**3.7**	**2.9**	**3.6**	**4.8**	**1.7**
4	**5.8**	**6.7**	**11.1**	**4.6**	**4.3**	**5.7**	**8.3**	**3.7**	**3.2**	**5.1**	**9.3**	**1.1**
5	**6.6**	**9.3**	**11.9**	**4.7**	**3.2**	**5.1**	**9.6**	**3.2**	**4.3**	**7.2**	**12.8**	**2.7**
6	7.7	9.3	14.3	6.4	6	7.7	11.6	5.0	3	4.1	6.8	1.4
7	11	13.4	19.4	7.7	8.2	10.8	16.5	6.1	3.8	6.2	12.3	2.8
8	10.8	14.4	20.2	7.5	4.9	7.7	13.6	3.1	7.8	8.7	11.1	2.8
9	8.7	11.8	18.4	5.6	5.4	8.7	15.4	3.0	3.4	4.6	10.1	1.1
10	10.6	12.9	18.4	7.7	7.9	9.8	13.5	5.8	4.1	5.7	10.1	2.1

Table 3.4. Thermodynamic and moisture parameters of KBNA, KFFC, and KTBW 1200 UTC composite soundings for each storm type. Mean θ_e is calculated over the 1000–850-hPa layer, and MLCAPE was calculated using the lowest 100 hPa. WFT types are bolded.

	KBNA				KFFC				KTBW			
Type	Mean θ_e (K)	MLCAPE (J kg^{-1})	Forecast SBCAPE (J kg^{-1})	TPW (mm)	Mean θ_e (K)	MLCAPE (J kg^{-1})	Forecast SBCAPE (J kg^{-1})	TPW (mm)	Mean θ_e (K)	MLCAPE (J kg^{-1})	Forecast SBCAPE (J kg^{-1})	TPW (mm)
1	**339.8**	**518**	**1,438**	**39.9**	**343.0**	**562**	**1,585**	**40.6**	**343.4**	**562**	**1,530**	**44.2**
2	**340.0**	**408**	**1,301**	**38.6**	**341.9**	**365**	**1,214**	**39.4**	**344.2**	**833**	**1,870**	**43.7**
3	**338.9**	**203**	**972**	**36.8**	**340.5**	**289**	**1,176**	**36.1**	**343.2**	**579**	**1,494**	**41.7**
4	**339.9**	**499**	**1,387**	**35.3**	**341.1**	**357**	**1,121**	**36.1**	**340.1**	**726**	**1,703**	**36.6**
5	**342.0**	**205**	**789**	**34.3**	**341.7**	**283**	**1,006**	**32.3**	**337.1**	**419**	**1,284**	**32.8**
6	338.1	218	1,006	36.6	339.0	211	973	35.8	343.0	561	1,455	41.4
7	330.9	0	192	34.5	336.6	66	723	37.1	344.0	142	1,031	40.9
8	332.3	0	383	32.8	336.0	24	558	34.3	338.8	264	1,099	35.1
9	328.4	0	0	27.2	330.6	0	32	26.9	335.1	0	505	29.7
10	329.8	0	91	29.2	334.5	0	391	29.7	339.7	151	821	31.2

Table 3.5. Mean humidity measures for both the lower (1000–850 hPa) and middle (850–500 hPa) troposphere from KFFC's composite soundings.

	1000–850-hPa		**850–500-hPa**	
Type	**RH (%)**	**w (g kg^{-1})**	**RH (%)**	**w (g kg^{-1})**
1	77	13.3	69	5.77
2	79	13.1	68	5.60
3	80	12.9	62	4.87
4	74	12.7	59	4.87
5	77	12.8	49	4.36

Table 3.6. Comparison of spatial and temporal metrics for pulse thunderstorms to the all-inclusive set of WFTs. The medians for each storm attribute are shown, and when applicable the interquartile range is shown in parenthesis.

	Storms	TFD	DUR	MAX REF	MAX SIZE	SOL
Pulse	5,378	7.51 (3.37)	208 (177)	65 (5)	470 (678)	0.49 (0.10)
All WFTs	885,496	7.89 (4.79)	60 (47)	55 (5)	42 (47)	0.53 (0.10)

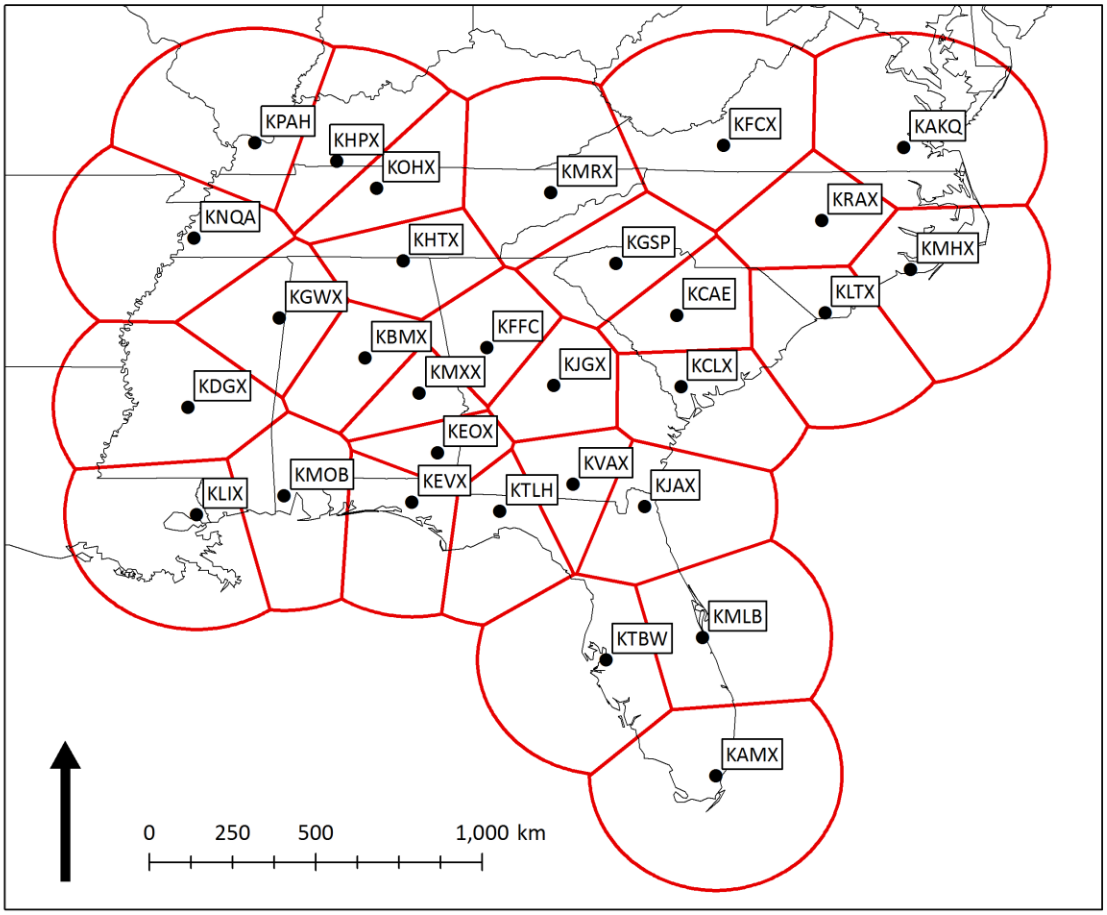

Figure 3.1. WSR-88D sites included in study. Red lines indicate regions nearest to each radar. Upper air soundings were also collected at three approximately collocated radiosonde and radar sampling sites along a diagonal transect through the center of the study area: Tampa, FL (KTBW), Peachtree City, GA (KFFC), and Nashville, TN (radar designation: KOHX; radiosonde designation: KBNA).

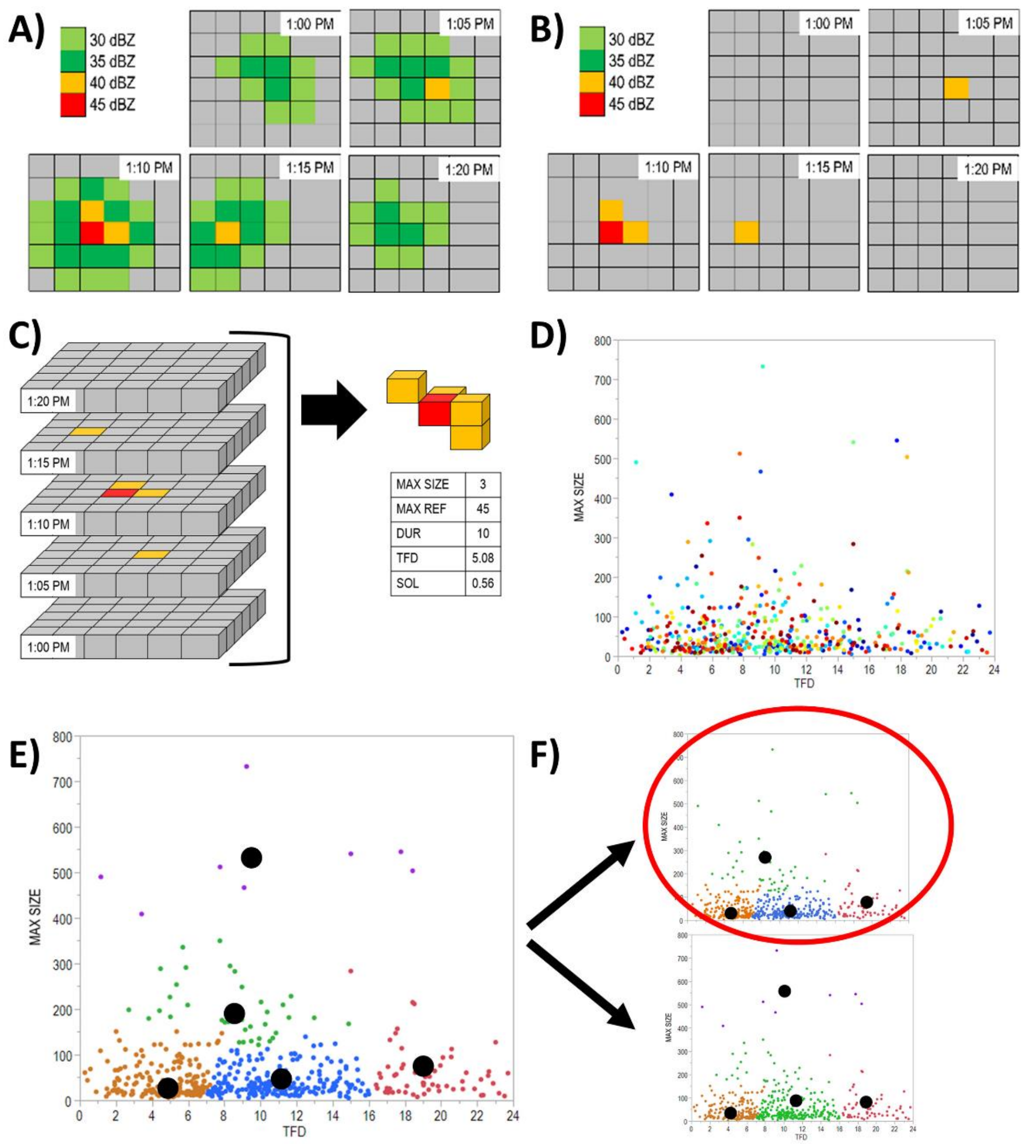

Figure 3.2. Illustration of the connected neighborhoods labeling and Ward's clustering workflow. Beginning with a hypothetical five-image sequence (A), reflectivities ≥40 dBZ are masked (B). The images are ordered sequentially, contiguous regions of convective reflectivities are extracted as thunderstorms, and five morphological variables are calculated (C). Storms are then clustered into statistically similar groups based on the five morphological characteristics with each storm beginning as an individual cluster (D). Storms are combined into groups (E) by iteratively merging the two clusters that will yield a new group with the smallest total within-cluster error of all possible mergers (F). Cluster centers are shown as black dots, and the total within-cluster error is proportional to the sum of all members' separation from their parent center. In pane (F), Ward's method combines the purple and green clusters from pane (E) because the new resulting cluster contains less total error than if, for instance, the green and blue clusters had been merged.

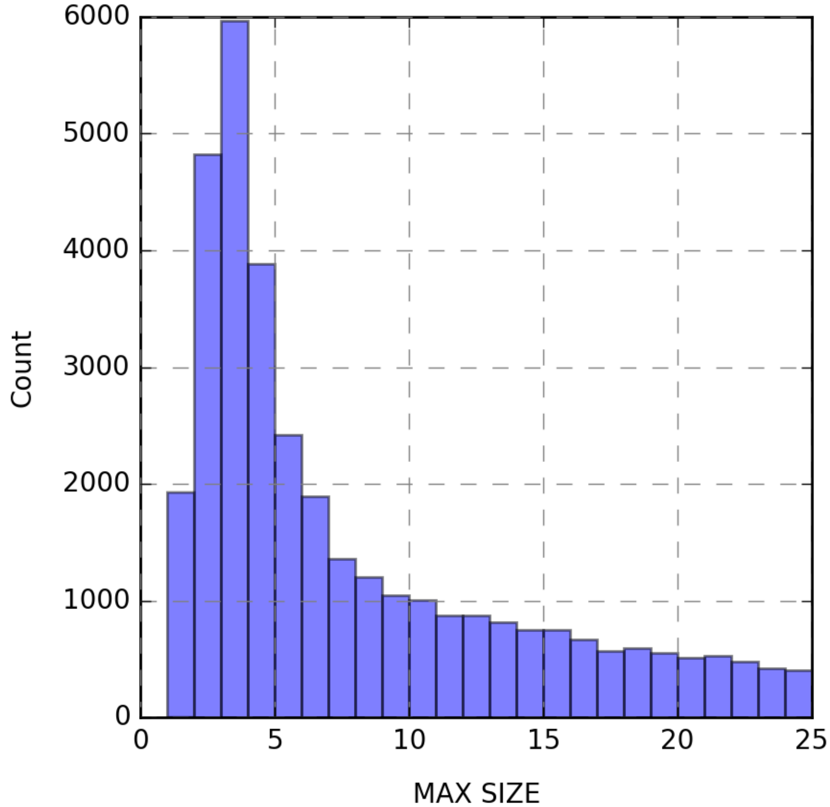

Figure 3.3. Recurring first-detection location MAX SIZE distribution. “Storms” originating from these recurring locations were disproportionately small, consistent with the appearance of ground clutter on radar. A MAX SIZE requirement of eight grid cells was implemented for storms originating in these locations to remove suspected non-meteorological echoes.

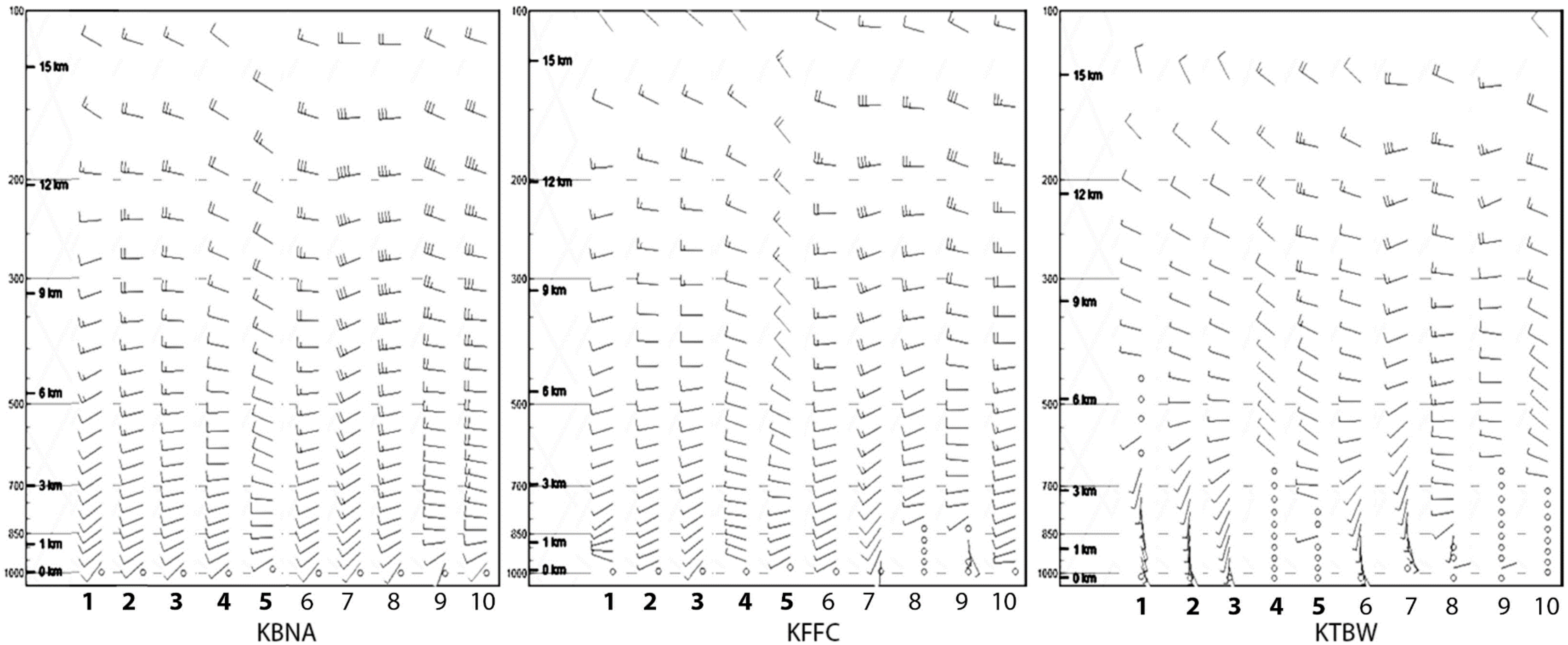

Figure 3.4. Composite KBNA, KFFC, and KTBW 1200 UTC vertical wind profiles for each storm type. WFT types are bolded.

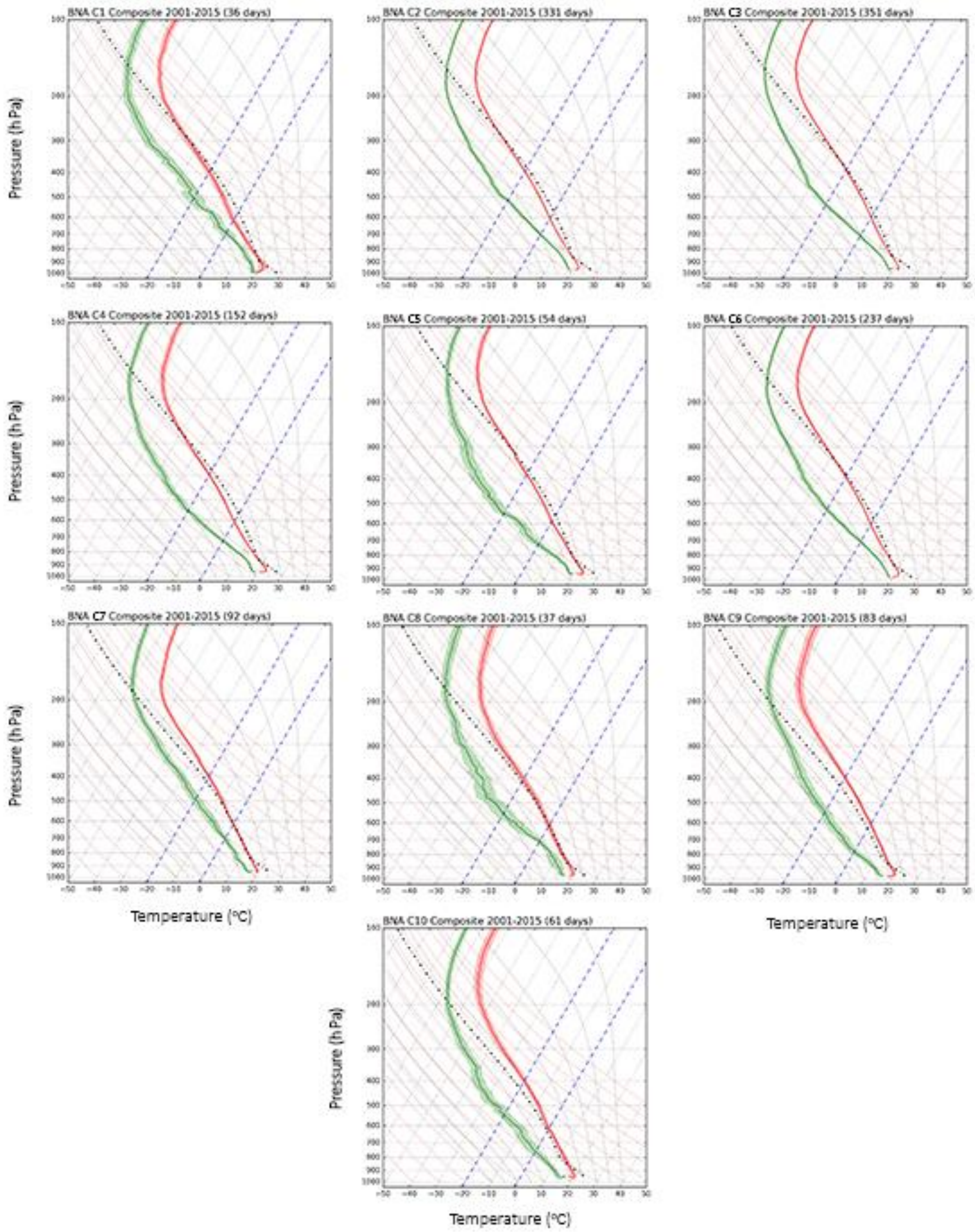

Figure 3.5. KBNA 1200 UTC composite soundings for the ten Ward's clusters. The 100-mb mixed-layer parcel trajectory is plotted as a black dashed line. The 95% confidence intervals for both the dewpoint and temperature traces are shown as green and red, respectively, shaded regions on either side of the traces.

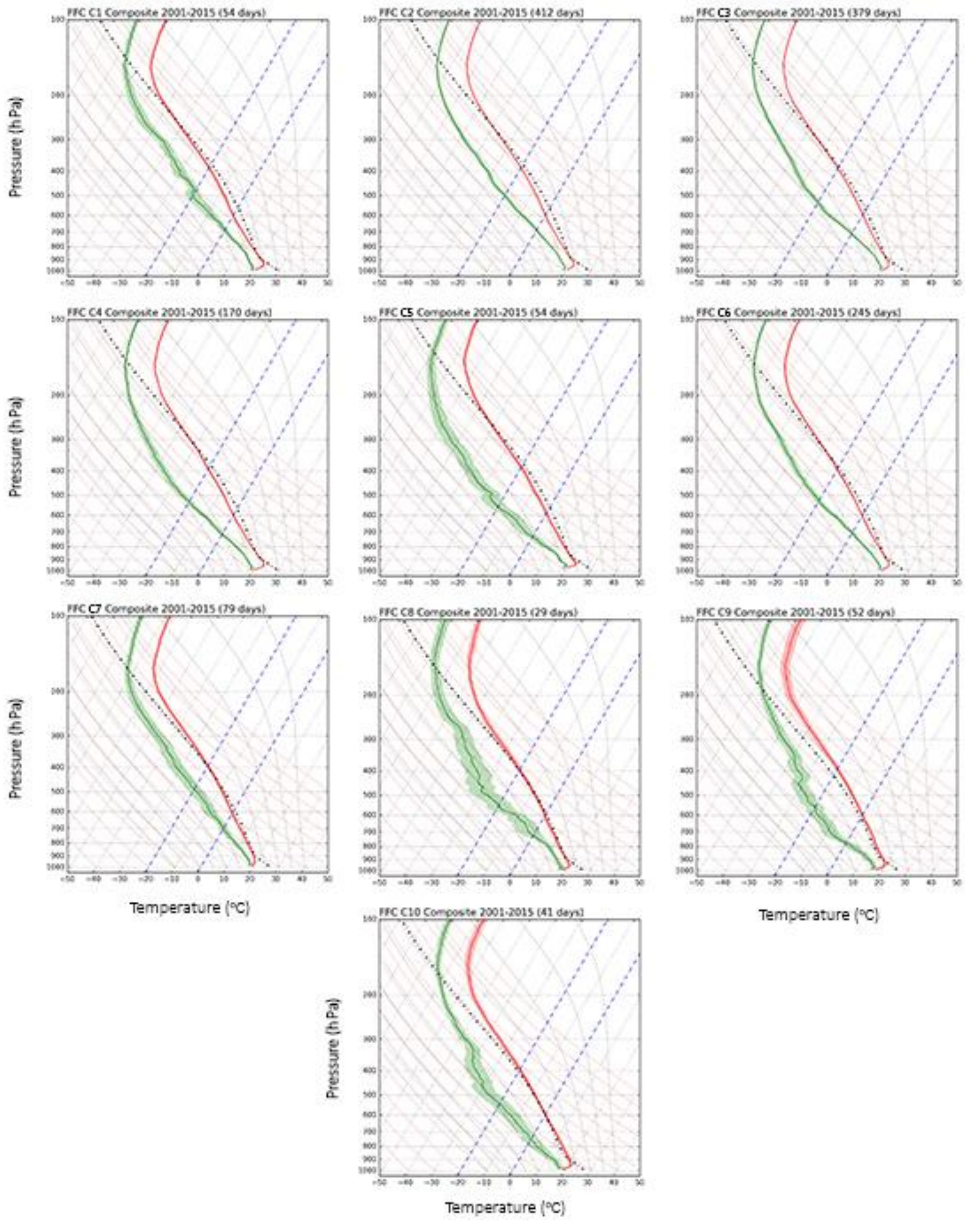

Figure 3.6. Same as Fig. 3.5 except for KFFC.

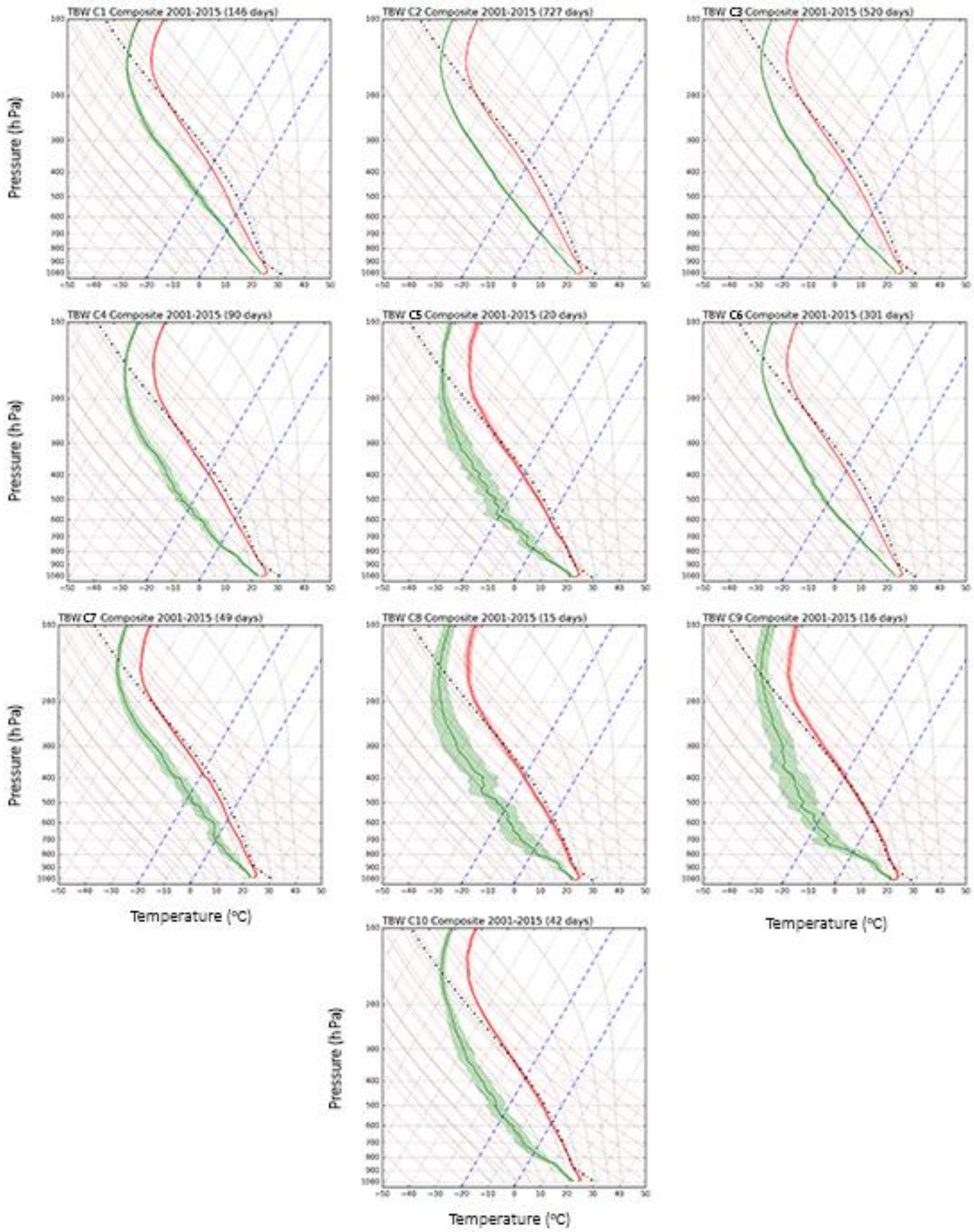

Figure 3.7. Same as Fig. 3.5 except for KTBW.

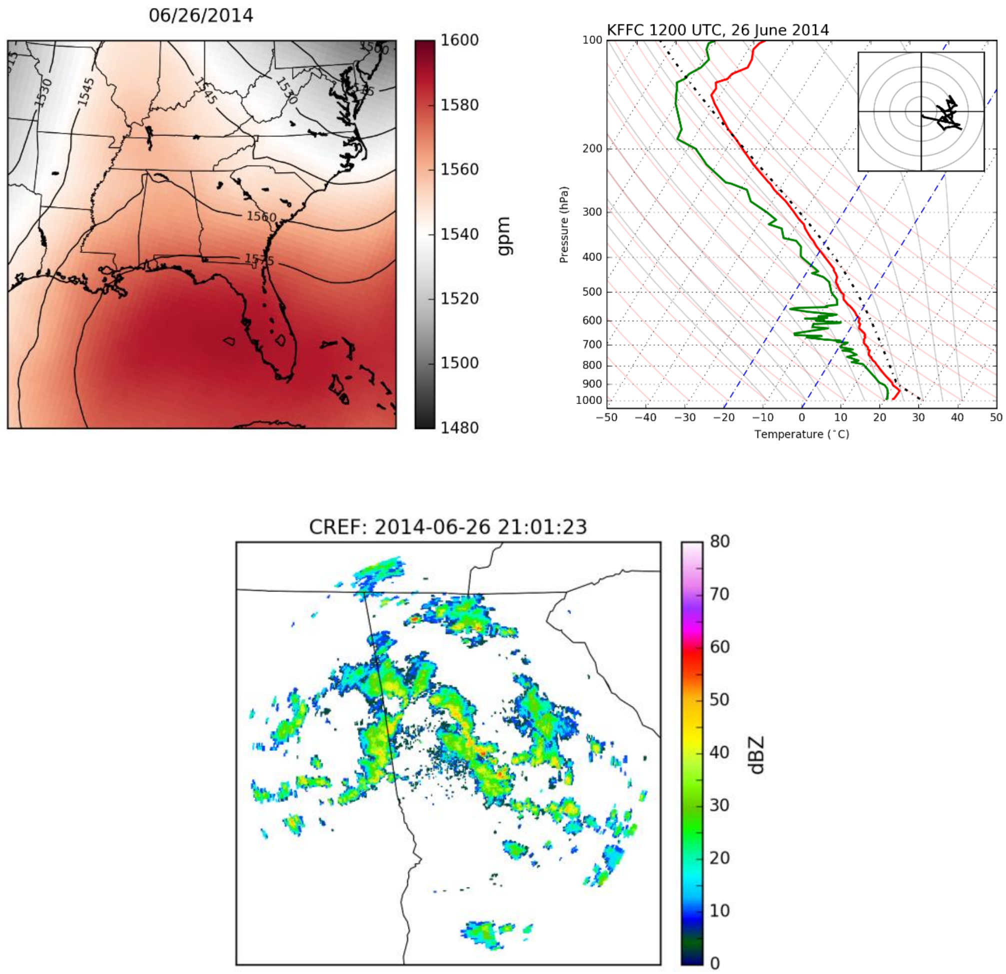

Figure 3.8. Example of a T2 day at KFFC. North Georgia is located on the northern fringe of Bermuda High which has expanded into the Gulf of Mexico (top left). The morning sounding from KFFC (top right) shows instability is present with an overall weak and disorganized wind field. (Hodograph rings placed at 10-kt intervals.) Despite the absence of jet-stream-aided forcing, the composite reflectivity near 2100 UTC shows that some convection is occurring in larger clusters yielding the T2 categorization on this day.

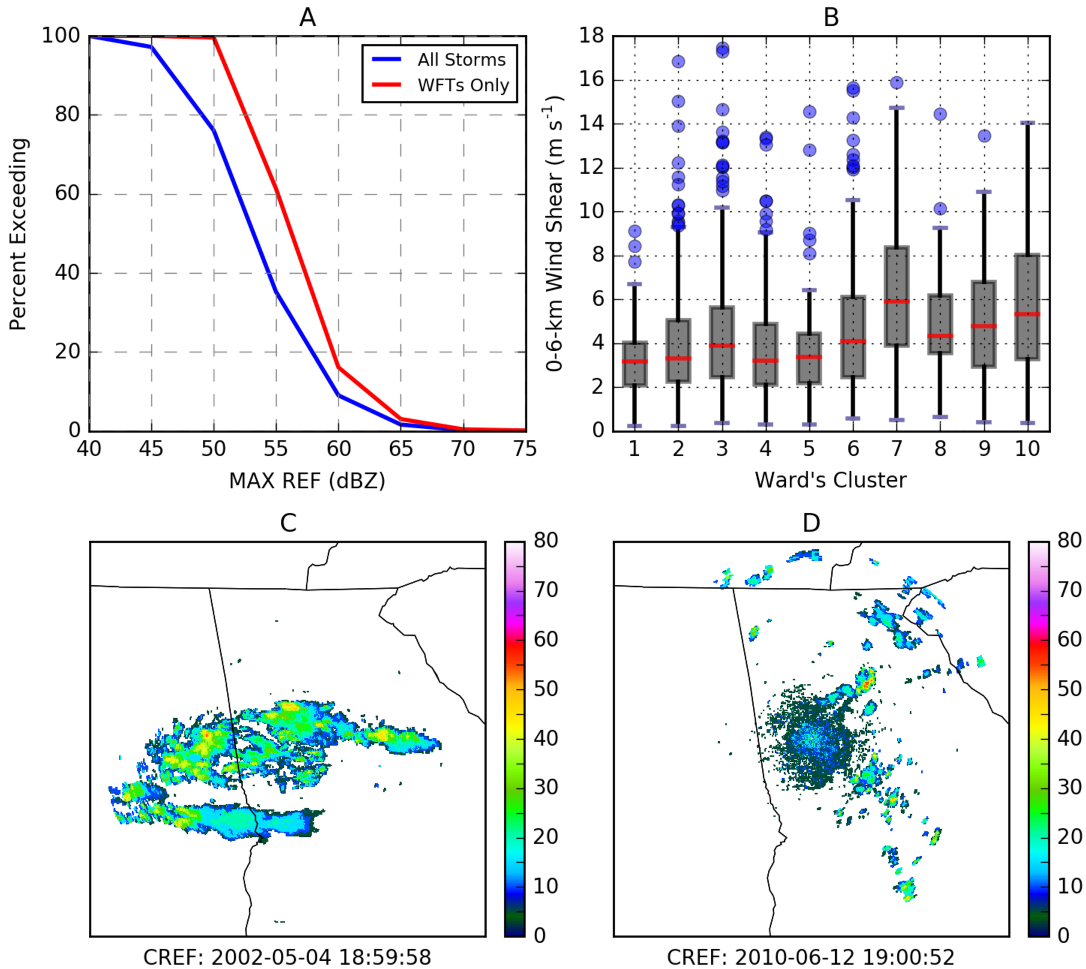

Figure 3.9. (A) Percent of storms meeting or exceeding the MAX REFs value on the *x*-axis. (B) Distributions of 0–6-km wind shear values for each of the Ward's clusters at KFFC. Examples of composite reflectivity imagery for a case where the WFT identification routine struggled (C) and for a more representative WFT case (D) are also pictured.

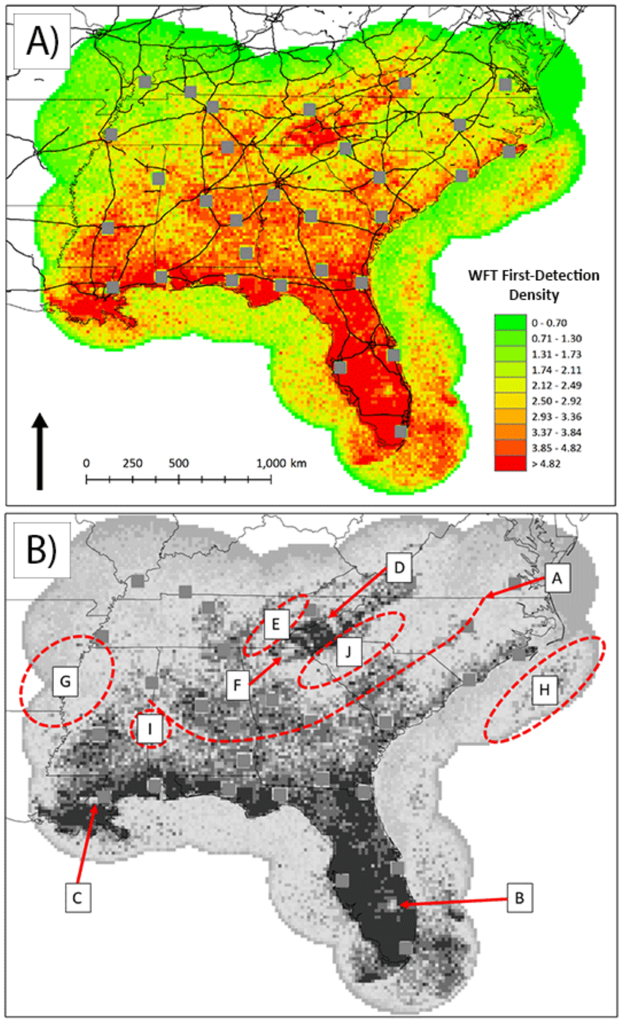

Figure 3.10. WFT first-detection density in events per year per 0.1˚x0.1˚ grid cell (A). Pane (B) labels notable features which are referenced in the text. Because the radar beam becomes less concentrated at increasing distance from the radar, small WFTs, detected by a more concentrated beam, are more common close to the radar, systematically driving the WFT climatology toward larger frequencies near radars and smaller concentrations farther from radars. To mitigate this effect, only WFTs with MAX SIZE ≥24 (the mode of the MAX SIZE distribution for all WFTs) were used to create the above images. The first-detection minima labeled in (B) were selected because they were evident in the absence of radar boundaries, but ranging effects may still have exacerbated their magnitude and shape.

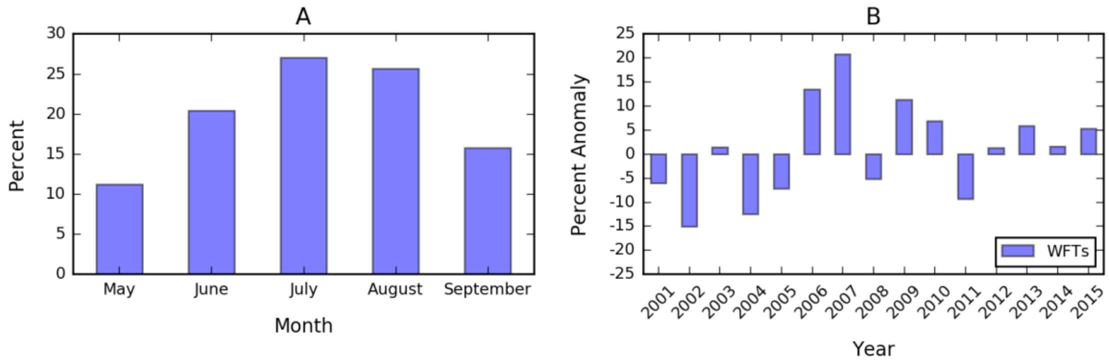

Figure 3.11. Distribution of WFT frequency by month (A) and year (B). The annual frequency is expressed in terms of the percent anomaly from the 15-yr Southeast average number of WFTs that occurred each year. For years 2002 and 2003, the 13-yr and 14-yr averages for KDGX and KHTX were added to the Southeast total as a rough correction for the absence of data from those two sites.

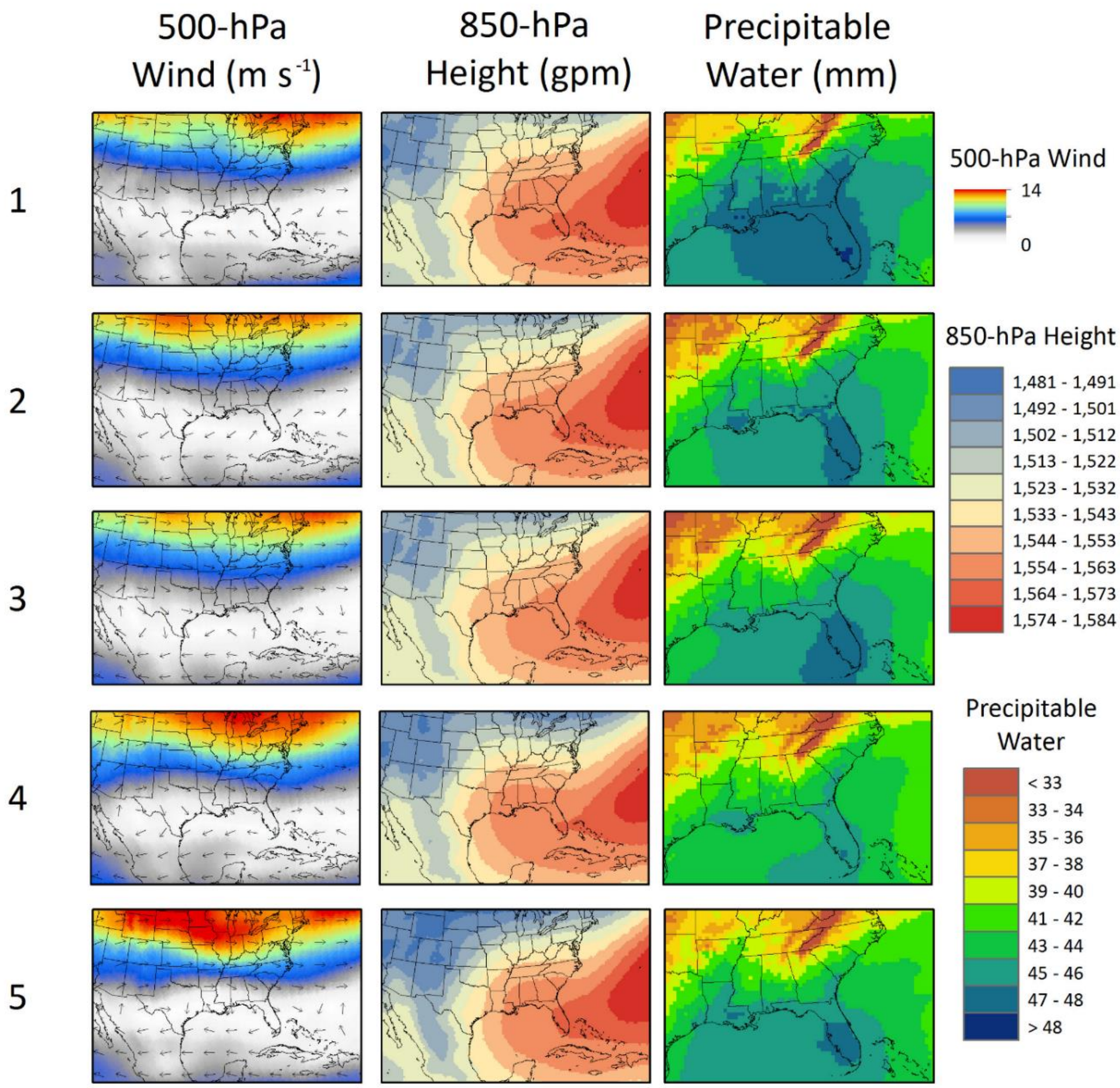

Figure 3.12. Synoptic composite maps of 500-hPa mean wind (left), 850-hPa height (center), and TPW (right) for the five WFT types. The 25th and 75th percentile maps for 850-hPa height and TPW are available as Figs. 3.13–3.14, respectively.

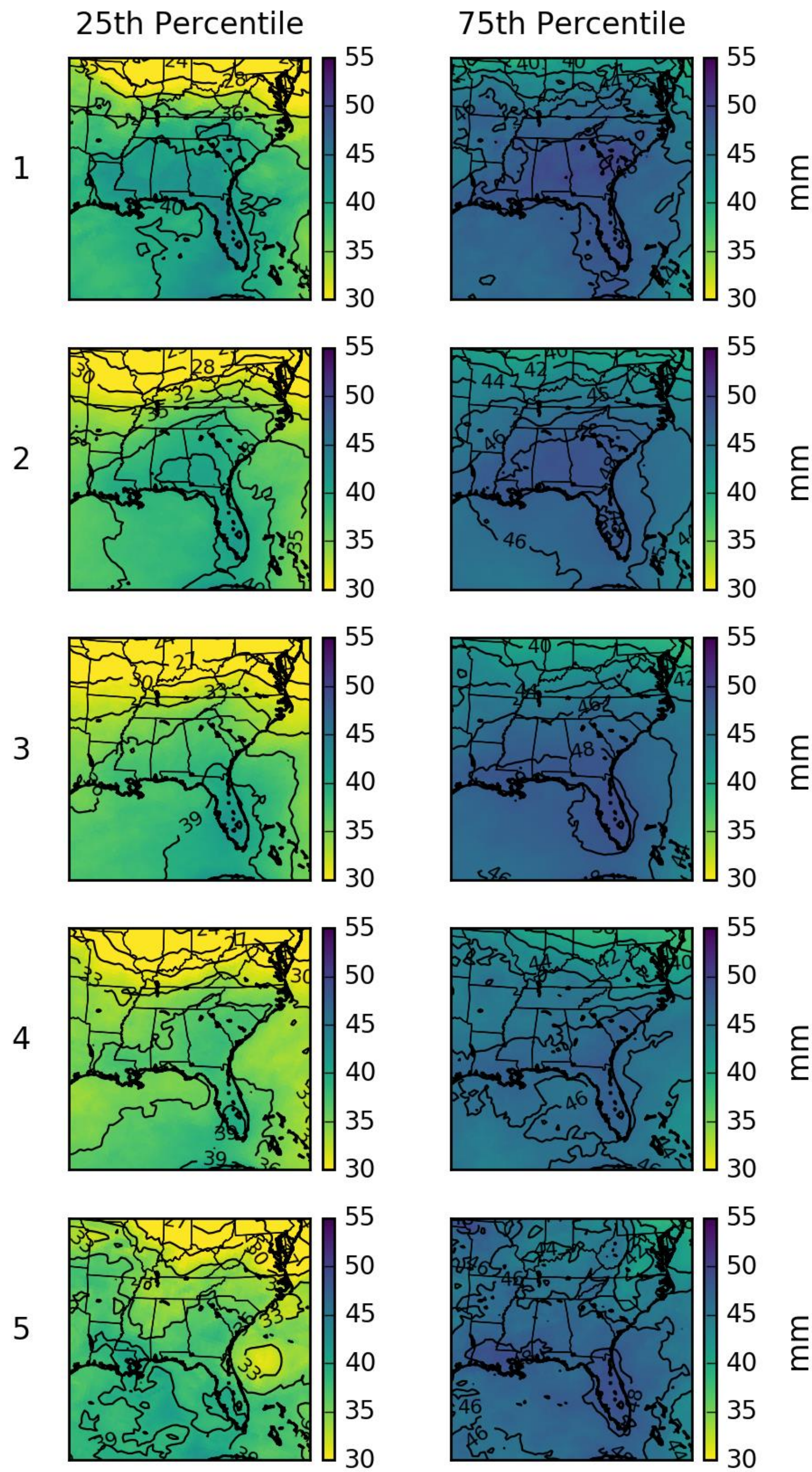

Figure 3.13. TPW quartiles to accompany the composite maps shown in Fig. 3.12.

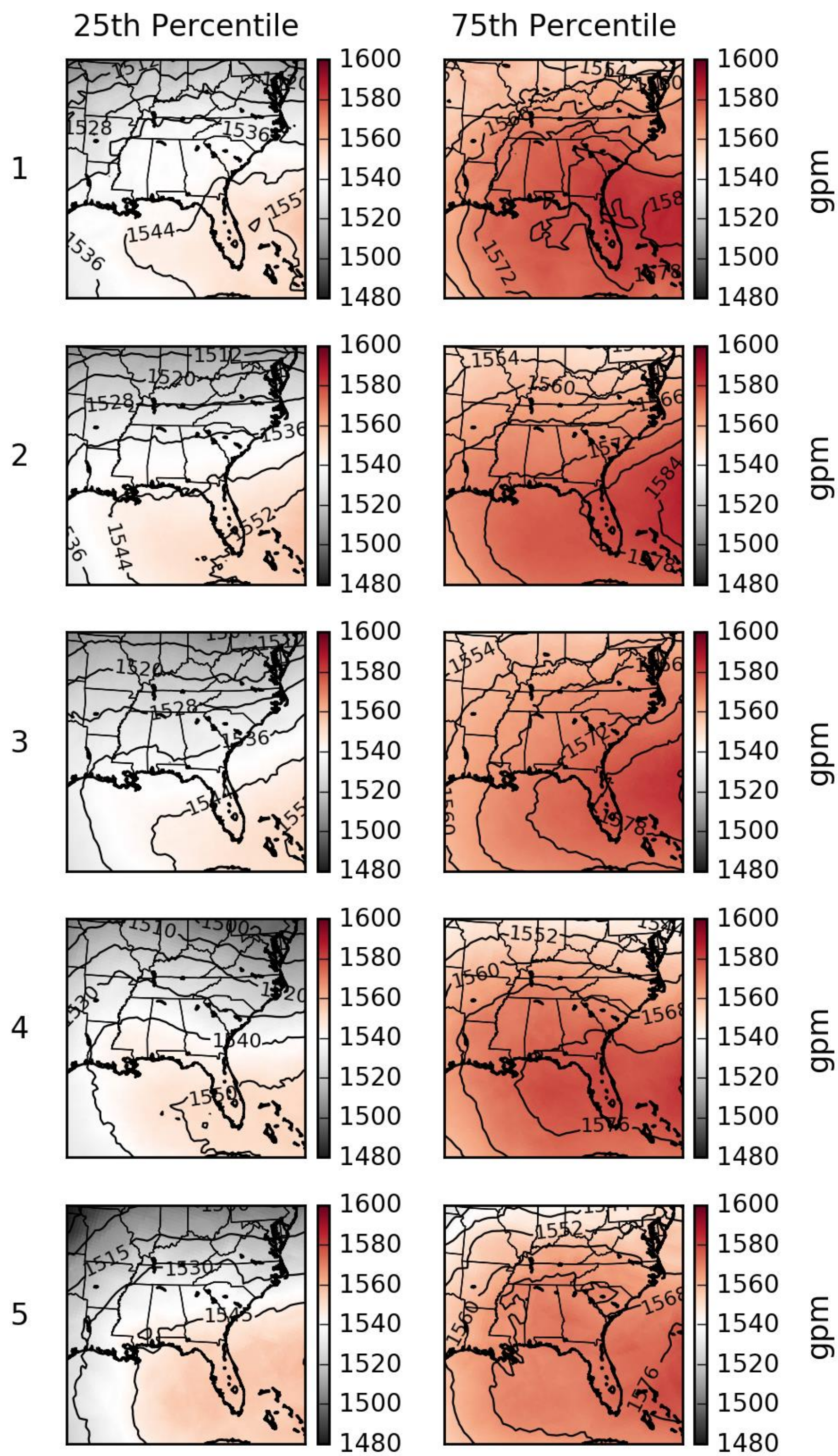

Figure 3.14. Geopotential height at 850 hPa quartiles to accompany the composite maps shown in Fig. 3.12.

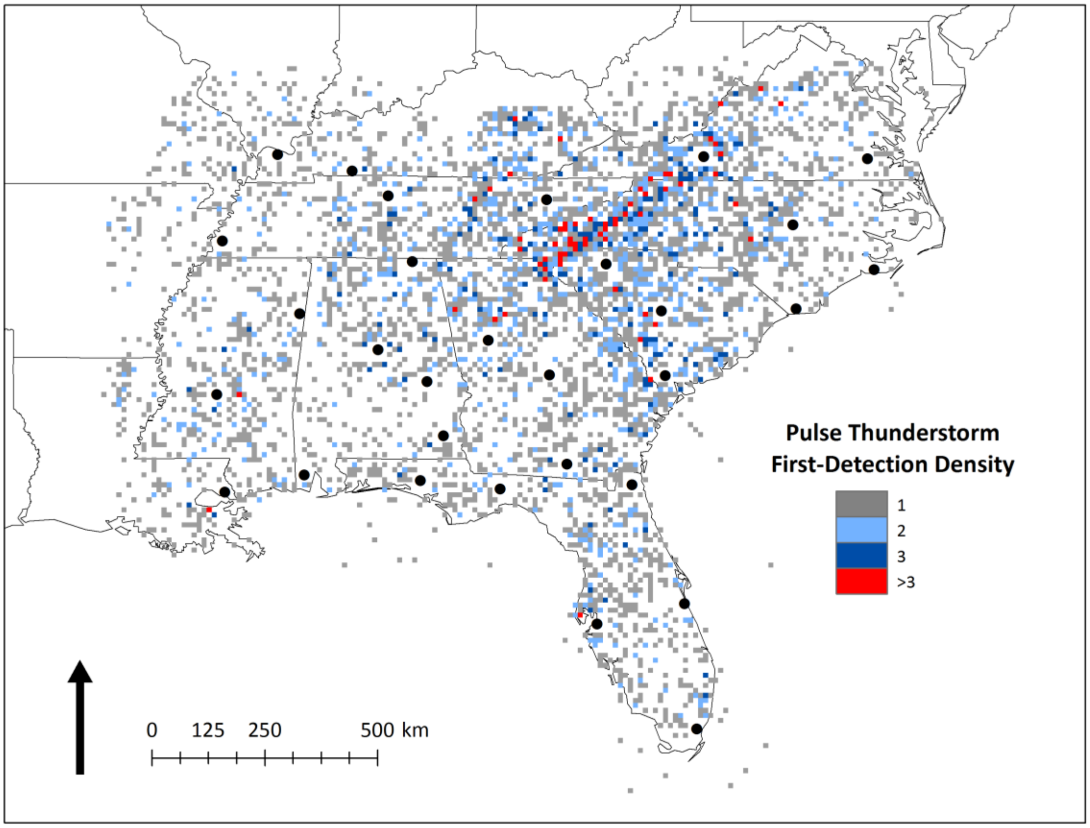

Figure 3.15. First detection density of all 5,378 pulse thunderstorms within the dataset. The number in the legend represents the total number of pulse thunderstorms during the entire 15-yr study period. WSR-88D sites are depicted as black dots.

CHAPTER 4

DETECTING SEVERE WEATHER POTENTIAL IN LOW SIGNAL-TO-NOISE RATIO REGIMES: WEAKLY FORCED THUNDERSTORM ENVIRONMENTS IN THE SOUTHEAST UNITED STATES [8]

[8] Miller, P. W., and T. L. Mote. Submitted to *Natural Hazards and Earth System Sciences*. 9 August 2017.

Abstract

Severe weather forecasting in weakly forced thunderstorm (WFT) environments is challenging due to a low signal (the large-scale difference in convective environment) to noise (other factors that compete with the large-scale difference) ratio (SNR). This study attempts to overcome the low SNR by examining >200,000 WFTs in the Southeast United States. Thirty near-storm convective parameters are calculated for each WFT from a high-resolution mesoscale model, the Rapid Refresh. Days on which at least one severe weather event was detected were considered supportive of severe weather and compared to days with no severe events using an odds ratio (OR). The OR calculates the relative proportions of severe to nonsevere WFT environments occurring above or beneath a convective parameter value. The result of the OR is a range of thresholds in which severe WFT environments were disproportionately concentrated above the threshold compared to below it. Only two convective parameters, vertical totals (VT) and total totals (TT), appreciably differentiate severe-wind-supporting (SWS) and severe-hail-supporting (SHS) days from control days. When VTs exceeded values between 24.6–25.1°C or TTs between 46.5–47.3°C, SWS days were roughly 5x more likely. Meanwhile, SHS days became roughly 10x more likely when VTs exceeded 24.4–26.0°C or TTs exceeded 46.3–49.2°C. The stronger performance of VT and TT is partly attributed to the more accurate RAP representation of these parameters. Under-reporting of severe weather and RAP error are hypothesized to exacerbate the low SNR, obscuring the few subtle environmental differences that might be used to forecast storm severity in WFT environments.

4.1 Introduction

Weakly forced thunderstorms (WFTs), convection forming in synoptically benign, weakly sheared environments, are a dual forecasting challenge. Not only is the exact location and time of convective initiation difficult to predict, but once present, the successful differentiation of severe WFTs from their benign counterparts is equally demanding. Consequently, severe weather warnings issued on WFTs in the U.S. are less accurate than more organized storm modes, such as squall lines and supercells (Guillot et al. 2008). American operational meteorologists have coined these severe WFTs “pulse thunderstorms” because the surge of the updraft that produces the severe weather occurs in a brief “pulse” (Miller and Mote 2017a). The United States National Weather Service defines “severe weather” as any of the following: winds ≥ 26 m s^{-1}, hail ≥ 2.54 cm in diameter, or a tornado.

Environments thought to support pulse thunderstorms are typically characterized by weak vertical wind shear and strong convective available potential energy (CAPE). However, not all weak-shear, high-CAPE environments facilitate pulse thunderstorms, nor are all pulse thunderstorms confined to environments with the weakest shear and/or strongest instability. The result is a low signal-to-noise ratio (SNR) which obstructs the reliable discernment of pulse-supporting environments. In this context, the “signal” refers to the true difference between the large-scale convective environments that support severe weather and those that do not. Meanwhile, the “noise” is represented the many processes than might cause storms to produce (not produce) severe weather in an environment where it was not expected (expected). Cell interactions, stabilization from prior convection, surface convergence, locally enhanced shear, etc, can act as noise in the operational setting.

Prior research directed at pulse thunderstorms is limited, and work has not typically included a representative proportion of nonsevere WFTs in their samples (Atkins and Wakimoto 1991; Cerniglia and Snyder 2002). If the sample contains too many pulse thunderstorms, the SNR may be artificially bolstered, results overstated, and the potential reliability in an operational setting diminished. For instance, in a meta-analysis of studies pertaining to new lightning-based storm warning techniques, Murphy (2017) found that the studies' reported FARs were directly proportional to the fraction of nonsevere storms contained in the sample. Samples that included a realistic ratio of severe-to-nonsevere storms demonstrated the weakest skill scores.

Most research considering pulse thunderstorms in the Southeast U.S. has typically focused on one of its primary severe weather mechanisms: the wet microburst. Severe wet microbursts generally occur in atmospheres characterized by a deep moist layer extending from the surface to 4–5 km above ground level (Johns and Doswell 1992). Above the moist layer lies a mid-level dry layer with lower equivalent potential temperature values (θ_e). In wet microburst environments, the difference between the maximum θ_e observed just above the surface and the minimum θ_e aloft exceeded 20 K, whereas non-microburst-producing thunderstorm days had differences less than 13 K (Roberts and Wilson 1989; Atkins and Wakimoto 1991; Stewart 1991; Wheeler and Spratt 1995). However, Atkins and Wakimoto (1991) examined only 14 microburst days versus three non-microburst days. Adding to the uncertainty, James and Markowski (2010) challenged the role of mid-level dry air in severe weather production. The results of their cloud-scale modeling experiment indicated that, for all but the highest instabilities tested, drier mid-level air did not correspond to increased downdraft and cold pool intensity.

Building on these findings, several severe weather forecasting parameters have been developed to distill the atmosphere's vertical thermodynamic profile into a single value representing the damaging wind potential. McCann (1994) developed a microburst-predicting "wind index" (WINDEX) to be used in the forecasting of wet downburst potential. However, although WINDEX performed well when tested in known microburst environments, no null cases were presented (McCann 1994). Additional severe wind potential indices include the wind damage parameter and the microburst index described by the United States Storm Prediction Center (SPC; http://www.spc.noaa.gov/exper/soundings/help/index.html). Tools such as Total Totals, K-index, the severe weather threat (SWEAT) index, etc, are also commonly used to forecast convective potential as well as the severity of thunderstorms.

However, the comparative utility of these environmental parameters within weakly forced regimes is unclear, particularly when they are tested with a realistic proportion of severe storms. Many of the results above were obtained by analyzing relatively small datasets, and they have not been tested against each other in a weakly forced environment. Therefore, this study seeks to compare the relative skill of convective parameters using a large WFT dataset to determine which are most appropriate for detecting environments supportive of pulse-thunderstorm-related severe weather.

4.2 Data and Methods

4.2.1 WFT selection and environmental characterization

This study uses the 15-yr WFT dataset developed by Miller and Mote (2017a) for the Southeast U.S. (Fig. 4.1). Their catalogue identifies thunderstorms as regions of spatiotemporally contiguous composite reflectivities meeting or exceeding 40 dBZ with WFTs representing the subset of generally small, short-lived thunderstorms that formed in weak-shear, strong-instability environments. The WFTs are spatially referenced according to their first-detection location, the centroid of the composite reflectivities constituting the first appearance on radar. The storms were then paired with severe weather reports from *Storm Data*, a storm event database maintained by the United States National Centers of Environmental Information, to differentiate benign WFTs from pulse thunderstorms. The entire 15-yr dataset contains 885,496 WFTs including 5316 pulse thunderstorms.

Meanwhile, the thermodynamic and kinematic environment of each WFT was characterized using the 0-hr Rapid Refresh (RAP; Benjamin et al. 2016) analysis. The RAP, implemented on 9 May 2012, is a 13-km non-hydrostatic weather model initialized hourly for the purpose of near-term mesoscale forecasting which is operated by the United States National Center for Environmental Prediction. The model has output available at 37 vertical levels spaced at 25-hPa intervals between 1000 and 100 hPa and 10-hPa intervals above 100 hPa. Several previous studies have relied upon the RAP's predecessor, the Rapid Update Cycle (RUC; Benjamin et al. 2004), to effectively characterize near-storm environments differentiating supercellular versus non-supercellular and tornadic versus non-tornadic thunderstorms (Thompson et al. 2007; Thompson et al. 2014).

For the grid cell containing each WFT's first-detection location, a RAP proxy sounding was created using the SHARPpy software package (Blumberg et al. 2017). Thus, each proxy sounding represents the model-derived storm environment for a point no more than 13-km and 30 min distant from the WFT first-detection location. The proxy soundings were used to calculate 30 near-storm environmental variables and indices, a complete list of which is provided in Table 4.1 with more thorough descriptions in Appendix A. The 30 variables were largely selected by virtue of their accessibility in SHARPpy. Four warm seasons of the Miller and Mote (2017a) dataset, containing 228,363 WFTs and 1481 pulse thunderstorms, overlapped with the RAP's operational archive period allowing >6 million near-storm parameters to contribute to the analysis.

4.2.2 RAP error assessment

Thompson et al. (2003) demonstrated the RUC-2 ability to adequately represent storm environments as evaluated using co-located radiosonde observations, and the Benjamin et al. (2016) RAP validation statistics show that the RAP is more accurate than its predecessor. Figure 4.2a shows the results of an error evaluation specific to the purposes of this study. Vertical error profiles were calculated for 3562 co-located RAP predictions and observed radiosonde profiles in the Southeast U.S. The comparisons contain 0000 and 1200 UTC soundings during the warm season (May–September) between 2012 and 2015 at three launch sites along a north-south trajectory through the Miller and Mote (2017a) domain: Nashville, Tenn., Peachtree City, Ga., and Tampa, Fla., corresponding to KOHX, KFFC, and KTBW in Fig. 4.1.

Similar to the Thompson RUC-2 analysis, the greatest, albeit small, temperature and moisture biases (mean errors) from the RAP reside near the surface and the upper atmosphere (Fig. 4.2a). Aided by the large sample of comparison soundings, the 95% confidence intervals indicate that the true bias of the selected RAP output variables at these sites can be estimated with reasonable confidence. The 95% mixing ratio confidence interval captures zero at all altitudes except 500 hPa, where the RAP predicted drier-than-observed values by 0.08 g kg^{-1}. Temperatures are warmer than observed throughout most of the troposphere with a maximum bias of 0.26°C at 850 hPa. In contrast, the RAP underestimated wind speeds on average throughout the depth of the troposphere. The largest bias, 0.46 m s^{-1}, was found at 925 hPa with similar errors above 500 hPa. The 95% confidence interval for wind speed error is largest near the tropopause, and demonstrates larger uncertainty than for temperature and mixing ratio. These results generally agree with the error statistics provided by Benjamin et al. (2016), and the reader should reference that paper for additional information, including validation statistics, about the RAP.

Although the RAP appears to resolve temperature, mixing ratios, and wind speeds more accurately than the RUC-2, the transmission of these errors onto the derived convective parameters can be large. Table 4.2 expresses error measures for surface-based (SBCAPE) and mean-layer CAPE (MLCAPE), 0–3-km and 0–6-km wind shear, total totals, and the theta-e index. Because the focus of this study is surface-based convection, only days when the observed surface-based CAPE was greater than zero were used to calculate the derived quantity error metrics. Similar to previous work (e.g., Lee 2002), parameters calculated via the vertical integration of a parcel trajectory, such as CAPE, are sensitive to errors in low-level temperature and moisture. The RAP's low-level temperature and moisture biases influence the lifted condensation level (LCL) calculation (negative MLLCL bias; Table 4.2) yielding a premature transition to the pseudo-adiabatic lapse rate and an overestimate of parcel instability (positive SBCAPE and MLCAPE biases; Table 4.2)[9]. Thompson et al. (2003) identified smaller CAPE errors generated by the RUC-2;

[9] The near-surface temperature and moisture errors in Fig. 4.2a are more pronounced following the upgrade to RAPv2 in February 2014. However, because the RAP is an operational tool and this work has operational relevance, no attempt was made to correct for this change.

however, the nature of the thermodynamic environments being examined is significantly different in this study. Similar to the RUC-2, the RAP is more adept at representing MLCAPE than SBCAPE with Fig. 4.2b, and consequently, the mean-layer parcel trajectory will be used for all parcel-related calculations.

Figures 4.2b-d demonstrate that although large outliers certainly occur, the majority of RAP-derived thermodynamic and kinematic parameters are concentrated within a narrower range of error. Figure 4.3 provides an example skewT-logP diagram for a large MLCAPE error shown in Fig. 4.2d. Though the difference in this case exceeded 1000 J kg^{-1}, the discrepancy can largely be attributed to the RAP's minor mischaracterization of low-level moisture. Otherwise, the depiction of the vertical profile is reasonably accurate. The advantage of the RAP to represent the near-storm environment is underscored when compared to results from coarser-scale models. For instance, the coefficients of determination (R^2) for RAP-derived SBCAPE and MLCAPE are appreciably larger than those calculated from the 32-km horizontal and 3-hr temporal resolution North American Regional Reanalysis (NARR; Mesinger et al. 2006) in Gensini et al. (2014b).

4.2.3 Assessing convective parameter skill

The quality of severe weather reports is a significant impediment to severe storm research (e.g., Weiss et al. 2002; Miller et al. 2016), particularly regarding the certainty with which nonsevere storms can be declared nonsevere. These storms may only appear benign because their associated severe weather was not reported. Consequently, the results of the proxy soundings are subdivided by nearest radar site (Fig. 4.1) and aggregated daily (1200–1200 UTC) with days containing at least one severe weather report considered supportive of severe weather whereas days with no severe weather reports will serve as the control. This approach is similar to the methods the Hurlbut and Cohen (2013) study of severe thunderstorm environments in the Northeast U.S. Severe-wind-supporting (SWS) days and severe-hail-supporting (SHS) days are treated separately because their thermodynamic environments have been shown to contain unique elements related to downdraft and hailstone production (Johns and Doswell 1992). Table 4.3 provides the specific subdivision details of the frequency of WFT days, SWS days, SHS days, and their respective control days. Figure 4.4 shows the annual average of WFT days for each radar site within the study area during the 2012–2015 warm seasons. As expected, WFT days are most frequent along coastlines and the Appalachian Mountains (Miller and Mote 2017a).

Given the low SNR in WFT environments, *t*-tests are deceiving. Statistically significant differences in the mean values of parameters on severe versus nonsevere days are routinely reported, but the considerable overlap between the distributions (e.g., Craven and Brooks 2004; Taszarek et al. 2017) can remove much practical value. This study explores the relationship between convective parameters and pulse thunderstorm environments by means of an odds ratio (OR; e.g., Fleiss et al. 2003). The OR is a common measure of conditional likelihood in human health and risk literature (e.g., Bland and Altman 2000) with precedent in the atmospheric sciences (e.g., Black and Mote 2015; Black et al. 2017). The OR looks past the descriptive statistics of the severe versus nonsevere distributions and more directly compares differences in where the data are concentrated.

Equation 4.1 shows the standard definition of the OR, essentially the ratio of two ratios,

$$OR = \frac{A/C}{B/D} \tag{4.1}$$

where the numerator represents the ratio of events (A) to non-events (C) when a condition is met whereas the denominator is the ratio of events (B) to non-events (D) when the same condition is not satisfied. In this context, “events” are SWS or SHS days whereas “non-events” would be the respective control days. Higher ORs indicate that events are more frequent (relative to non-events) when the condition is met, or conversely, that events are less frequent when the condition is not met. For this study, a condition might be a convective parameter exceeding a specified threshold. For instance, if the SWS OR equals 4 for the condition MLCAPE > 1000 J kg^{-1}, then an SWS day is 4x more likely when MLCAPE is greater than 1000 J kg^{-1} than when it is less than 1000 J kg^{-1}.

We employ a modified form of the OR in which both the numerator and denominator are standardized by the climatological ratio of events to non-events (Eq. 4.2), allowing the components of the OR to be separated and interpreted independently by comparison to climatology.

$$OR = \frac{\frac{A/C}{(A+B)/(C+D)}}{\frac{B/D}{(A+B)/(C+D)}} \tag{4.2}$$

The modification does not change the value of the quotient OR, but it does improve the interpretability of the numerator and denominator. When the numerator or denominator is near zero (one), then the likelihood of SWS or SHS days is much lower than (nearly equal to) climatology. The climatological odds ratio was 0.069 for SWS days and 0.025 for SHS days. A 95% confidence interval for the OR was calculated using the four-step method presented in Black et al. (2017).

4.3 Results

4.3.1 Convective environments of pulse thunderstorm wind events

During the four-year study period, pulse thunderstorm wind events were documented somewhere in the study area on 49% of WFT days, although the average frequency within any single subdivision was 6.7% (Table 4.3). Table 4.4 shows the 30 convective parameters analyzed from the proxy soundings as well as the number of subdivisions for which each parameter is a statistically significant differentiator of SWS days. A significance threshold of $p < 0.10$ guided the selection of potentially useful parameters which would be examined in more detail. Nine of the 30 variables are statistically significant across at least two-thirds of the study area: VT, TT, MLCAPE, MLLCL, MICROB, DCAPE, TEI, RH_LOW, and ThE_LOW.

Figure 4.5a-h depicts the distributions for several parameters from Table 4.4 for control versus SWS days. These eight parameters are either significant across much of the domain (VT and TT), demonstrate larger relative changes on SWS days (MLCAPE and MLLCL), and/or are traditional operational severe wind forecasting tools (DCAPE, TEI, WNDG, MICROB). However, as the distributions clearly illustrate, any difference in the mean values between the control days and SWS days is small compared to the spread about their means. This results in the characteristically low SNR described in the Section 4.1. Any attempt to establish a forecasting value indicative of pulse-wind potential will yield many missed events occurring beneath the threshold and/or false alarms associated with control days above it.

Thus, Fig. 4.6 employs the OR to characterize the relative skill that some knowledge of the convective environment can contribute to a severe versus nonsevere designation. For each variable in Fig. 4.5, a progressively larger value is selected, and the OR is calculated at each step. Figure 4.6 displays the OR as well as both the numerator and denominator terms for each iteration. Often high ORs result when a near-zero number of severe events exist below the threshold inflating the OR calculation. In these situations, the OR is indicating that severe weather is very unlikely, rather than that the severe weather risk is enhanced. These results are not particularly useful because forecasters would not have needed a decision-support tool in these environments in the first place. Ideally, large ORs will result when the numerator indicates an appreciable increase against the climatology while the denominator simultaneously indicates an appreciable decrease below climatology. Further, these ORs would ideally occur in a range where the severe weather risk may be uncertain. In Fig. 4.6, the OR is shown in a gray line, but the line is drawn in black whenever the OR results from a numerator ≥2 and a denominator ≤0.5. ORs resulting from this combination indicate that the threshold yields a simultaneous two-fold increase (decrease) in the likelihood of SWS days above (below) the specified value. These ORs will be hereon referenced as "two-fold" ORs, and represent a goal scenario.

Figures 4.6a-h show ORs for the same eight parameters in Fig. 4.5. Of all eight parameters, only VT and TT achieve two-fold ORs for any range of thresholds, as indicated by the black segments in Fig. 4.6a-b. The maximum two-fold OR for VT is 5.16 at 24.6°C, meaning that SWS days are 5.16x more likely when this threshold is met. TT offers slightly more skill with a maximum two-fold OR of 5.70 at 46.5°C. MLCAPE and MLLCL demonstrate consistently lower ORs between 2 and 4. Surprisingly, the four wind-specific variables in Fig. 4.6e-h are relatively poor differentiators of SWS days in the WFT regime.

The maximum OR achieved by any of these parameters is approximately 10 driven by very low values of DCAPE with corresponding wide confidence intervals.

Though ORs are greater at lower VT and TT thresholds, these values are also somewhat common. Placing the aforementioned values (24.6°C and 46.5°C, respectively) in the context of the 12,759 WFT environments included in this study, they represent the 58.8th and 58.9th percentiles of their distributions. Alternatively, the maximum VT threshold that yields a two-fold OR is 25.1°C, which corresponds to the 70.9th percentile of all VTs in the dataset; however, the OR for this value is smaller, 4.77. This result illustrates the trade-off involved by seeking climatologically exceptional values to serve as guidance. As greater values are selected as the threshold, meteorologists can focus on a fewer number of days. However, the OR decreases as more severe weather events occur in environments not satisfying the threshold. As for TT, the maximum two-fold OR value is 47.3°C, corresponding to the 70.6th percentile, but demonstrates an OR of 5.16. This means that when TT meets or exceeds 47.3°C, pulse thunderstorm severe wind events are 5.16x more likely than when it does not.

4.3.2 Convective environments of pulse thunderstorm hail events

Table 4.5 replicates Table 4.4 except for SHS days. Many of the same parameters that are statistically significant differentiators of SWS days also rank high for SHS days. However, fewer parameters in Table 4.5 are statistically significant over two-thirds of the domain. Whereas 10 parameters in Table 4.4 showed spatially expansive statistical skill on SWS days, only three quantities do so on SHS days. We attribute this result to the pattern in Table 4.3 and Fig. 4.4b-c whereby there are fewer SHS days than SWS days, which increases uncertainty related to the statistical tests and impedes the confident detection of differences.

Nonetheless, VT and TT are once again skillful differentiators, and are now joined by their related parameter CT. Additionally, several new convective variables demonstrate statistical significance across roughly half of the domain on SHS days that demonstrated little skill on SWS days: PW, PEFF, HGT0, and ApWBZ. For comparison, Fig. 4.7a-d duplicates Fig. 4.5a-d now comparing distributions between the control and SHS days while Fig. 4.7e-h displays boxplots for the SHS-specific convective parameters listed above. The distributions for MLCAPE and MLLCL are similar; however, there is a larger separation between control and SHS days for VT and TT than was apparent on SWS days. This observation is corroborated by the relative changes in VT and TT on SHS days that are several percentage points larger than for SWS days (Table 4.5). PW, PEFF, HGT0, and ApWBZ demonstrate smaller differences.

Figure 4.8 replicates Fig. 4.6 except by representing SHS days and substituting the four wind-specific parameters (DCAPE, TEI, WNDG, MICROB) with the four hail parameters listed above (PW, PEFF, HGT0, ApWBZ). The ORs for VT and TT are large, greater than 10, throughout the entire range of thresholds tested, and contain larger swathes of two-fold ORs. The maximum two-fold OR for VT is 13.1 at 24.4°C, and the maximum two-fold-OR-achieving VT threshold is 26.0°C with an OR of 9.61. These values relate to the 53.4th and 86.0th percentiles of the VT distribution. As for TT, the maximum two-fold OR is 14.98 at 46.3°C, and the maximum two-fold-OR threshold is 49.2°C with an OR of 11.79. These two TT cut-offs translate to the 55.7th and 88.4th percentiles. Similar to SWS days, MLCAPE and MLLCL show little skill with ORs generally between 1–2. PW, PEFF, HGT0, and ApWBZ perform more capably than MLCAPE and MLLCL; however, they do not produce any two-fold ORs. Values for these metrics are generally around 4 with several instances of higher ORs driven by a small denominator with wide 95% confidence intervals.

4.3.3 Separating marginal pulse thunderstorm days

Because the severe weather generated by pulse thunderstorms is often near the lower limit used to define severe weather in the United States, some pulse thunderstorm environments may closely resemble nonsevere regimes. Consequently, the influence of these "marginal" pulse thunderstorm days on the OR analysis is further scrutinized. For this purpose, "marginal" SWS and SHS days are defined as those on which only one severe wind or hail report was received. Marginal days constitute 48.7% of the SWS days and 57.7% of the SHS days in Table 4.3. Figure 4.9 replicates the OR analysis for VT and TT, the two most promising environmental parameters from Sections 4.3.1 and 4.3.2, but with only marginal SWS and SHS days being considered. Comparing Figs. 4.6a-b and 4.8a-b to Fig. 4.9, marginal SWS and SHS days resemble the OR patterns of the broader set of SWS (Fig. 4.6a-b) and SHS (Fig. 4.8a-b) days. Though the ORs for the marginal subset are slightly smaller than for the broader group, they bear similar OR patterns as the thresholds are increased. Overall, marginal SWS and SHS days are generally characterized by similar VT and TT values as when all SWS and SHS days were aggregated. Corroborating this finding, an OR analysis comparing marginal SWS and SHS days to those with >1 severe event (not shown) revealed that ORs generally remained near 1 regardless of the VT or TT threshold selected. Thus, although marginal pulse thunderstorm days are by no means easily distinguishable from non-severe WFT days, they do not appear to be particularly more challenging to differentiate than active pulse thunderstorm days.

4.4 Discussion

The relative changes in the convective variables in Table 4.4 on SWS days versus control days correspond well to previous microburst research. Compared to the nonsevere control days, SWS days are characterized by a drier near surface layer (i.e., lower RH, higher LCLs). Simultaneously, steep mid-level lapse rates (i.e., larger VT and TT) aid an increase in CAPE which supports stronger updrafts. As the strong updraft transitions to a downdraft-dominant storm, the drier surface layer supports evaporative cooling, downdraft acceleration, and severe outflow winds. This same conceptual model has been promoted by previous severe convective wind research (e.g., Wolfson 1988; Atkins and Wakimoto 1991; Kingsmill and Wakimoto 1991).

The results of SHS days also support previous findings (Moore and Pino 1990; Johns and Doswell 1992; Púčik et al. 2015). The distributions in Fig. 4.7 (and relative changes in Table 4.5) indicate that SHS days are characterized by relative decreases in PW, a lower freezing level, a lower wet-bulb freezing level, and dry near-surface air. Smaller PWs result in less waterloading and greater parcel buoyancy (larger VT, TT, and MLCAPE) which maximizes updraft strength. Meanwhile, lower freezing levels and a dry layer between 1000–850 hPa support evaporative cooling which can together yield a lower wet-bulb zero height, and more efficient growth of hailstones. Interestingly, these two concepts are both represented in the PEFF calculation (Appendix A) which was not developed as a hail indicator. PEFF as defined by Noel and Dobur (2002), equals the product of PW and the mean 1000–700-hPa RH. As both values decrease, PEFF becomes smaller and hail is more likely for the reasons stated above.

The poor performance of MLLCLs and MLCAPEs in differentiating SWS and SHS days from their controls is surprising given their prominence in severe storm forecasting. In contrast, VT and TT were among the strongest indicators of both SWS and SHS days. Recalling from Section 4.2.2, VT and TT are also very well represented by the RAP. TTs were replicated by the model with a <1°C bias and a MAE representing only 3% of the average value (Table 4.2). Additionally, mid-level temperatures, from which VT is computed, also compared very well to the observed soundings (Fig. 4.2a). Thus, the strong performance of VT and TT compared to other more heavily moisture-weighted metrics may be due to their more accurate representation in the proxy soundings.

Regardless, because the severe weather SNR is already low in WFT environments, any systematic error introduced by the data source (in this case the RAP) may significantly dampen, or even remove, whatever environmental differences exist. As Section 4.2.2 indicated and previous work has also concluded, low-level moisture biases can impede the accurate calculation of convective parameters relying on those terms (e.g., Thompson et al. 2003; Gensini et al. 2014b). In this study, MLCAPE, MLLCL, PW, PEFF, and others were vulnerable to such errors. The poorer performance of these variables' ORs (relative to the lapse-rate-based parameters) and the sensitivity of PW, PEFF, and ApWBZ to simulated RAP errors suggests that model inaccuracies may be obscuring their potential skill to detect severe weather environments. The perception of the WFT environment as a difficult-to-forecast regime may partly be driven by model inconsistency exacerbating an already small SNR.

Another confounding factor is the quality of the *Storm Data* severe weather reports. Section 4.3.3 discussed that marginal SWS and SHS days are more similar to days with >1 report than days with no reports. Thus, the basis for the similarity may be that severe weather was simply under-reported on “marginal” days. Extending this logic, the pulse regime’s low SNR may also be partially attributed to under-reporting of severe weather on “nonsevere” days. Given that the severe weather generated by pulse convection is often short-lived, isolated, and narrowly exceeds severe criteria, the notion that some pulse-related severe weather events go undetected is likely. If some “nonsevere” days existing above the tested parameter thresholds in Figs. 4.6 and 4.8 did in fact host severe weather, then the ORs would have been larger than those found in Sections 4.3.1 and 4.3.2.

4.5 Conclusions

Hazardous weather within WFT environments is characterized by a lower SNR than other severe thunderstorm regimes. Though past research has developed promising tools for forecasting pulse thunderstorm environments, their relatively small sample sizes may have understated the SNR, and by corollary overstated the reliability of their tools. With recent research suggesting that the performance of new severe weather forecasting tools is closely tied to the proportion of nonsevere thunderstorms in the sample (Murphy 2017), this study sought to test the relative skill of 30 convective forecasting parameters using realistic proportions of severe and nonsevere WFT environments (severe: 7.9%; nonsevere: 92.1%). Future research may consider broadening the methods of Murphy (2017) to standardize the skill values across previous studies of severe convective environments.

Only 13 (5) of the 30 convective parameters tested were statistically significant ($p < 0.10$) differentiators of SWS (SHS) days across at least half of the domain. Though the distinctive variables for SWS and SHS days were consistent with previous theories of severe microburst and hail formation, considerable overlap between the distribution of values on severe and nonsevere days is problematic. Similarities between the SWS, SHS, and their corresponding control distributions inhibit consistent identification of pulse thunderstorm potential based on the value of any individual parameter. Nonetheless, VT and TT did perform more skillfully than the others. When VTs exceed values between 24.6–25.1°C or TTs between 46.5–47.3°C, the relative likelihood of a wind event increases roughly 5x. Meanwhile, hail events become roughly 10x more likely when VTs exceed values between 24.4–26.0°C or TTs between 46.3–49.2°C.

The noteworthy performance of VT and TT, two quantities calculated from the more reliable RAP output fields, is unlikely a coincidence. Our findings suggest that the already weak severe weather SNR in WFT environments is exacerbated by model limitations in the low-level moisture and temperature fields. Meteorologists may perhaps alleviate the challenges of the WFT environment by examining convective parameters that are well-represented by models, such as VT, TT, and other measures of lapse rate. Future research might seek to track the transmission of the model errors through calculation of forecast skill statistics, and more concretely ascertain the contribution of model error to the SNR.

4.6 Acknowledgments

The authors thank Alan Black for providing comments on an earlier draft of this manuscript.

4.7 References

Atkins, N. T., and R. M. Wakimoto, 1991: Wet microburst activity over the southeastern United States: Implications for forecasting. *Wea. Forecasting*, **6,** 470–482, doi:10.1175/1520-0434(1991)006<0470:WMAOTS>2.0.CO;2.

Benjamin, S. G., and Coauthors, 2004: An hourly assimilation–forecast cycle: The RUC. *Mon. Wea. Rev.*, **132,** 495–518, doi:10.1175/1520-0493(2004)132<0495:AHACTR>2.0.CO;2.

Benjamin, S. G., and Coauthors, 2016: A North American hourly assimilation and model forecast cycle: The Rapid Refresh. *Mon. Wea. Rev.*, **144,** 1669–1694, doi:10.1175/MWR-D-15-0242.1.

Black, A. W., and T. L. Mote, 2015: Characteristics of Winter-Precipitation-Related Transportation Fatalities in the United States. *Wea. Climate Soc.*, **7,** 133–145, doi:10.1175/WCAS-D-14-00011.1.

Black, A. W., G. Villarini, and T. L. Mote, 2017: Effects of Rainfall on Vehicle Crashes in Six U.S. States. *Wea. Climate Soc.*, **9,** 53–70, doi:10.1175/WCAS-D-16-0035.1.

Bland, J. M., and D. G. Altman, 2000: The odds ratio. *BMJ,* **320,** 1468.

Blumberg, W. G., K. T. Halbert, T. A. Supinie, P. T. Marsh, R. L. Thompson, and J. A. Hart, 2017: SHARPpy: An open source sounding analysis toolkit for the atmospheric sciences. *Bull. Amer. Meteor. Soc.*, **In press**, doi:10.1175/BAMS-D-15-00309.1.

Cerniglia, C. S., and W. R. Snyder, 2002: Development of warning criteria for severe pulse thunderstorms in the Northeastern United States using the WSR-88D. National Weather Service. Eastern Region Technical Attachment No. 2002-03, 14 pp. [Available online at http://docs.lib.noaa.gov/noaa_documents/NWS/NWS_ER/Eastern_Region_Tech_Attachment/TA_2002-03.pdf.]

Craven, J. P., and H. E. Brooks, 2004: Baseline climatology of sounding derived parameters associated with deep, moist convection. *Natl. Wea. Dig*, **28,** 13-24.

Fleiss, J. L., B. Levin, and M. C. Paik, 2003: *Statistical Methods for Rates and Proportions.* 3rd ed. Wiley, 800 pp.

Gensini, V. A., T. L. Mote, and H. E. Brooks, 2014: Severe-thunderstorm reanalysis environments and collocated radiosonde observations. *J. Appl. Meteor. Climatol.*, **53,** 742–751, doi:10.1175/JAMC-D-13-0263.1.

Guillot, E. M., T. M. Smith, V. Lakshmanan, K. L. Elmore, D. W. Burgess, and G. J. Stumpf, 2008: Tornado and severe thunderstorm warning forecast skill and its relationship to storm type. *24th Int. Conf. Interactive Information Processing Systems for Meteor., Oceanogr., and Hydrol.*, New Orleans, LA, American Meteorological Society. [Available online at http://ams.confex.com/ams /pdfpapers/132244.pdf.]

Hurlbut, M. M., and A. E. Cohen, 2013: Environments of Northeast U.S. severe thunderstorm events from 1999 to 2009. *Wea. Forecasting*, **29,** 3-22, doi:10.1175/WAF-D-12-00042.1.

James, R. P., and P. M. Markowski, 2010: A numerical investigation of the effects of dry air aloft on deep convection. *Mon. Wea. Rev.*, **138,** 140–161, doi:10.1175/2009MWR3018.1.

Johns, R. H., and C. A. I. Doswell, 1992: Severe local storms forecasting. *Wea. Forecasting*, **7,** 588–612, doi:10.1175/1520-0434(1992)007<0588:SLSF>2.0.CO;2.

Kingsmill, D. E., and R. M. Wakimoto, 1991: Kinematic, dynamic, and thermodynamic analysis of a weakly sheared severe thunderstorm over northern Alabama. *Mon. Wea. Rev.*, **119,** 262–297, doi:10.1175/1520-0493(1991)119<0262:KDATAO>2.0.CO;2.

Lee, J. W., 2002: Tornado proximity soundings from the NCEP/NCAR reanalysis data. Thesis. Dept. of Meteorology, University of Oklahoma, 61 pp.

McCann, D. W., 1994: WINDEX - a new index for forecasting microburst potential. *Wea. Forecasting*, **9,** 532–541, doi:10.1175/1520-0434(1994)009<0532:WNIFFM>2.0.CO;2.

Mesinger, F., and Coauthors, 2006: North American regional reanalysis. *Bull. Amer. Meteor. Soc.*, **87,** 343–360, doi:10.1175/bams-87-3-343.

Miller, P., and T. Mote, 2017: A climatology of weakly forced and pulse thunderstorms in the Southeast United States. *J. Appl. Meteor. Climatol.*, **In press**.

Miller, P. W., A. W. Black, C. A. Williams, and J. A. Knox, 2016: Quantitative assessment of human wind speed overestimation. *J. Appl. Meteor. Climatol.*, **55,** 1009–1020, doi:10.1175/JAMC-D-15-0259.1.

Moore, J. T., and J. P. Pino, 1990: An interactive method for estimating maximum hailstone size from forecast soundings. *Wea. Forecasting*, **5,** 508–525, doi:10.1175/1520-0434(1990)005<0508:AIMFEM>2.0.CO;2.

Murphy, M., 2017: Preliminary results from the inclusion of lightning type and polarity in the identification of severe storms. Preprints. *8th Conf. on the Meteor. Appl. of Lightning Data*, Seattle, WA, American Meteorological Society, 7.3. [Available online at https://ams.confex.com/ams/97Annual/webprogram/Manuscript/Paper308037/murphy_8mald_paper7.3.pdf.]

Noel, J., and J. C. Dobur, 2002: A pilot study examining model-derived precipitation efficiency for use in precipitation forecasting in the eastern United States. *Natl. Wea. Dig.*, **26,** 3–8.

Púčik, T., P. Groenemeijer, D. Rýva, and M. Kolář, 2015: Proximity soundings of severe and nonsevere thunderstorms in Central Europe. *Mon. Wea. Rev.*, **143,** 4805–4821, doi:10.1175/MWR-D-15-0104.1.

Roberts, R. D., and J. W. Wilson, 1989: A proposed microburst nowcasting procedure using single-Doppler radar. *J. Appl. Meteor.*, **28,** 285–303, doi:10.1175/1520-0450(1989)028<0285:APMNPU>2.0.CO;2.

Stewart, S. R., 1991: The prediction of pulse-type thunderstorm gusts using vertically integrated liquid water content (VIL) and the cloud top penetrative downdraft mechanism. NOAA. Technical Memorandum NWS SR-136, 20 pp. [Available online at http://docs.lib.noaa.gov/noaa_documents/NWS/NWS_SR/TM_NWS_SR_136.pdf.]

Taszarek, M., H. E. Brooks, and B. Czernecki, 2017: Sounding-derived parameters associated with convective hazards in Europe. *Mon. Wea. Rev.*, **145,** 1511-1528, doi:10.1175/MWR-D-16-0384.1.

Thompson, R. L., C. M. Mead, and R. Edwards, 2007: Effective storm-relative helicity and bulk shear in supercell thunderstorm environments. *Wea. Forecasting*, **22,** 102–115, doi:10.1175/WAF969.1.

Thompson, R. L., B. T. Smith, A. R. Dean, and P. T. Marsh, 2014: Spatial Distributions of Tornadic Near-Storm Environments by Convective Mode. *Electronic J. Severe Storms Meteor.*, **8,** 1–22.

Thompson, R. L., R. Edwards, J. A. Hart, K. L. Elmore, and P. Markowski, 2003: Close proximity soundings within supercell environments obtained from the Rapid Update Cycle. *Wea. Forecasting*, **18,** 1243–1261, doi:10.1175/1520-0434(2003)018<1243:CPSWSE>2.0.CO;2.

Weiss, S. J., J. Hart, and P. Janish, 2002: An examination of severe thunderstorm wind report climatology: 1970–1999. Preprints. *21st Conf. Severe Local Storms*, San Antonio, TX, American Meteorological Society, 11B.2. [Available online at https://ams.confex.com/ams/SLS_WAF_NWP/techprogram/paper_47494.htm.]

Wheeler, M., and S. M. Spratt, 1995: Forecasting the potential for central Florida microbursts. NOAA. Technical Memorandum NWS SR-163, 9 pp. [Available online at www.weather.gov/media/mlb/research/SR_TechMemo163.pdf.]

Wolfson, M., 1988: Characteristics of microbursts in the continental United States. *Lincoln Lab Journal*, **1,** 49–74.

Table 4.1. List of the 30 convective parameters computed from the proxy soundings where CAPE, CIN, LCL, LFC, and EL and correspond to convective available potential energy, convective inhibition, lifted condensation level, level of free convection, and equilibrium level, respectively.

Abbrev.	**Full Name**	**Units**
MLCAPE	Mean-layer CAPE	J kg^{-1}
MLCIN	Mean-layer CIN	J kg^{-1}
MLLCL	Mean-layer LCL	m
MLLFC	Mean-layer LFC	m
MLEL	Mean-layer EL	m
K_IND	K index	°C
TT	Total totals	°C
CT	Cross totals	°C
VT	Vertical Totals	°C
PW	Precipitable Water	mm
HGT0	Height of 0°C temperature isotherm	hPa
ApWBZ	Approximate height of 0°C wet bulb temperature	m
W_LOW	Mean low-level mixing ratio	g kg^{-1}
W_MID	Mean mid-level mixing ratio	g kg^{-1}
RH_LOW	Mean low-level relative humidity	--
RH_MID	Mean mid-level relative humidity	--
ThE_LOW	Mean low-level theta-e	K
ThE_MID	Mean mid-level theta-e	K
ML_BRN	Mean layer bulk Richardson number	--
Tc	Convective temperature	°C
PEFF	Precipitation efficiency	--
DCAPE	Downdraft CAPE	J kg^{-1}
WNDG	Wind damage parameter	--
TEI	Theta-e index	°C
MICROB	Microburst composite index	--
SWEAT	Severe weather and threat index	--
0-3-km_SHR	0–3-km vertical wind shear	m s^{-1}
0-6-km_SHR	0–6-km vertical wind shear	m s^{-1}
0-8-km_SHR	0–8-km vertical wind shear	m s^{-1}
EBWD	Effective layer vertical wind shear	m s^{-1}

Table 4.2. RAP error statistics for surface-based CAPE (SBCAPE) and several of the variables listed in Table 4.1. The statistics are presented similarly to Thompson et al. (2003) by providing the mean RAP-derived value, the mean arithmetic error (bias), and the mean absolute error (MAE).

Parameter	Mean	Bias	MAE	R^2
SBCAPE	1354.3	141.3	530.4	0.59
MLCAPE	943.4	112.6	338.0	0.64
MLLCL	1077.4	-32.9	151.8	0.82
Total Totals	44.8	0.51	1.54	0.74
TEI	21.1	-2.30	3.80	0.69
0–3-km Shear	6.33	-0.48	1.38	0.82
0–6-km Shear	8.39	-0.28	1.40	0.88

Table 4.3. WFT, SWS, and SHS day frequency by radar site.

Site	WFT Days	Wind Control	SWS Days	% SWS	Hail Control	SHS Days	% SHS
KAKQ	376	351	25	6.6	363	13	3.5
KAMX	581	569	12	2.1	575	6	1.0
KBMX	376	364	12	3.2	372	4	1.1
KCAE	401	339	62	15.5	377	24	6.0
KCLX	450	407	43	9.6	440	10	2.2
KDGX	426	403	23	5.4	416	10	2.3
KEOX	384	366	18	4.7	382	2	0.5
KEVX	467	449	18	3.9	463	4	0.9
KFCX	408	318	90	22.1	370	38	9.3
KFFC	400	358	42	10.5	387	13	3.3
KGSP	417	334	83	19.9	383	34	8.2
KGWX	362	349	13	3.6	354	8	2.2
KHPX	299	282	17	5.7	294	5	1.7
KHTX	373	343	30	8.0	369	4	1.1
KJAX	555	520	35	6.3	546	9	1.6
KJGX	384	356	28	7.3	377	7	1.8
KLIX	504	492	12	2.4	501	3	0.6
KLTX	452	439	13	2.9	444	8	1.8
KMHX	497	496	1	0.2	495	2	0.4
KMLB	540	532	8	1.5	532	8	1.5
KMOB	451	444	7	1.6	446	5	1.1
KMRX	415	349	66	15.9	384	31	7.5
KMXX	357	346	8	2.2	350	4	1.1
KNQA	356	336	20	5.6	345	11	3.1
KOHX	349	336	13	3.7	345	4	1.1
KPAH	330	305	25	7.6	318	12	3.6
KRAX	367	337	30	8.2	355	12	3.3
KTBW	546	525	21	3.8	535	11	2.0
KTLH	482	461	21	4.4	479	3	0.6
KVAX	457	430	27	5.9	452	5	1.1
Mean	425	398	27	6.7	415	10	2.5

Table 4.4. Summary of convective parameters on SWS days. The “Sites” column indicates the number of spatial subdivisions within which the difference between the SWS mean and the control mean was accompanied by $p < 0.10$; the “percent change” column shows the relative increase or decrease of the mean on SWS days.

Parameter	Sites	Percent change
VT	28	5.1
TT	27	4.2
MLCAPE	25	31.2
MICROB	23	44.0
DCAPE	22	17.3
TEI	22	13.1
MLLCL	21	12.9
ThE_LOW	21	0.9
RH_LOW	20	-5.5
WNDG	19	41.2
CT	19	3.2
Tc	19	5.8
MLEL	18	8.0
SWEAT	14	7.8
W_LOW	10	3.0
K_IND	8	3.8
RH_MID	7	-3.2
ThE_MID	6	0.1
PEFF	6	-3.8
0-6-km_SHR	6	-4.5
0-8-km_SHR	6	-6.5
ApWBZ	5	-0.5
HGT0	4	0.1
W_MID	3	0.0
MLBRN	3	-0.7
PW	2	0.9
0-3-km_SHR	2	-1.2
MLCIN	0	6.6
MLLFC	0	0.9
EBWD	0	-1.9

Table 4.5. Same as Table 4.4, except for SHS days.

Parameter	**Sites**	**Percent change**
VT	27	8.0
TT	27	7.5
CT	21	7.1
PEFF	16	-11.0
MLLCL	15	13.2
HGT0	14	2.4
ApWBZ	14	-6.0
RH_LOW	14	-5.3
DCAPE	13	23.3
MLCAPE	12	28.8
PW	12	-6.7
W_MID	11	-9.2
ThE_MID	10	-0.7
WNDG	10	27.4
RH_MID	9	-7.8
TEI	7	10.4
MICROB	7	21.6
SWEAT	7	10.1
W_LOW	6	-2.1
Tc	6	3.2
0-6-km_SHR	6	9.7
0-8-km_SHR	5	6.9
MLEL	4	3.8
K_IND	3	2.7
ThE_LOW	3	-0.1
0-3-km_SHR	3	5.3
MLCIN	1	17.7
MLLFC	1	4.1
MLBRN	1	-15.8
EBWD	1	9.5

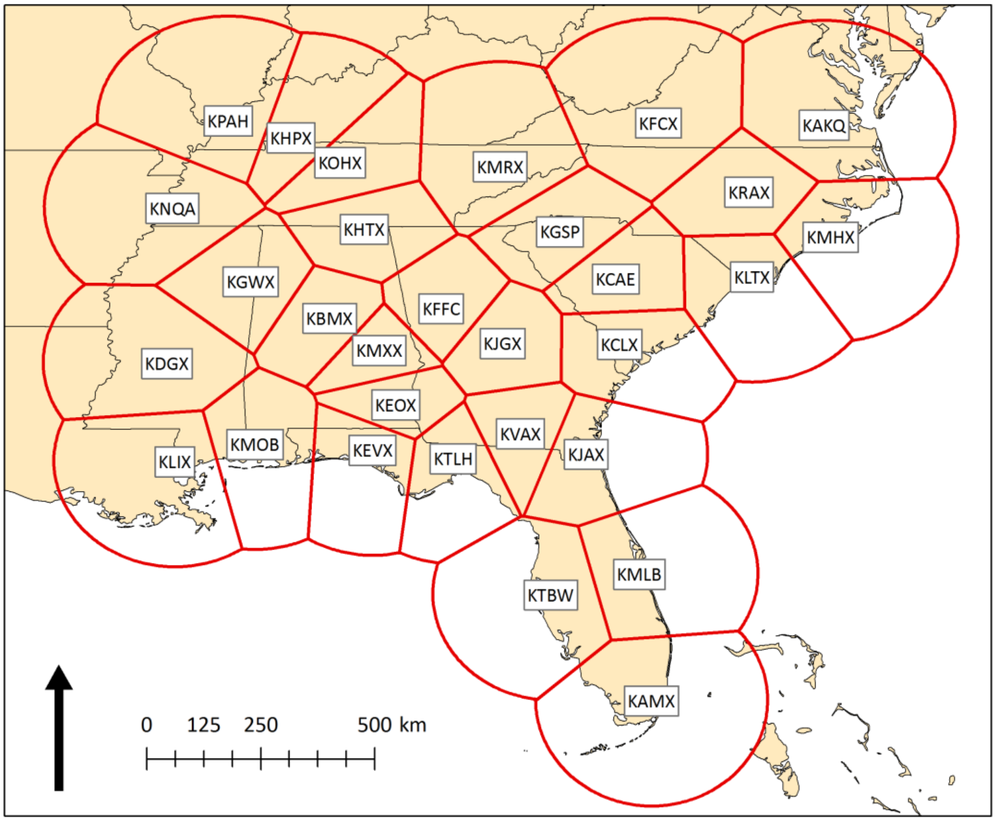

Figure 4.1. WSR-88D sites contributing to the Miller and Mote (2017) WFT climatology.

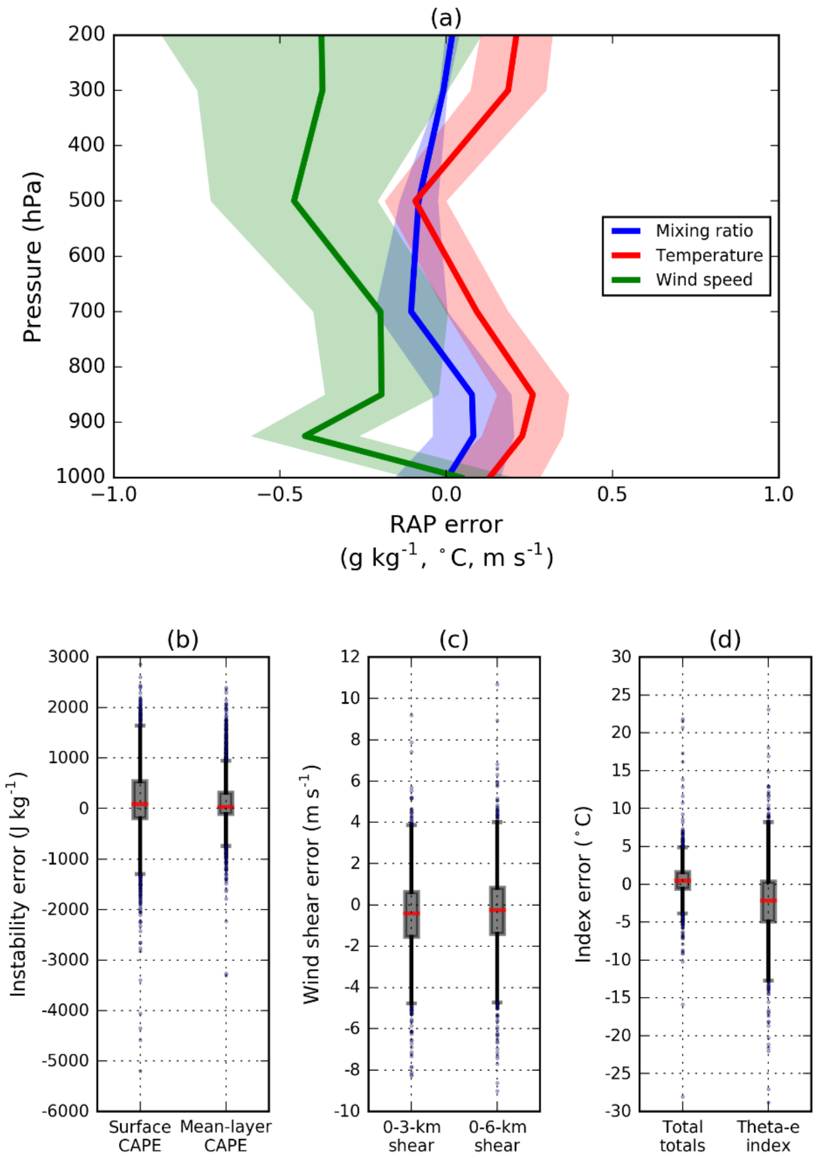

Figure 4.2. Vertical profiles of RAP output errors measured by co-located radiosonde observations (A). Errors were calculated at 1000, 925, 850, 700, 500, 300, and 200 hPa. The 95% confidence interval for the mean error (solid lines) is shaded. Boxplots of the resulting error for six derived quantities is shown in (B)-(D). The interquartile range (IQR), representing the middle 50% of values, is depicted by the gray box. Values lying more than 1.5*IQR from the median (red line) are marked with dots.

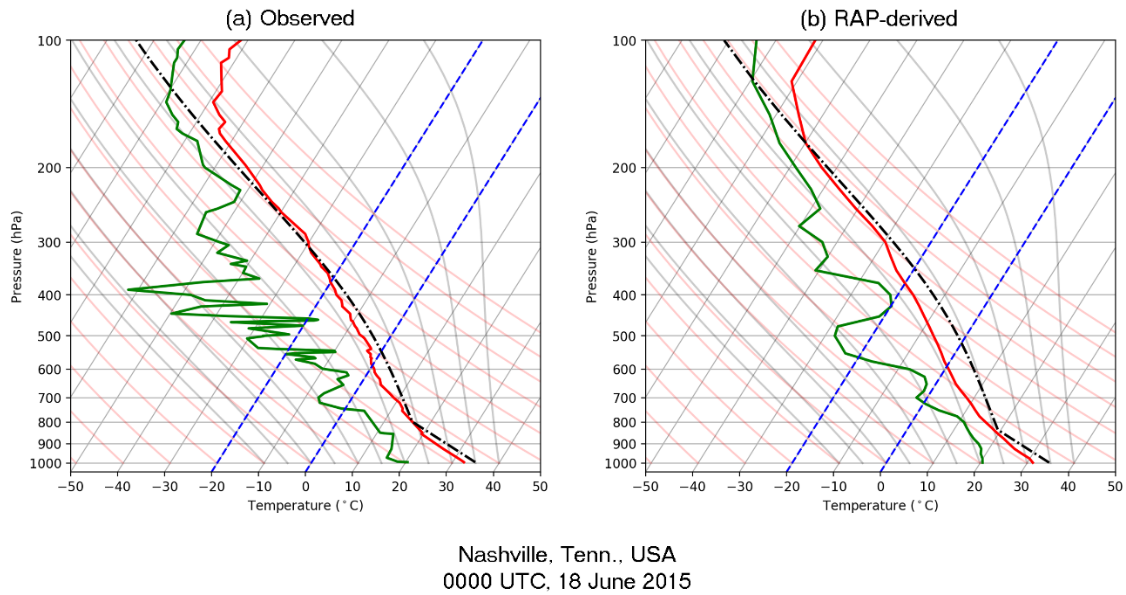

Figure 4.3. Comparison of observed (A) versus RAP-derived (B) soundings for a case when the MLCAPE discrepancy exceeded 1000 J kg^{-1} (observed: 1028 J kg^{-1}; RAP: 2051 J kg^{-1}). Minor mischaracterizations of low-level moisture contributed to a large response in MLCAPE during the vertical integration of the parcel trajectory.

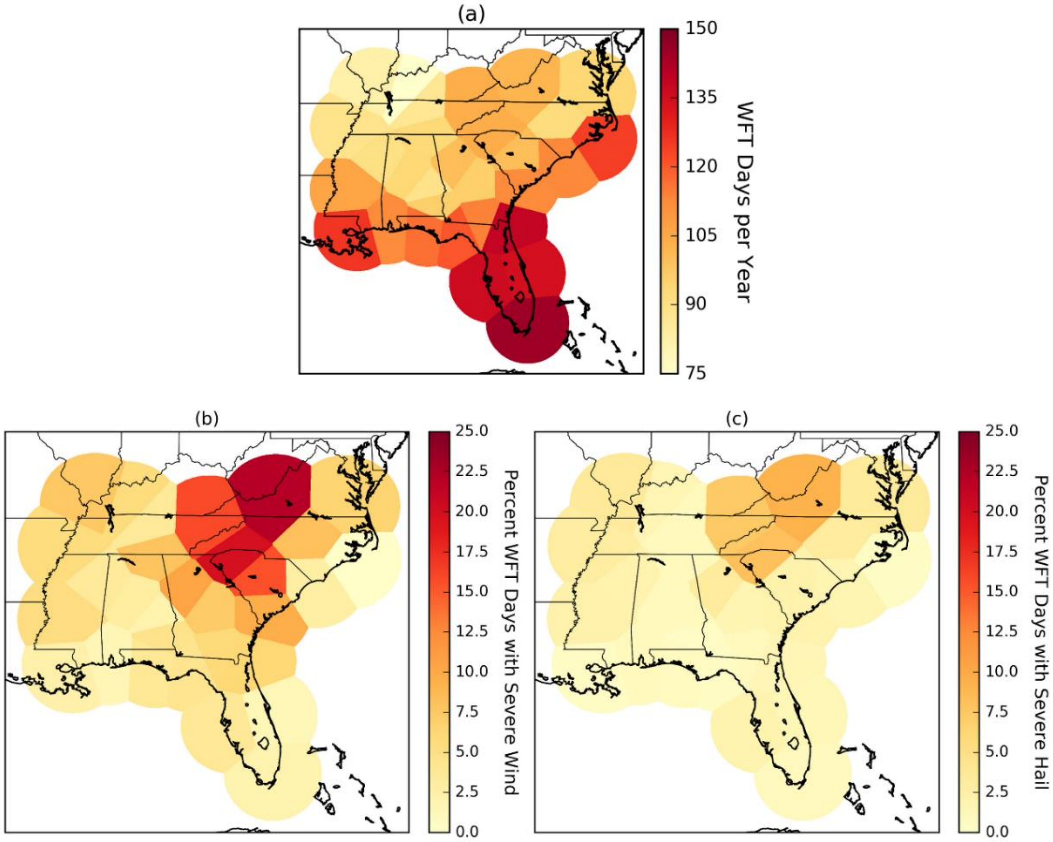

Figure 4.4. Average number of WFT days during the four-year study period (A) compared to the proportion of WFT days associated with severe wind (B) and severe hail (C) events.

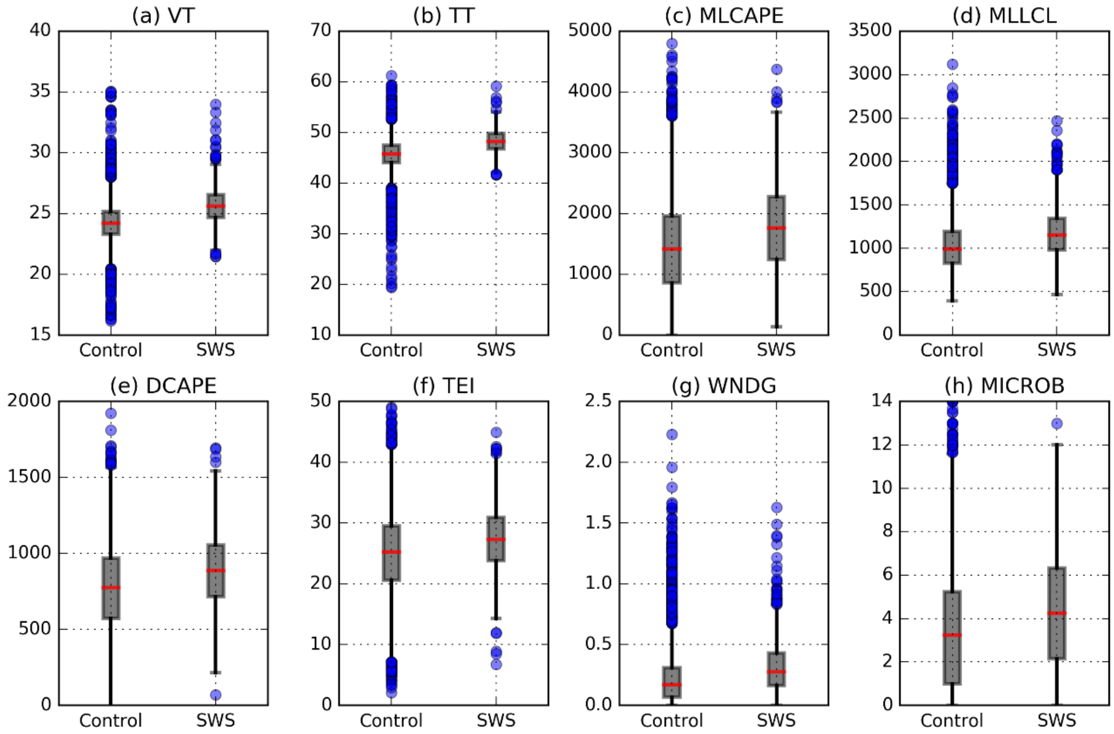

Figure 4.5. Boxplots of selected convective parameters that demonstrated skill in differentiating between the control days and SWS days.

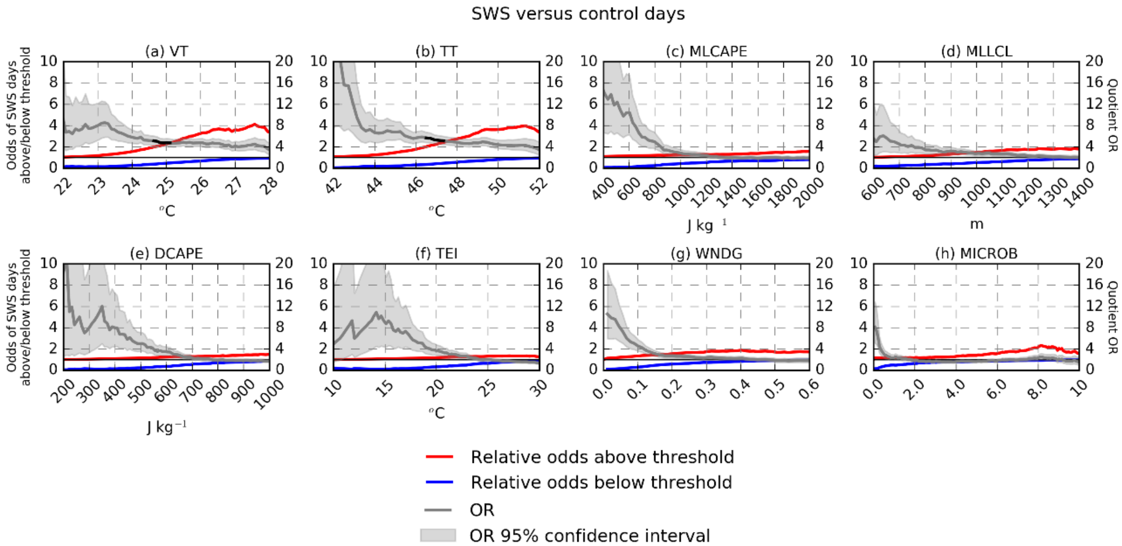

Figure 4.6. ORs for the same eight convective parameters shown in Fig. 4.5. Whenever the OR, defined by Eq. (4.2), results from a numerator (red) ≥2 and a denominator (blue) ≤0.5, then the OR is drawn in black. The left y-axis expresses values corresponding to the OR's numerator and denominator (red and blue lines), and the right y-axis corresponds to the OR value (gray line). At very low and very high threshold values, the variance of the OR may be undefined, and the 95% OR confidence interval cannot be computed.

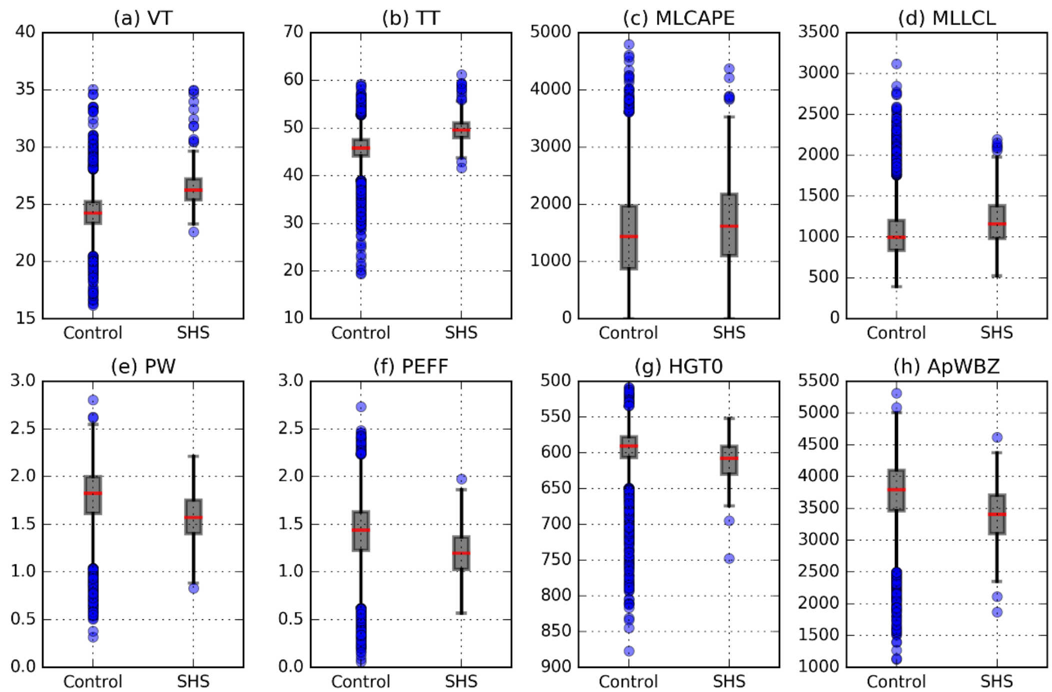

Figure 4.7. Same as Fig. 4.5 except for SHS days. Panes (A)-(D) replicate the same variables shown in Fig. 4.5 whereas (E)-(H) are replaced with four SHS-specific parameters from Table 4.5.

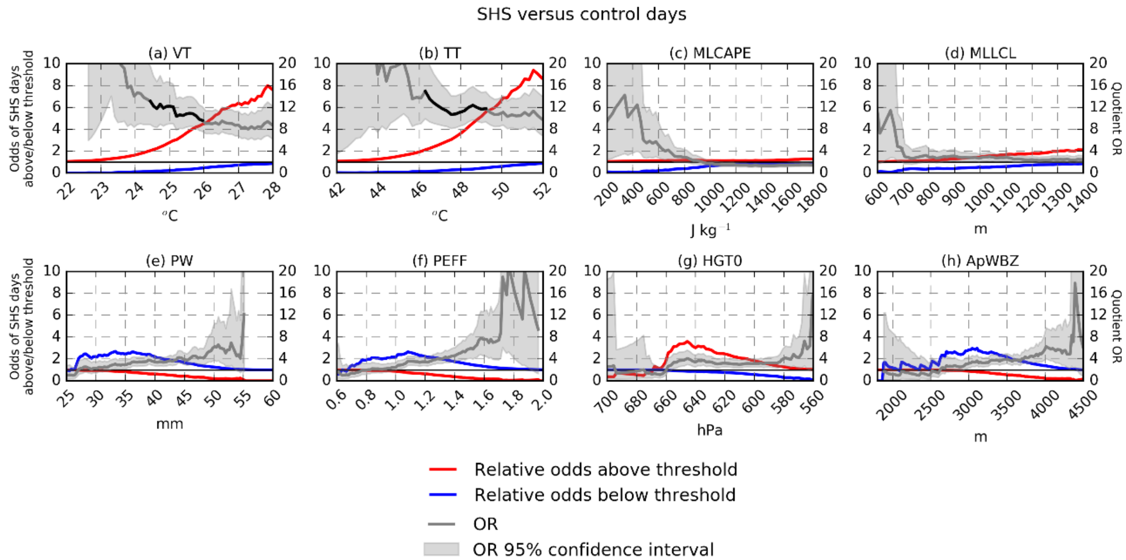

Figure 4.8. Same as Fig. 4.6 except for SHS days. Panes (A)-(D) replicate the same variables shown in Fig. 4.6 whereas (E)-(H) are replaced with four SHS-specific parameters from Table 4.5. At very low and very high threshold values, the variance of the OR may be undefined, and the 95% OR confidence interval cannot be computed.

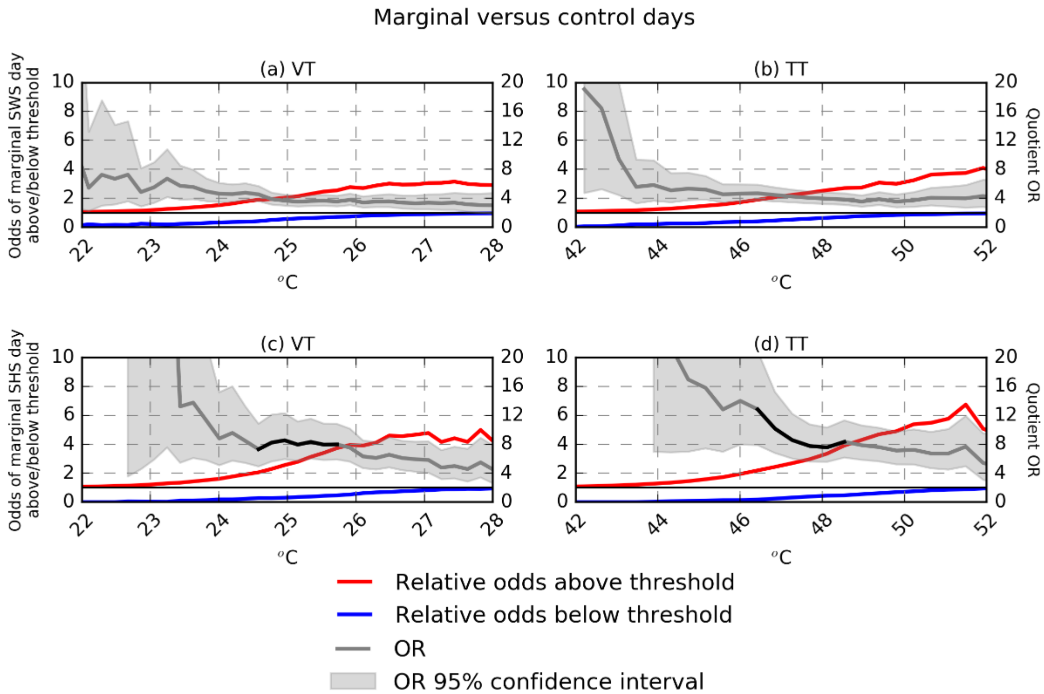

Figure 4.9. Same as Fig. 4.6a-b (A-B) and Fig. 4.8a-b (C-D) except that only marginal SWS and SHS days are used to calculate the OR. At very low and very high threshold values, the variance of the OR may be undefined, and the 95% OR confidence interval cannot be computed.

CHAPTER 5

THE ALGORITHMIC DETECTION OF PULSE THUNDERSTORMS WITHIN A LARGE, MOSTLY NONSEVERE SAMPLE [10]

[10] Miller, P. W., and T. L. Mote. Submitted to *Meteorological Applications*. 22 September 2017.

Abstract

The accurate differentiation of pulse thunderstorms from benign weakly forced thunderstorms (WFTs) is both a historical and contemporary forecasting challenge. Little research has been directed toward WFTs, and the few existing efforts are characterized by small sample sizes and inflated proportions of pulse thunderstorms. The purpose of this study is to determine if pulse thunderstorms can be successfully differentiated from nonsevere WFTs within a large, mostly nonsevere sample, a more operationally realistic scenario. Random forests, a decision-tree-based machine learning technique, is applied to radar, total lightning, and environmental parameters of >84,000 WFTs, of which <1% are pulse thunderstorms. In particular, differential reflectivity (Z_{DR}) fields are mined for occurrences of Z_{DR} troughs, suggested by recent work as an indication of impending downbursts.

The random forest approach struggled to identify pulse thunderstorms from the 84,000-storm sample, but performed accurately in a subset of the most active geographic regions and convective environments. The critical success index (CSI) was 46.0%, which out-performs the U.S. National Weather Service CSI (34.8%) for severe thunderstorm warnings issued on pulse thunderstorms. Unfortunately, the presence of Z_{DR} troughs contributed little skill to the random forest. Though forming at higher rates in pulse thunderstorms (61%) than nonsevere WFTs (5.1%), nonsevere WFTs with troughs were roughly 9x more common than pulse thunderstorms with the same feature.

Overall, the random forest shows promise as a potential decision aid for identifying pulse thunderstorms. Performance may be further improved if collinearity amongst the radar parameters and likely under-reporting of severe weather can be overcome.

5.1 Introduction

Severe weather in synoptically weakly forced environments is often localized, short-lived, and difficult to predict. These storms have consequently been dubbed "pulse thunderstorms" owing to the brevity of their severe weather production and represent a subset of the weakly forced thunderstorms (WFTs) that form without appreciable dynamical support. Though severe weather forecasting and detection is the subject of rigorous study in the United States, comparatively little attention has been given to pulse thunderstorms despite their perennial activity across much of the southern and eastern U.S. (Miller and Mote 2017a). Consequently, pulse thunderstorms remain a challenging subject of the warning decision process (Guillot et al. 2008).

To date, only a handful of large-scale research efforts have engaged this thunderstorm mode. Following World War II, the immense volume of data collected by the Thunderstorm Project (Byers and Braham 1949) informed our concept of the basic thunderstorm lifecycle. The observations collected during the Project are still the most comprehensive available for WFTs despite their age and the antiquated technology that produced them. Though several other research efforts have since revisited WFTs (Browning et al. 1968; Lhermitte and Gilet 1975; Kropfli and Miller 1976; LeMone and Zipser 1980; Miller et al. 1983; Cunning et al. 1986), these studies were handicapped by the temporal and spatial coarseness to their observations, problems described by Kingsmill and Wakimoto (1991).

Unfortunately, despite its exceptional thoroughness and ground-breaking findings, the Thunderstorm Project was not primarily concerned with the severity of the WFTs it observed (Byers and Braham 1949). The team did, however, document a "pressure nose" associated with a narrow swath of high winds along the outflow of a storm. This feature would later be termed a "microburst" (Fujita 1981), and several microburst-related field campaigns were launched during the late 1970s and 1980s (Wilson and Wakimoto 2001). The Northern Illinois Meteorological Research on Downbursts (NIMROD), the Joint Airport Wind Shear (JAWS), and the Microburst and Severe Thunderstorm (MIST) projects thoroughly investigated downburst-producing storms that included, but were not limited to, WFTs.

Fortunately, a number of case studies have observed promising storm-scale signatures associated with severe downbursts. In a dual-polarization radar and photogrammetric study of a microburst-producing WFT, Wakimoto and Bringi (1988) identified a descending reflectivity core, mid-level radial convergence signature, and Z_{DR} trough that accompanied the microburst. As the updraft penetrated above the freezing level and glaciated, the release of latent heat intensified the updraft, enhancing entrainment and leading to mid-level convergence on radar. The Z_{DR} trough resulted from a narrow shaft of small hail (<1 km) penetrating beneath the freezing level. On plan-position indicator scans, this feature appears as a small area of near-zero dB surrounded by higher dB. The latent heat consumption of the melting hail is believed to enhance downdraft cooling and microburst intensity. Most recently, Kuster et al. (2016) and Mahale et al. (2016) performed complementary radar analyses of a downburst-producing multicell thunderstorm, and found the lead time offered by these features to be valuable in forecast operations.

To our knowledge, the only non-case-study radar analysis of pulse convection was conducted by Cerniglia and Snyder (2002). Their study of 89 WFTs found that the maximum echo top of the 45-, 50-, 55-, 60-, and 65-dBZ reflectivity as well as vertically integrated liquid (VIL) density (Amburn and Wolf 1997), probability of hail (POH), and probability of severe hail (POSH) were successful differentiators of pulse thunderstorms, regardless of the type of severe weather the storm produced. However, their sample over-represented pulse thunderstorms with 64 of the 89 storms (72%) tied to severe weather. This is important given that a recent meta-analysis of lightning-based severe weather warning studies found that the studies' reported skill scores were closely related to the proportion of severe storms in the sample (Murphy 2017).

Given that previous work on this topic has been limited to case studies or small sample sizes, the transferability of their findings to a more realistic representation of storms is unknown. This study distinguishes itself from previous efforts by examining a much larger thunderstorm sample, specifically those forming in synoptically quiescent conditions in the Southeast United States. More than 80,000 WFTs, containing <1% pulse thunderstorms, are mined for occurrences of Z_{DR} troughs as well as more general radar, total lightning, and environmental metrics. Machine learning techniques are applied to the dataset with the goal of identifying pulse convection. The purpose of this study is to determine if pulse thunderstorms can be successfully differentiated from nonsevere WFTs within a large, mostly nonsevere sample.

5.2 Data and methods

5.2.1 Weakly forced thunderstorm dataset

The study relies upon the WFT and pulse thunderstorm dataset created by Miller and Mote (2017; hereafter MM17). The original 15-yr dataset (2001–2015) includes 885,496 WFTs extracted from composite reflectivity imagery from 30 radar sites in the

Southeast U.S. (Fig. 5.1). WFTs were identified as spatiotemporally contiguous areas of 40-dBZ composite reflectivities that also formed in weakly sheared environments. Miller and Mote (2018) added to this dataset by calculating thermodynamic and kinematic environmental parameters for each WFT between 2012–2015 using the Rapid Refresh model (Benjamin et al. 2016). Though Miller and Mote (2018) calculated 30 environmental parameters, only six (vertical totals, total totals, and CAPE, CIN, LCL, and LFC for the mean-layer parcel) that they showed to be relatively reliably replicated by the Rapid Refresh are considered in this analysis.

For this study, 12 new radar variables (Table 5.1) as well as total lightning observations are added to the Miller and Mote (2018) database. However, the dataset is narrowed to contain only the 84,664 WFTs that initiated over land during June and July 2012–2015. These months were shown by MM17 to be the seasonal maximum for pulse thunderstorm activity. Pulse thunderstorms constitute 0.97% (819/84,663) of WFTs in the dataset, with the severe weather reports (winds ≥ 26 m s^{-1}, hail ≥ 2.54 cm in diameter, or a tornado) being furnished by *Storm Data*.

5.2.2 Addition of new radar-derived measurements

The 12 new radar fields shown in Table 5.1 were selected for their ability to discern features that previous research has advocated as indicators of pulse thunderstorm potential (Wakimoto and Bringi 1988; Paxton and Shepherd 1993; Cerniglia and Snyder 2002). The reflectivity products (N0Q, N1Q, N2Q, N3Q, NAQ, and NBQ) were selected to detect suspended high reflectivity cores whereas the differential reflectivity product (N0X) was used to infer the proximity of a hail shaft near the surface. The radar products were regridded from their native, radial format to the same 0.01˚-resolution (~1 km) Cartesian grid used by MM17 with the NOAA Weather and Climate Toolkit (https://www.ncdc.noaa.gov/wct/). Whenever a product in Table 5.1 was collocated with a WFT (i.e., recorded at the same latitude and longitude during the same volume scan), its value was appended to the MM17 dataset. The altitude of the beam above radar level was also calculated at each grid cell (as described in Appendix B) to accompany all reflectivity-related observations.

As mentioned in the Introduction, Z_{DR} troughs are not identified purely by their Z_{DR} value, but by the spatial structure of the Z_{DR} field. Thus, each Z_{DR} image was processed to label local Z_{DR} minima, and note the presence of these features coinciding with the WFTs documented by MM17. Figure 5.2 shows an example of this five-step processing workflow. A minimum filter was applied to a 3x3 moving neighborhood of cells, with all cells in the block reset to the minimum value in the block. The original Z_{DR} field was then compared to the filtered field, and any values that remained unchanged (i.e., they served as the minimum for their 3x3 neighborhood) were considered as possible Z_{DR} troughs. The difference between the local minima and the median value of its surrounding cells was also recorded. Potential Z_{DR} troughs were further required to be near-zero (-0.5–0.5 dB), could not be less than 5 dB from its median surrounding Z_{DR}, and be collocated with a base reflectivity (N0Q) of at least 50 dBZ. These criteria were informed by consulting the characteristics of Z_{DR} troughs documented by Wakimoto and Bringi (1988) and Kuster et al. (2016).

Many WFT grid cells did not receive values for every radar product in Table 5.1. For instance, the higher-tilt scanning angles commonly overshot convection at greater distances from the radar. Additionally, the National Weather Service (NWS) was still in the process of upgrading the WSR-88D network with dual-polarization capabilities in June 2012, the first month of the data set used here. Eighteen of the 30 WSR-88Ds used in this study had already received the upgrade by June 2012. All 30 had received the upgrade by June 2013. In any instances where a radar product was unavailable, rather than excluding the storm, the attributes were recorded as “missing” and the storm was retained.

In addition to the purely radar-based products described above, five post-processed radar parameters (Table 5.1) were also paired with WFTs if they were collocated in space and time. Enhanced echo tops (EET) and digital vertically integrated liquid (DVL) were selected based on the results of Cerniglia and Snyder (2002), who testing the coarser-resolution versions of these products. Additionally, Amburn and Wolf (1997) showed that the ratio of these two parameters, VIL density, is also a reliable hail indicator that is robust to ranging effects occurring when storms are too near the radar to be fully sampled. Probability of hail (POH), probability of severe hail (POSH), and the maximum estimated hail size (MEHS) were also retrieved based on the results of Cerniglia and Snyder (2002). These products are calculated for each storm centroid identified by the storm cell identification and tracking (SCIT) algorithm (NOAA 2006). The POH calculation is based on the presence of high reflectivities located above the freezing level whereas POSH and MEHS are determined using empirical relationships derived from the severe hail index (SHI) introduced by Witt et al. (1998b). If a storm was not large or strong enough to receive a SCIT centroid, which also initiated the POH, POSH, and MEHS calculations, then these values were reported as “missing.” Table 5.1 provides a simple key relating the radar products to the abbreviations introduced in this section.

5.2.3 Total lightning observations

Total lightning data, the sum of cloud-to-ground and intracloud flashes, from the Earth Networks Total Lightning Network (ENTLN) were also integrated into the dataset. The ENTLN is a ground-based network of wideband sensors (1 Hz to 12 MHz) which can detect both very high frequency (VHF) and very low frequency (VLF) emissions of cloud-to-ground and intracloud flashes, respectively (Liu and Heckman 2011). Though cloud-to-ground flashes emit a VLF signal which can travel great distances and be detected with high efficiency, intracloud flashes emit VHF energy which can only be detected if a line-of-sight exists to nearby sensors (Cummins and Murphy 2009). Consequently, the intracloud flash detection efficiency suffers in areas of low sensor density and complex terrain. The ENTLN was operational during the entire 2012–2015 period; however, the continual addition of sensors to the network, upgrades to the waveform processing algorithm (Zhu et al. 2017), as well as the issues described above caused the detection efficiency to vary across the spatial and temporal zones of study. Each ENTLN flash was georeferenced with a latitude and longitude and given a timestamp. Flashes were paired with WFT-attributed grid cells and summed by the volume scan during which they occurred. This pairing effectively created a ~1-km, ~5-min total lightning flash density history for each WFT.

5.2.4 Identification of characteristic radar and total lightning attributes of pulse thunderstorm

Given the enormous volume of four-dimensional (x, y, z, t) data being considered, radar parameters were necessarily reduced into a series of one-dimensional values.

Following the methods of Cerniglia and Snyder (2002), radar information was summarized by taking the most extreme values observed at any location within the storm during the its entire lifetime. Table 5.2 shows the final list of summarized radar, total lightning, and environmental variables that were compared against storm severity.

The “random forests” machine learning procedure was employed to distinguish pulse thunderstorms from nonsevere WFTs using the characteristics in Table 5.2. Random forests was selected for its reported robustness to “noise” within the dataset (Breiman 2001a) and its successful precedent in the atmospheric sciences, several of which have included radar data. Previous such applications include near-term predictions of mesoscale convective system formation (Ahijevych et al. 2016), storm mode classification (Gagne et al. 2009), and quantitative precipitation forecasts (Gagne et al. 2014). In this context, “noise” includes any number of processes not captured by any of the variables (e.g., cell interactions, mid-altitude convergence, etc) as well as errors within the dataset (e.g., severe/nonsevere misclassifications, Rapid Refresh errors, etc). Although random forest classification is often called a “black box” for its complex and unintuitive structure, it has been demonstrated to perform more accurately than a single decision tree (Breiman 2001b). Given that the purpose of this paper is to assess the possibility of successfully identifying pulse thunderstorms, by any means, the accuracy of random forests was prioritized above the interpretability of a single tree.

A random forest consists of an ensemble of individual decision trees with each tree trained on a subset of the available variables and storms. Each tree in the forest “votes” for a pulse versus nonsevere designation with the most popular category representing the final designation (Breiman 2001a). The forest was grown using the JMP Pro 13 statistical software package with the 13 radar and lightning variables and six convective environmental parameters shown in Table 5.2. One-third of the dataset was set aside as a validation portion. Eight storms were required to split a branch, and 10 of the 19 radar, lightning, and environmental variables were sampled to form each tree. Tree splits were determined by optimizing the LogWorth statistic, which is a transformation of the chi-square p-value (Sall 2002). The LogWorth increases as the split variable and its split value lead to more dramatic segregations of pulse thunderstorms from nonsevere WFTs. The number of splits was capped at 200, and each forest was limited to 100 trees.

Four traditional forecast verification parameters are used to measure the performance of the random forest: probability of detection (POD), false alarm rate (FAR), critical success index (CSI), and the Heidke skill score (HSS) described by Doswell et al. (1990). Because of the infrequency of pulse thunderstorms in the dataset, the HSS is better designed to credit the skill required to extract these events against the overwhelming likelihood of selecting a nonsevere WFT by chance.

5.2.5 Limitations

Due to the volume of data contributing to the analysis, storms were summarized by their most extreme values. This step, though necessary for computational purposes, effectively removes the temporal component of each storm. However, for a forecaster, the temporal component often offers insight toward severe weather potential, especially for maximizing the lead time of the warning. Though it is uncertain whether the maximum values ingested by the tree could still provide lead time on warnings, lead time is not a consideration of this study. The absence of temporal information will be further discussed in Section 5.4.

5.3 Results

5.3.1 Random forest classification

The random forest was generated using the dataset and forest settings described in Section 5.2.4. Despite the suitability of a random forest for this task, it nonetheless struggled to reliably identify pulse thunderstorms. The algorithm performed more accurately on the training storms (CSI=42%) than the validation set (CSI=24%), but neither performance was strong. Table 5.3 contains the complete contingency table outcomes and skill statistics for the validation sample. Though generally robust to noise, the possible mislabeling of genuine pulse thunderstorms as "nonsevere" storms may explain the poor accuracy (Alpaydin 2010, p. 192). The deficiencies of *Storm Data* are well-documented, including spatial and temporal errors (Williams et al. 1999), overestimation of wind speeds (Miller et al. 2016), skewness toward locations receiving a severe weather warning (Lenning et al. 1998), concentration in highly populated areas (Weiss et al. 2002), etc. The latter shortcoming is particularly relevant in this study. Because the severe weather associated with pulse thunderstorms tends to be brief, isolated, and only marginally severe, the likelihood of these events being reported outside of densely populated areas is much lower.

The random forest was accordingly retrained with all storms weighted by the population density of their mean latitude and longitude. Population density was characterized using the Global Population of the World version 4 (GPWv4), a ~1-km gridded population density product maintained by Columbia University (CIESN 2016). The GPWv4 was aggregated to 25-km to dampen high values in downtown districts of major cities and better characterize the general differences between highly populated and sparsely populated areas of the Southeast U.S. Under this framework, the most confident severe/nonsevere designations (i.e., those that occurred in high population areas) are prioritized. The weighted forest performed more much effectively on the training dataset, achieving a CSI of 74% and HSS of 0.85. However, the CSI of the validation dataset decreased to 20% with a HSS of 0.33. The deterioration of skill from the training to validation suggests that the forest is "overfitting" the training sample. The forest conforms too tightly to the noise of the training storms, and loses its flexibility to accurately accommodate a new sample of storms.

To reduce overfitting, the dataset was narrowed to include only storms forming in favorable convective environments and in areas where pulse thunderstorms are most common. In this "concentrated" subset, the signal-to-noise is higher, and the complexity of the trees can be reduced. The concentrated subset consisted of the 2,299 WFTs (with 6.1% pulse thunderstorms) that (1) occurred in the KFCX and KGSP radar polygons (Fig. 5.1) and (2) formed in environments with total totals (TT) greater than or equal to 49 ˚C. Miller and Mote (2018) showed that these two regions contained the highest frequencies of pulse thunderstorms in the Southeast U.S. Further, TT ≥ 49 ˚C was associated with a roughly 5x increase in pulse thunderstorm likelihood. Because the subset contained fewer pulse thunderstorms (n=141), performance statistics for the validation dataset were sensitive to the storms that were captured in the 33% random validation sample. Thus, skill scores for the third forest, trained and validated on this concentrated subset, were averaged for ten training/validation dataset combinations. The concentrated forest performed more accurately, particularly for the validation dataset. The CSI increased to 90% (HSS = 0.95) for the training dataset and 46% (HSS = 0.61) for the validation storms. For reference, Guillot et al. (2008) calculated the CSI for NWS severe thunderstorm warnings issued on pulse thunderstorms to be 34.8%. Although deterioration in the skill scores between the training and validations samples suggests that overfitting still hampers performance, additional attempts to reduce the complexity of the forest yielded only negligible improvements.

The relative utility of the variables to the pulse/nonsevere classification can be ranked by summing the value of the likelihood-ratio chi-square statistic (G^2) at every split in the forest based on each variable. G^2 is proportional to the ratio of the observed proportions of pulse and nonsevere WFTs after versus expected proportions prior to the split. This statistic follows a chi-squared distribution and yields very similar results to the LogWorth statistic referenced in Section 5.2.4. [See the JMP documentation (JMP 2017) for more information about the parameter rankings.] Consequently, a variable's importance reflects both how frequently it served as a split and how effectively it segregated pulse and nonsevere WFTs when it did. For the third forest, the most valuable parameter to differentiate between pulse thunderstorms and benign WFTs was VILD, contributing 28.3% of the total G^2. VILD was closely followed by its two constituent terms, VIL and ET, which combine to account for an additional 28.9% of the total G^2. HGT REF was responsible for 9.5%, and the other 15 parameters were collectively responsible for the remaining total. Table 5.4 includes a ranking of all 19 parameters based on their contributions to the forest.

5.3.2 Z_{DR} troughs

A unique contribution of this work is the inclusion of Z_{DR} trough information. Unfortunately, Z_{DR} TROF, Z_{DR} GRD, and HGT TROF contribute a combined 1.9% of the total G^2. As shown in Table 5.4, decision tree nodes based off these variables were the least effective of all 19 variables at segregating the dataset into severe and nonsevere subgroups. The paltry contributions of Z_{DR}-related variables is likely driven by the infrequency of Z_{DR} troughs within the dataset. Roughly 11% of WFTs in the 84,000-storm dataset formed before dual-polarization capabilities existed at their nearest WSR-88D. Of the WFTs with Z_{DR} information, only 5.6% of WFTs possessed a Z_{DR} trough at some point during their lifetime. Thus, 95% of the WFTs in the dataset had no HGT TROF or Z_{DR} GRD variables for the random forest to leverage.

However, the Z_{DR} trough may yet have the potential to be useful forecasting tool. For instance, Z_{DR} troughs occurred at a much higher rate among pulse thunderstorms (61%) than nonsevere WFTs (5.1%). In fact, WFTs with a Z_{DR} trough were roughly 28x more likely to be a pulse thunderstorm. Figure 5.3 also shows that for storms with this feature, the trough was typically "deeper," meaning Z_{DR} GRD was larger for pulse thunderstorms (pooled *t*-test yields $p < 0.01$). Nonsevere WFTs showed a mean Z_{DR} GRD of -0.99 whereas pulse thunderstorms had a mean of -1.49. Despite these encouraging differences, there remained an abundance on nonsevere WFTs with Z_{DR} troughs. For perspective, the FAR for designating severity solely based on a Z_{DR} trough would exceed 90% (FAR=90.3%; POD=60.8%; CSI=9.2%; HSS=0.15). There were roughly 9x more nonsevere WFTs with troughs than pulse thunderstorms with the same feature.

5.3.3 Examination of performance hurdles

Although a relatively successful forest was trained on a concentrated subset of WFTs, the poor performance on the all-inclusive dataset was further examined. Figure 5.4 explores the performance struggles in greater detail with a principal components analysis (PCA) on 16 of the 19 variables. (The Z_{DR}-related variables were omitted given the infrequency of Z_{DR} troughs and the "missing" data that resulted.) The PCA shows that the 16 radar, lightning, and environmental parameters are largely co-linear. The first principal component (PC1), strongly correlated with the radar variables, and the second principal component (PC2), correlated to the environmental variables (Table 5.5), together capture over half (53.2%) of the variability in the dataset. Even MFD, which is not radar-derived, co-varies with the radar-detected parameters. The correlation coefficients between MFD and MREF (0.41), VIL (0.70), and MEHS (0.71) are relatively large.

Regardless of the specific product, any radar-sensed parameter is ultimately related to the number and size of hydrometeors in the atmosphere. Though individual products can offer more detailed information about their phase, altitude, total concentration, etc, covariance is nonetheless unavoidable. Further, lightning activity results from the static charge accumulated through mixed-phase hydrometeor collisions (Williams 1988). Storms with greater reflectivities (i.e., greater concentrations of hydrometeors) will also be favored for increased flash densities. Even the inclusion of storm-scale lightning information only offers incremental insight beyond the information gleaned by reflectivity alone. Additionally, larger and more abundant hydrometeors (i.e., strong reflectivities) must be held aloft by strong updrafts. Thus, convective environmental parameters are also weakly co-linear with the radar-sensed information. For instance, the correlation coefficient between VT and VIL is 0.33. Even though PC1 largely captures the radar variables, it is also weakly correlated with the environmental information as well. This result is evident in Fig. 5.4b where all of the environmental variables except CIN point in the same direction as the radar variables in PC1 axis.

Figure 5.5 illustrates another dimension of the performance challenge. All the WFTs are plotted in a 2-d data space using PC1 and PC2. Figure 5.5a shows that pulse thunderstorms are largely concentrated in the portion of the data space with large PC1 scores. However, Fig. 5.5b shows that this same sub-region of the dataset is also densely occupied by nonsevere WFTs. This result is problematic for not only random forests, but any predictive modeling procedure. Conceptually, machine learning techniques seek to define sub-regions of the n-dimensional data space where one classification is dominant. Even though pulse thunderstorms are clearly concentrated in one area of data space, they are still not the *dominant* storm type in much of this sub-region. Consequently, the random forest frequently misclassifies pulse thunderstorms as nonsevere WFTs due to the abundance of nonsevere storms nearby. The result is a low POD, which drives the low CSIs apparent in the most inclusive dataset (Table 5.3). This pattern will be further discussed in the next section.

5.4 Discussion

As stated in Section 5.1, the purpose of this research is to assess the transferability of previous pulse-thunderstorm forecasting guidelines to a large, mostly null sample. The results clearly indicate that many nonsevere WFTs possess similar radar, lightning, and environmental characteristics to pulse thunderstorms, diminishing the possibility of differentiating the two based on these variables. However, in certain settings (i.e., active regions and favored environments), such a task is possible. Based on these findings, algorithmic methods show promise for pulse thunderstorm detection, especially if higher quality data can be incorporated.

Section 5.3 identified two key limiting performance factors: collinearity and under-reporting in *Storm Data*. Though Cerniglia and Snyder (2002) identified a number of potentially useful radar-derived differentiators, Section 5.3.3 showed that they are mostly redundant, and efforts to provide orthogonal radar-based data vectors were met with limited success. For instance, because Z_{DR} corresponds to the shape, rather than the size and concentration, of hydrometeors, the addition of this parameter was thought to compliment the other radar parameters. However, the infrequency of Z_{DR} troughs and the abundance of nonsevere trough-possessing storms largely neutralized its ability to differentiate pulse thunderstorms from nonsevere WFTs. This result leads to two possibilities: (1) that the presence of small hail below the freezing level does not regularly translate into severe microburst winds, or (2) the Z_{DR} trough signature is more complex than could be discerned by the relatively simple detection algorithm used here. Future studies may consider using enhanced image processing algorithms to develop more robust methods of automatically identifying Z_{DR} troughs.

Another significant impediment that emerged in Section 5.3.1 was the likely under-reporting of pulse thunderstorms in *Storm Data*. As Fig. 5.5 demonstrated, the close proximity of pulse thunderstorms and nonsevere WFTs in the 2-d data space caused the pulse thunderstorm signal to be overwhelmed by the abundant nonsevere WFTs surrounding them. Given the isolated, brief, and marginal nature of pulse-thunderstorm-generated severe weather, it is reasonable to believe that many of these "nonsevere" WFTs did in fact produce severe weather that was not recorded in *Storm Data*. If these storms were recorded as severe, rather than nonsevere, the random forest would be more adept at labeling pulse thunderstorms in these sections of data space, and overfitting would also likely relax. This possibility is reasonable in light of recent studies using high-resolution storm reports (Ortega et al. 2009; Blair et al. 2017). For instance, during the Hail Spatial and Temporal Observing Network Effort (HailSTONE) field project, Blair et al. (2017) found that 32% of the severe-hail-producing storms sampled by field observers lacked a corresponding *Storm Data* report. Additionally, *Storm Data* hail diameters consistently under-represented the maximum hail diameters sampled by the field team.

Although pulse thunderstorms and nonsevere WFTs were frequently characterized by similar values of the radar, lightning, and environmental variables considered here, the storms may be more clearly separated in unconsidered dimensions (i.e., additional non-collinear parameters). For instance, the presence and/or strength of a mid-level convergence signature is one possibility supported by previous research. Similarly, as referenced in Section 5.2.5, the time rates of change of radar and lightning variables may also be insightful. For instance, Schultz et al. (2011) determined that the time derivative of the total flash rate, not the flash rate itself, was a useful indication of impending severity. Paxton and Shepherd (1993) identified VIL and ET growth (decay) rate as indicators of strengthening (collapsing) updrafts and subsequent severe weather. Future research might consider adding time derivatives of radar variables to the forest instead of maximum values. The inclusion of additional, orthogonal radar and lightning parameters may ultimately help reduce the complexity of the random forest procedure, and may support the eventual use of a single, more interpretable tree.

5.5 Conclusion

This study assessed the feasibility of detecting pulse thunderstorms within a large, mostly nonsevere sample of WFTs. Although previous studies have investigated the environments and radar characteristics of pulse convection, these works have traditionally contained unrealistic proportions of pulse thunderstorms. Consequently, the frequency of nonsevere WFTs that also possess these characteristics, confounding the severe weather detection, is uncertain. With pulse thunderstorms constituting <1% of this study's sample, a random forest struggled to correctly differentiate pulse thunderstorms from nonsevere WFTs in the broadest sample. However, accurate performance (CSI=46%; HSS=0.61), even surpassing comparable NWS skill measures, was achieved for a concentrated subset of WFTs that occurred in geographically favorable areas and favorable convective environments. However, even in this concentrated subset, pulse thunderstorms only represented 6.1% of the sample. Overall, performance was hindered by collinearity of the radar and lightning variables and hypothesized under-reporting of pulse thunderstorm-related severe weather.

Ultimately, the results of this study demonstrate that algorithmic modeling methods, such as random forests, are promising means of pulse thunderstorm detection, given the relatively strong performance in the concentrated subset. Meanwhile, in the short term, these findings aid forecasters by identifying the radar variables that most strongly differentiated between pulse thunderstorms and nonsevere WFTs. The random forest decision-making structure was dominated by VILD as well as its two constituent terms, VIL and ET. Additionally, Z_{DR} troughs, though contributing little to the random forest, did show promise as a potential pulse thunderstorm indicator. Storms with Z_{DR} troughs were 28x more likely to produce severe weather, and severe trough-possessing storms were also characterized by a “deeper” Z_{DR} trough. Nonetheless, the number of pulse thunderstorms with Z_{DR} troughs was dwarfed by nonsevere WFTs with the same feature.

The results of this study raise important questions regarding Z_{DR} trough characteristics, which should serve as the focus of future research. Are there substantive differences between the Z_{DR} troughs of nonsevere WFTs and pulse thunderstorms? Did nonsevere trough-featuring WFTs actually produce severe weather that was simply unreported? Additionally, future work might expand the parameters ingested by the random forest to include time derivatives of radar and lightning behavior. With the addition of refined Z_{DR} trough information and radar-based time derivatives to the random forest, the complexity of the algorithm can hopefully be reduced until is easily interpretable by severe weather warning meteorologists.

5.6 Acknowledgements

The authors thank Lynne Seymour for her comments on an earlier version of this manuscript.

5.7 References

Ahijevych, D., J. O. Pinto, J. K. Williams, and M. Steiner, 2016: Probabilistic forecasts of mesoscale convective system initiation using the random forest data mining technique. *Wea. Forecasting*, **31,** 581-599.

Alpaydin, E., 2010: *Introduction to Machine Learning.* 2nd ed. The MIT Press, 415 pp.

Amburn, S. A., and P. L. Wolf, 1997: VIL density as a hail indicator. *Wea. Forecasting*, **12,** 473–478.

Benjamin, S. G., and Coauthors, 2016: A North American hourly assimilation and model forecast cycle: The Rapid Refresh. *Mon. Wea. Rev.*, **144,** 1669–1694, doi:10.1175/MWR-D-15-0242.1.

Blair, S. F., and Coauthors, 2017: High-resolution hail observations: Implications for NWS warning operations. *Wea. Forecasting*, **32,** 1101–1119.

Breiman, L., 2001a: Random Forests. *Machine Learning*, **45,** 5–32, doi:10.1023/A:1010933404324.

——, 2001b: Statistical modeling: The two cultures (with comments and a rejoinder by the author). *Statistical science*, **16,** 199–231.

Browning, K., T. Harrold, A. Whyman, and J. Beimers, 1968: Horizontal and vertical air motion and precipitation growth, within a shower. *Quart. J. Roy. Meteorol. Soc.*, **94,** 498-509.

Byers, H. R., and R. R. Braham, 1949: *The Thunderstorm: Report of the Thunderstorm Project.* US Government Printing Office, 287 pp.

Center for International Earth Science Information Network, 2016: Documentation for the Gridded Population of the World, Version 4. http://dx.doi.org/10.7927/H4D50JX4.

Cerniglia, C. S., and W. R. Snyder, 2002: Development of warning criteria for severe pulse thunderstorms in the Northeastern United States using the WSR-88D. National Weather Service. Eastern Region Technical Attachment No. 2002-03, 14 pp. [Available online at http://docs.lib.noaa.gov/noaa_documents/NWS/NWS_ER/Eastern_Region_Tech_Attachment/TA_2002-03.pdf.]

Cummins, K. L., and M. J. Murphy, 2009: An overview of lightning locating systems: history, techniques, and data uses, with an in-depth look at the US NLDN. *IEEE Trans. Electromagn. Compat.*, **51,** 499–518, doi:10.1109/temc.2009.2023450.

Cunning, J. B., H. W. Poor, and M. Demaria, 1986: An investigation of the development of cumulonimbus systems over south Florida. Part II: In-cloud structure. *Mon. Wea. Rev.*, **114,** 25-39.

Doswell, C. A., R. Davies-Jones, and D. L. Keller, 1990: On summary measures of skill in rare event forecasting based on contingency tables. *Wea. Forecasting*, **5,** 576–585, doi:10.1175/1520-0434(1990)005<0576:OSMOSI>2.0.CO;2.

Fujita, T. T., 1981: Tornadoes and downbursts in the context of generalized planetary scales. *J. Atmos. Sci.*, **38,** 1511–1534.

Gagne, D. J., A. McGovern, and J. Brotzge, 2009: Classification of convective areas using decision trees. *J. Atmos. Oceanic Technol.*, **26,** 1341-1353, doi:10.1175/2008JTECHA1205.1.

Gagne, D. J., A. McGovern, and M. Xue, 2014: Machine learning enhancement of storm-scale ensemble probabilistic quantitative precipitation forecasts. *Wea. Forecasting*, **29,** 1024–1043, doi:10.1175/WAF-D-13-00108.1.

Guillot, E. M., T. M. Smith, V. Lakshmanan, K. L. Elmore, D. W. Burgess, and G. J. Stumpf, 2008: Tornado and severe thunderstorm warning forecast skill and its relationship to storm type. *24th Int. Conf. Interactive Information Processing Systems for Meteor., Oceanogr., and Hydrol.*, New Orleans, LA, American Meteorological Society. [Available online at http://ams.confex.com/ams/pdfpapers/132244.pdf.]

JMP, 2017: JMP 12 Online Documentation. Accessed 20 July 2017. [Available online at http://www.jmp.com/support/help/Statistical_Details_8.shtml#1277120.]

Kingsmill, D. E., and R. M. Wakimoto, 1991: Kinematic, dynamic, and thermodynamic analysis of a weakly sheared severe thunderstorm over northern Alabama. *Mon. Wea. Rev.*, **119,** 262–297, doi:10.1175/1520-0493(1991)119<0262:KDATAO>2.0.CO;2.

Kropfli, R., and L. Miller, 1976: Kinematic structure and flux quantities in a convective storm from dual-Doppler radar observations. *J. Atmos. Sci.*, **33,** 520–529.

Kuster, C. M., P. L. Heinselman, and T. J. Schuur, 2016: Rapid-update radar observations of downbursts occurring within an intense multicell thunderstorm on 14 June 2011. *Wea. Forecasting*, **31,** 827–851, doi:10.1175/WAF-D-15-0081.1.

LeMone, M. A., and E. J. Zipser, 1980: Cumulonimbus vertical velocity events in GATE. Part I: Diameter, intensity and mass flux. *J. Atmos. Sci.*, **37,** 2444–2457.

Lenning, E., H. E. Fuelberg, and A. I. Watson, 1998: An evaluation of WSR-88D severe hail algorithms along the Northeastern Gulf Coast. *Wea. Forecasting*, **13,** 1029–1045, doi:10.1175/1520-0434(1998)013<1029:AEOWSH>2.0.CO;2.

Lhermitte, R. M., and M. Gilet, 1975: Dual-Doppler radar observation and study of sea breeze convective storm development. *J. Appl. Meteor.*, **14,** 1346–1361.

Liu, C., and S. Heckman, 2011: The application of total lightning detection and cell tracking for severe weather prediction. *5th Conf. on the Meteor. Appl. Lightning Data*, Seattle, WA, American Meteorological Society, 1–10

Mahale, V. N., G. Zhang, and M. Xue, 2016: Characterization of the 14 June 2011 Norman, Oklahoma, downburst through dual-polarization radar observations and hydrometeor classification. *J. Appl. Meteor. Climatol.*, **55,** 2635–2655, doi:10.1175/JAMC-D-16-0062.1.

Miller, L. J., J. E. Dye, and B. E. Martner, 1983: Dynamical-microphysical evolution of a convective storm in a weakly-sheared environment. Part II: Airflow and precipitation trajectories from Doppler radar observations. *J. Atmos. Sci.*, **40,** 2097–2109.

Miller, P., and T. Mote, 2017: A climatology of weakly forced and pulse thunderstorms in the Southeast United States. *J. Appl. Meteor. Climatol.*, **In press**.

——, 2018: Detecting severe weather potential in low signal-to-noise ratio regimes: weakly forced thunderstorm environments in the Southeast United States. *Natural Hazards and Earth System Sciences*, **In review**.

Miller, P. W., A. W. Black, C. A. Williams, and J. A. Knox, 2016: Quantitative assessment of human wind speed overestimation. *J. Appl. Meteor. Climatol.*, **55,** 1009–1020, doi:10.1175/JAMC-D-15-0259.1.

Murphy, M., 2017: Preliminary results from the inclusion of lightning type and polarity in the identification of severe storms. Preprints. *8th Conf. on the Meteor. Appl. of Lightning Data*, Seattle, WA, American Meteorological Society, 7.3. [Available online at https://ams.confex.com/ams/97Annual/webprogram/Manuscript/Paper308037/murphy_8mald_paper7.3.pdf.]

NOAA, 2006: Doppler radar meteorological observations. Part C. WSR-88D products and algoritms. NOAA. FCM-H11C-2006, 390 pp. [Available online at http://www.ofcm.gov/fmh11/fmh11partc/pdf/FMH-11-PartC-April2006.pdf.]

Ortega, K. L., T. M. Smith, K. L. Manross, A. G. Kolodziej, K. A. Scharfenberg, A. Witt, and J. J. Gourley, 2009: The severe hazards analysis and verification experiment. *Bull. Amer. Meteor. Soc.*, **90,** 1519–1530, doi:10.1175/2009bams2815.1.

Paxton, C. H., and J. M. Shepherd, 1993: Radar diagnostic parameters as indicators of severe weather in central Florida. NOAA. Technical Memorandum NWS SR-149, 13 pp. [Available online at https://repository.library.noaa.gov/view/noaa/7316/Share.]

Sall, J., 2002: Monte Carlo Calibration of Distributions of Partition Statistics, 15 pp. [Available online at https://www.jmp.com/content/dam/jmp/documents/en/white-papers/montecarlocal.pdf.]

Schultz, C. J., W. A. Petersen, and L. D. Carey, 2011: Lightning and severe weather: A comparison between total and cloud-to-ground lightning trends. *Wea. Forecasting*, **26,** 744–755, doi:10.1175/waf-d-10-05026.1.

Wakimoto, R. M., and V. Bringi, 1988: Dual-polarization observations of microbursts associated with intense convection: The 20 July storm during the MIST project. *Mon. Wea. Rev.*, **116,** 1521–1539, doi:10.1175/1520-0493(1988)116<1521:DPOOMA>2.0.CO;2.

Weiss, S. J., J. Hart, and P. Janish, 2002: An examination of severe thunderstorm wind report climatology: 1970–1999. Preprints. *21st Conf. Severe Local Storms,* San Antonio, TX, American Meteorological Society, 11B.2. [Available online at https://ams.confex.com/ams/SLS_WAF_NWP/techprogram/paper_47494.htm.]

Williams, E., and Coauthors, 1999: The behavior of total lightning activity in severe Florida thunderstorms. *Atmos. Res.*, **51,** 245–265, doi:10.1016/s0169-8095(99)00011-3.

Williams, E. R., 1988: The electrification of thunderstorms. *Sci. Amer.*, **259,** 88–99.

Wilson, J. W., and R. M. Wakimoto, 2001: The discovery of the downburst: TT Fujita's contribution. *Bull. Amer. Meteor. Soc.*, **82,** 49–62.

Witt, A., M. D. Eilts, G. J. Stumpf, J. T. Johnson, E. D. W. Mitchell, and K. W. Thomas, 1998: An enhanced hail detection algorithm for the WSR-88D. *Wea. Forecasting*, **13,** 286–303, doi:10.1175/1520-0434(1998)013<0286:aehdaf>2.0.co;2.

Zhu, Y., and Coauthors, 2017: Evaluation of ENTLN performance characteristics based on the ground-truth natural and rocket-triggered lightning data acquired in Florida. *J. Geophys. Res.: Atmos.*, **In press**, doi:10.1002/2017JD027270.

Table 5.1. Radar and radar-derived and total lightning products collected for study. Because the tilt angles can vary by scanning strategy, the most common angle is provided. An asterisk indicates that the product is not available for all scanning strategies.

Product	**Description**
N0Q	Reflectivity at 0.5˚ tilt
N1Q	Reflectivity at 1.5˚ tilt
N2Q	Reflectivity at 2.4˚ tilt
N3Q	Reflectivity at 3.4˚ tilt
NAQ*	Reflectivity at 0.9˚ tilt
NBQ*	Reflectivity at 1.8˚ tilt
N0X	Z_{DR} at 0.5˚ tilt
EET	Enhanced echo tops
DVL	Digital VIL
POH	Probability of hail
POSH	Probability of severe hail
MEHS	Maximum estimated hail size

Table 5.2. List of summarized radar attributes and environmental variables that were used to build the random forest.

Property	Units	Abbreviation
Maximum reflectivity at any height	dBZ	MREF
Height above radar level of maximum reflectivity	m	HGT REF
Maximum reflectivity nearest to surface	dBZ	NSFC REF
Binary indication of Z_{DR} trough signature	--	Z_{DR} TROF
Height above radar level of lowest Z_{DR} minimum	m	HGT TROF
Maximum Z_{DR} gradient observed at a Z_{DR} minimum	dB km^{-1}	Z_{DR} GRD
Maximum echo top	m	ET
Maximum VIL	g m^{-2}	VIL
Maximum VIL Density	g m^{-3}	VILD
Maximum total lightning flash density	km^{-1}	MFD
Maximum POH	%	POH
Maximum POSH	%	POSH
Maximum MEHS	in	MEHS
Total Totals	˚C	TT
Vertical Totals	˚C	VT
Mean-layer convective available potential energy	J kg^{-1}	CAPE
Mean-layer convective inhibition	J kg^{-1}	CIN
Mean-layer lifted condensation level	m	LCL
Mean-layer level of free convection	m	LFC

Table 5.3. Contingency table data and performance statistics for the validation samples for the three random forest frameworks tested. The values for the concentrated subset scenario reflect the average of ten training/validation sample combinations.

Scenario	Predicted: Severe Observed: Severe	Predicted: Benign Observed: Severe	Predicted: Severe Observed: Benign	Predicted: Benign Observed: Benign	FAR	POD	CSI	HSS
All storms, no population	72	201	21	27556	22.6	26.4	24.5	0.39
All storms, with population	61	206	38	24455	38.4	22.8	20.0	0.33
Concentrated subset	26	19	13	690	31.5	58.6	45.9	0.61

Table 5.4. Column contributions to the concentrated subset random forests. Because the forest was sensitive to the storms contained in the random validation sample, the statistics below are averages across ten random forests created using different randomly selected training/validation sample combinations. The "sum of likelihood-ratio chi-square" column represents the total that would be obtained if all the G^2 values from splits using that parameter were summed across all the trees in the random forest.

Parameter	Splits	Sum of likelihood ratio chi-square	Portion
VILD	302	7529	28.3
VIL	172	4942	18.6
ET	242	2733	10.3
HGT REF	248	2507	9.5
MEHS	148	974	3.7
POSH	130	922	3.5
TT	188	806	3.0
MFD	229	768	2.9
LCL	179	764	2.9
POH	81	672	2.5
NSFC REF	167	662	2.5
CAPE	196	645	2.4
CIN	183	585	2.2
LFC	147	580	2.2
MREF	119	462	1.8
VT	161	461	1.7
Z_{DR} TROF	75	182	0.7
HGT TROF	63	170	0.6
Z_{DR} GRD	65	169	0.6

Table 5.5. Correlations between the parameters in Table 5.2 and the first two principal components of the dataset. Only storms without missing data for any of the parameters (n=65,352) could be included with the PCA. Z_{DR} TROF, HGT TROF, and Z_{DR} GRD were not included in the PCA because the infrequency of Z_{DR} troughs led contributed to too many "missing" values.

Parameter	**PC 1**	**PC 2**
MREF	0.28	-0.10
HGT REF	0.17	0.03
NSFC REF	0.29	-0.10
Z_{DR} TROF	--	--
HGT TROF	--	--
Z_{DR} GRD	--	--
ET	0.30	-0.03
VIL	0.37	-0.05
VILD	0.28	-0.08
MFD	0.30	-0.09
POH	0.35	-0.03
POSH	0.29	-0.07
MEHS	0.36	-0.05
TT	0.15	0.30
VT	0.17	0.46
CAPE	0.11	-0.16
CIN	-0.01	-0.45
LCL	0.12	0.43
LFC	0.02	0.48

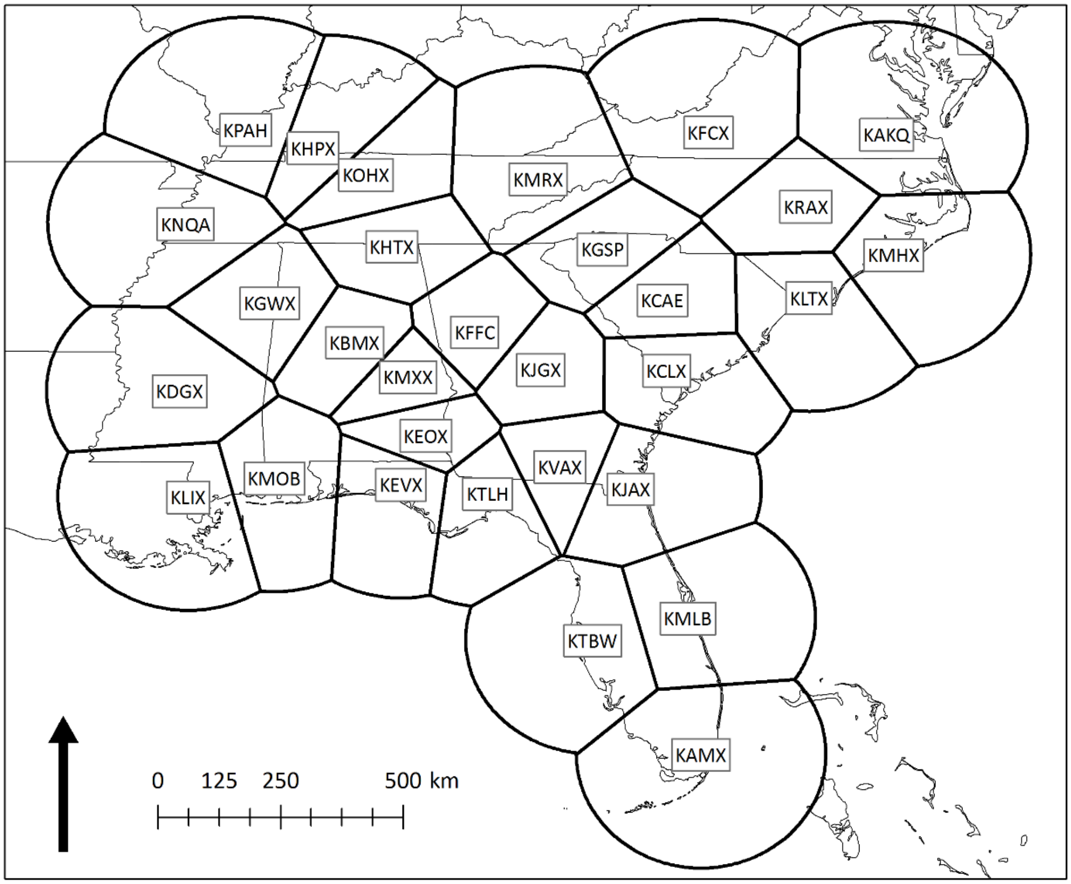

Figure 5.1. Thirty Weather Surveillance Radar – 1998 Doppler (WSR-88D) sites contributing to the Miller and Mote (2017a) WFT dataset.

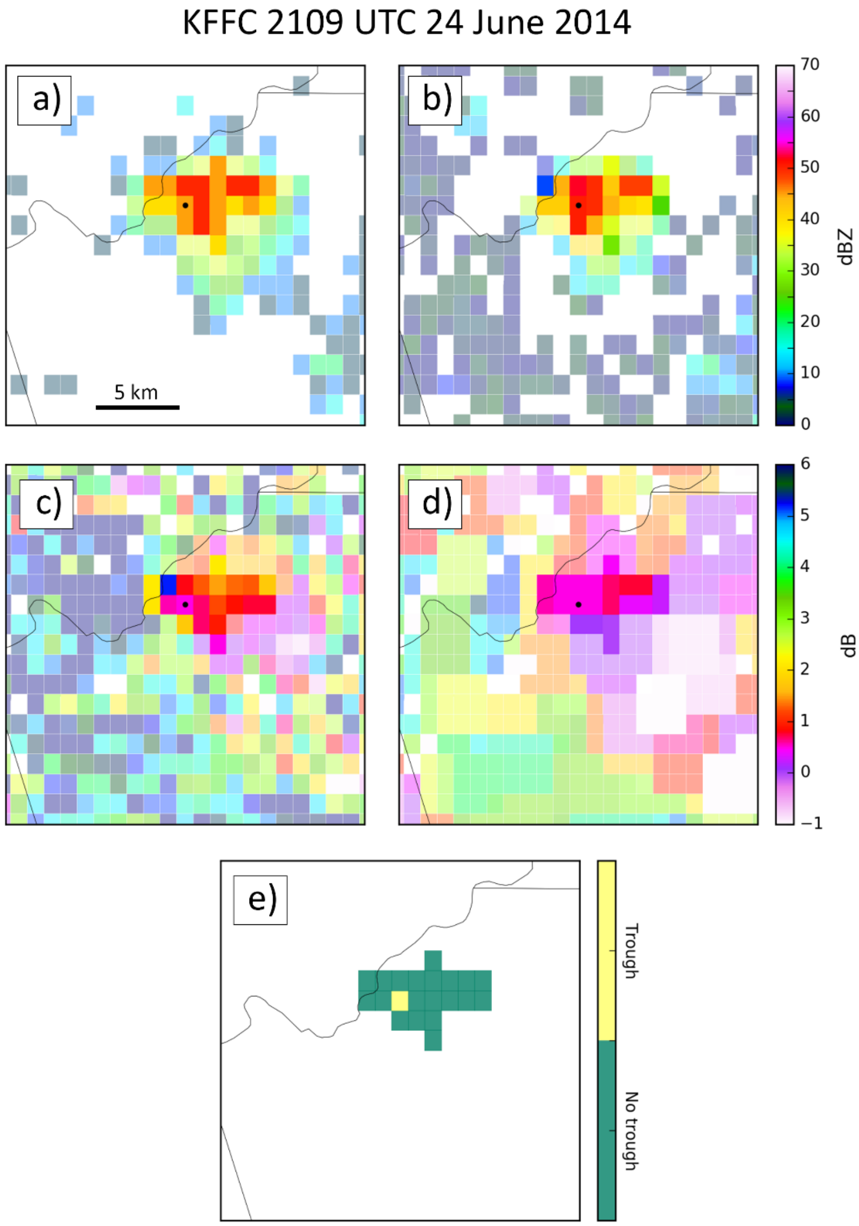

Figure 5.2. Z_{DR} trough detection algorithm workflow for a WFT in western Georgia (33.45˚N, 84.90˚W) on 24 June 2014. Only thunderstorm grid cells with composite reflectivities ≥40 dBZ can be considered for Z_{DR} troughs as dictated by the original Miller and Mote (2017a) dataset (A). Grid cells meeting this criterion are shown in full color whereas the coloring is partially muted for those not satisfying it. The grid cell that will eventually be designated as a Z_{DR} trough is stippled. Because the Z_{DR} trough is composed of hail, the base reflectivity at the level of the trough was required to be ≥50 dBZ (B). The corresponding Z_{DR} field (C) was transformed using a minimum filter (D). Any Z_{DR} grid cells that remained unchanged by the minimum filter, meaning they served as the local minimum, and were near-zero ($-0.5 \leq Z_{DR} \leq 0.5$), were designated as Z_{DR} troughs (E).

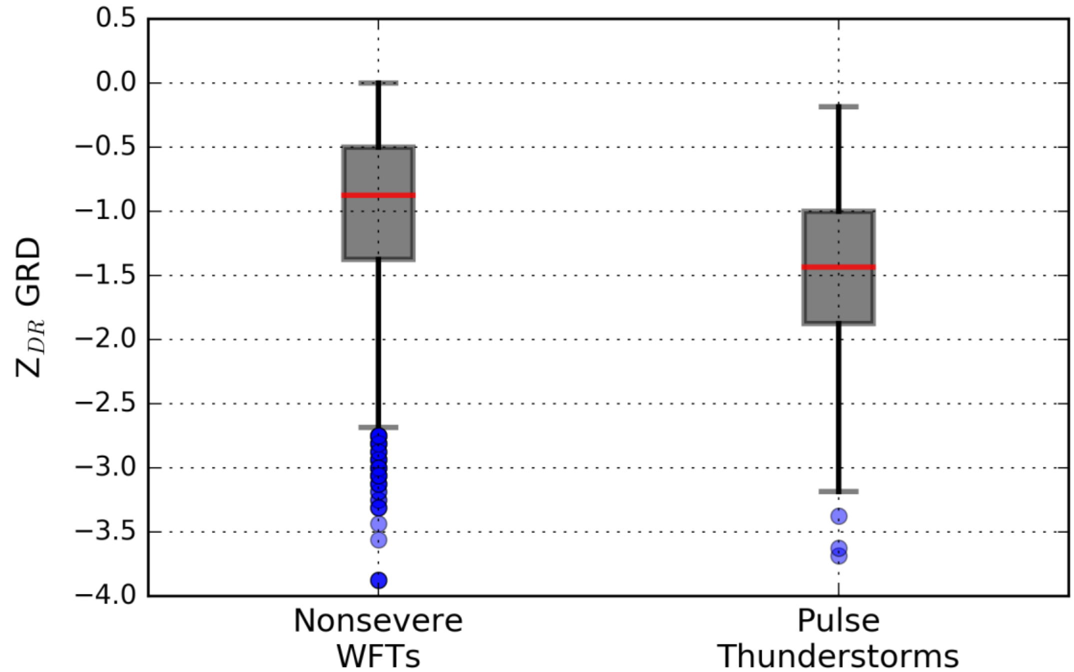

Figure 5.3. Boxplots comparing the Z_{DR} GRD between pulse thunderstorms and nonsevere WFTs. Pulse thunderstorms are generally characterized by "deeper" Z_{DR} troughs (i.e., a greater difference between the Z_{DR} minimum and its median surrounding value). However, considerable overlap between the distributions prevents its use as an independent severe weather indicator.

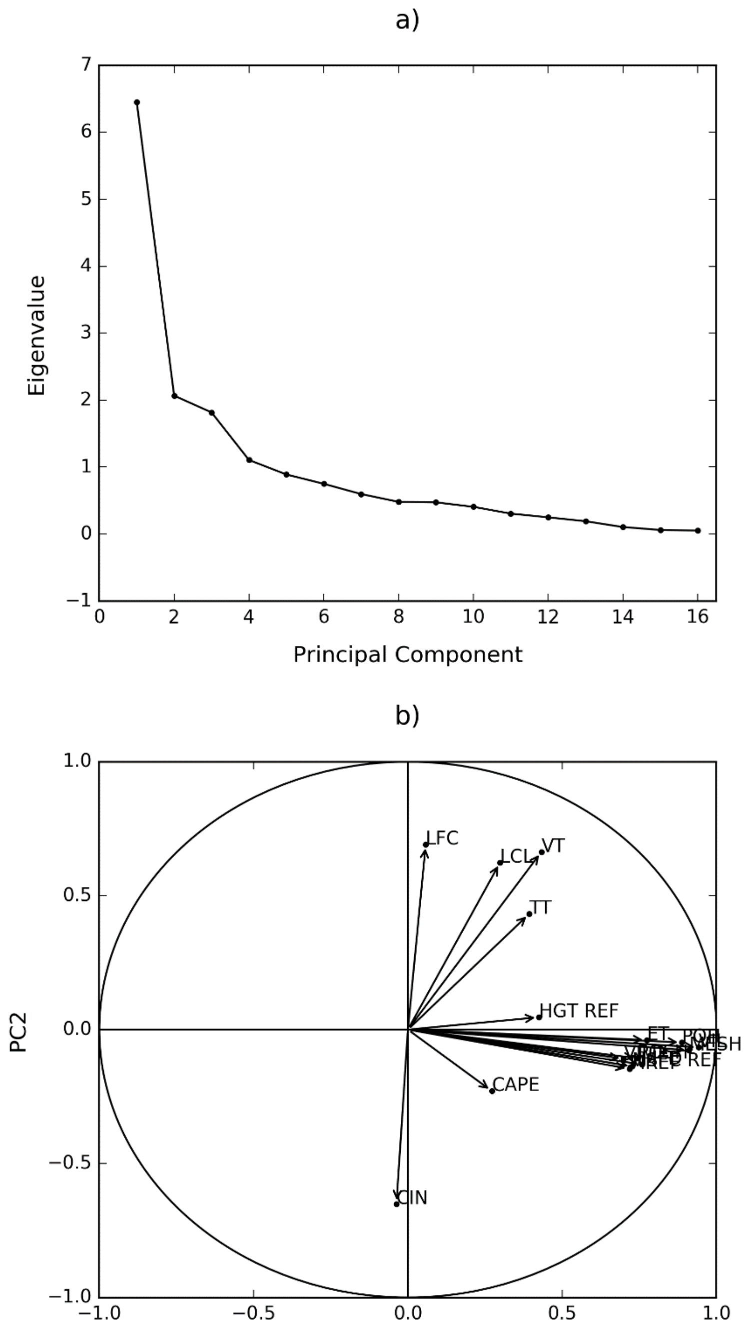

Figure 5.4. Results of principal components analysis of 16 radar, lightning, and environmental parameters. The parameters are significantly collinear with the variability disproportionately concentrated in the first principal component (A). The 10 radar and lightning variables are largely described by PC1 whereas PC2 captures the environmental variables (B).

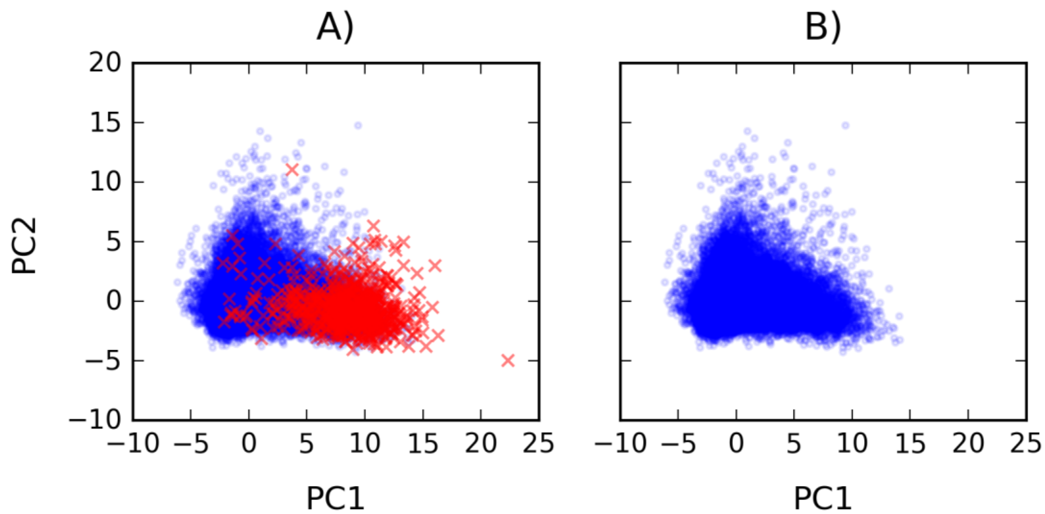

Figure 5.5. Scatterplots of WFTs in the transformed PC1 and PC2 data space. Pulse thunderstorms (red) are primarily located in the section of data space with high PC1 values (A). However, the same region of data space is also densely occupied by nonsevere WFTs (blue) (B) which diminishes the ability of the random forest to accurately detect pulse thunderstorms.

CHAPTER 6

SUMMARY AND CONCLUSIONS

6.1 Overview

Disorganized thunderstorms are the primary severe weather threat in the Southeastern U.S. during the warm season. However, despite their ubiquity there has been little scientific inquiry directed toward these storms. Even the lexicon used to describe them has remained uncertain and poorly defined for the last several decades, impeding the reproducibility and comparability of the few research efforts on this topic. For climate scientists, the lack of even a basic disorganized thunderstorm climatology prevents the establishment of connections with the global climate system. Meanwhile, the meteorologist's ability to nowcast severe disorganized thunderstorms had advanced little in the last decade.

Forming in the absence of a synoptic-scale forcing mechanism and its attendant shear regime, disorganized thunderstorms are typically benign features with limited severe-weather potential. Consequently, forecasting severe disorganized storms poses a "needle in a haystack" dilemma for operational forecasters. The challenge is two-fold: (1) the convective environments that support severe disorganized storms are poorly distinguished from benign thunderstorm environments, and (2) individual severe disorganized thunderstorms closely resemble their benign counterparts. Nowhere is this problem more evident than the Southeast U.S. A perennial feature of the summertime climate in this region, disorganized thunderstorms are the primary warm season severe weather threat.

Further, they are also the primary source severe thunderstorm warning false alarms (Guillot et al. 2008).

This dissertation, possibly the largest contribution to disorganized thunderstorm research since the 1940s (Byers and Braham 1949), addresses their climatology (Section 3), convective environments (Section 4), and storm-scale radar and lightning attributes (Section 5). Additionally, this project engages the nomenclature and terminology used to describe disorganized thunderstorms with the aspiration that consistent verbiage will facilitate a more coherent research program in the future (Section 2).

6,2 Summary

Section 2 performs a content analysis of disorganized-thunderstorm-related documents dating back to the 1970s. The purpose of this effort is to decipher the meanings of numerous terms used to reference disorganized convection, and ultimately, propose a standard nomenclature for research moving forward. The content analysis mined textual references to disorganized convection and examined patterns in the adjectives and nouns used in association with disorganized thunderstorm terminology. The content analysis revealed that none of the existing disorganized thunderstorms terminology accurately reflected the phenomenon being described, and new term “weakly forced thunderstorm” (WFT) was suggested for this purpose. Further, word associations revealed that the common disorganized thunderstorm descriptor “pulse thunderstorm” represented the special case of a severe-weather-producing WFT.

Section 3 examines 15 years of radar imagery collected at 30 sites in the Southeast U.S. to establish a WFT and pulse thunderstorm climatology for this region. The findings corroborate many heretofore unsubstantiated assumptions of WFT activity. For instance, WFT activity is concentrated along the Gulf and Atlantic coastlines with a secondary maximum in the Southern Appalachians. However, the maximum of pulse thunderstorm activity, the Blue Ridge Mountains, is displaced from the overall WFT maximum in the Florida Peninsula.

Section 4 leverages the WFT database developed in Section 3 to investigate the convective environmental parameters that best differentiate between benign WFT environments and those that support pulse thunderstorms. The initiation locations of WFTs are paired with model output from the Rapid Refresh (RAP), and thirty near-storm convective parameters are calculated for each WFT. Overall, only two RAP parameters, also the two parameters most accurately represented by the model, satisfactorily distinguish between benign WFT and pulse thunderstorm environments: Vertical Totals (VT) and Total Totals (TT). VT (TT) are tied to a roughly 5x (10x) increase in severe wind (hail) events when meeting the 70^{th} (85^{th}) percentile.

Lastly, Section 5 builds upon Sections 3 and 4 by contributing additional radar- and total-lightning-based variables to each WFT in the dataset. A decision-tree-based machine learning algorithm, random forests, is trained on the dataset to differentiate nonsevere WFTs from pulse thunderstorms based on the storm-scale and convective environmental attributes. The random forest struggles to accurately classify pulse thunderstorms when trained using all WFTs in the Southeast U.S. However, when trained using WFTs from the most active pulse thunderstorm sub-region from Section 3 and the most active convective environments from Section 4, the random forest exceeds NWS warning skill.

The random forest shows promise as a pulse thunderstorm detection technique. Furthermore, this dissertation shows that accurate pulse thunderstorm detection is most achievable when information beyond simply radar-based information is considered. The classifications were most accurate when additional context was provided about the convective environment and geographic region. However, even in this concentrated dataset, pulse thunderstorms represented only 6.1% of WFTs, a much more realistic proportion that previous research efforts. Thus, there is reason to believe that this technique will more readily apply to an operational setting.

6.3 Conclusions

Because fewer than 1% of the 125,000 WFTs occurring annually in the Southeast U.S. produce severe weather, the operational forecasting challenge is apparent. This dissertation addresses the challenge of accurately detecting the small subset of pulse thunderstorms within an overwhelmingly nonsevere WFT population. Previous efforts directed at this problem have offered promising results, but achieved them through case studies or with unrealistic proportions (roughly 50%) of pulse thunderstorms (Wakimoto and Bringi 1988; Atkins and Wakimoto 1991; Kingsmill and Wakimoto 1991; Cerniglia and Snyder 2002). Recent research suggests that the skill of experimental nowcasting tools is closely tied to the proportion of nonsevere storms upon which it is tested (Murphy 2017).

The work completed herein finds that when the proportion of pulse thunderstorms is accurately represented, relationships between convective environment, storm-scale radar and lightning characteristics, and storm severity become more difficult to discern. Though statistically significant differences in the mean convective environments and storm-scale attributes may exist, the spread about the mean removes most operational practicality to the findings. This result is described as a low signal-to-noise ratio. Section 4 found that the convective parameters differentiating between nonsevere WFT and pulse environments most reliably were also that were represented most accurately by the RAP. Thus, the subtle differences in convective environment may be overshadowed by model errors and severe-nonsevere misclassifications. Similarly, the random forest prediction in Section 5 only performed capably after corrections were made for missing storm reports and the algorithm was trained on a concentrated (though still realistic) sub-sample. The performance of the forest when trained for the whole Southeast U.S. is likely more closely related to the introduction of noise from misreported severe weather than methodological shortcomings.

In sum, this dissertation project represents a long overdue contribution to disorganized convection. The results reveal the true magnitude of the pulse thunderstorm forecasting challenge facing forecasters, as well as identify the current roadblocks to accurate forecasting. Until model inaccuracies and storm reporting deficiencies are overcome, research meteorologists will struggle to identify reliable characteristic traits of pulse thunderstorms. In the meantime, the suggestion of a standard disorganized thunderstorm nomenclature and the availability of a regional WFT climatology will equip researchers with the basic resources to undertake future work.

REFERENCES

Adler, R. F., and A. J. Negri, 1988: A satellite infrared technique to estimate tropical convective and stratiform rainfall. *J. Appl. Meteor.*, **27,** 30–51, doi:10.1175/1520-0450(1988)027<0030:ASITTE>2.0.CO;2.

Ahijevych, D., J. O. Pinto, J. K. Williams, and M. Steiner, 2016: Probabilistic forecasts of mesoscale convective system initiation using the random forest data mining technique. *Wea. Forecasting*, **31,** 581-599.

Alpaydin, E., 2010: *Introduction to Machine Learning.* 2nd ed. The MIT Press, 415 pp.

Amburn, S. A., and P. L. Wolf, 1997: VIL density as a hail indicator. *Wea. Forecasting*, **12,** 473–478.

AMS, 2016: Glossary of Meteorology. Accessed 18 January 2016. [Available online at http://glossary.ametsoc.org/.]

Ashley, W. S., and C. W. Gilson, 2009: A reassessment of U.S. lightning mortality. *Bull. Amer. Meteor. Soc.*, **90,** 1501–1518, doi:10.1175/2009BAMS2765.1.

Ashley, W. S., M. L. Bentley, and J. A. Stallins, 2012: Urban-induced thunderstorm modification in the Southeast United States. *Climatic Change*, **113,** 481-498.

Atkins, N. T., and R. M. Wakimoto, 1991: Wet microburst activity over the southeastern United States: Implications for forecasting. *Wea. Forecasting*, **6,** 470–482, doi:10.1175/1520-0434(1991)006<0470:WMAOTS>2.0.CO;2.

Beasley, W. H., D. E. Williams, and P. T. Hyland, 2008: Analysis of surface electric-field contours in relation to cloud-to-ground lightning flashes in air-mass thunderstorms at the Kennedy Space Center. *20th International Lightning Detection Conference*, Tucson, Arizona, Vaisala. [Available online at http://es.vaisala.com/Vaisala%20Documents/Scientific%20papers/Analysis_of_surface_electric-field_contours.pdf.]

Bedka, K. M., 2011: Overshooting cloud top detections using MSG SEVIRI Infrared brightness temperatures and their relationship to severe weather over Europe. *Atmos. Res.*, **99,** 175–189, doi:http://dx.doi.org/10.1016/j.atmosres.2010.10.001.

Benjamin, S. G., and Coauthors, 2004: An hourly assimilation–forecast cycle: The RUC. *Mon. Wea. Rev.*, **132,** 495–518, doi:10.1175/1520-0493(2004)132<0495:AHACTR>2.0.CO;2.

Benjamin, S. G., and Coauthors, 2016: A North American hourly assimilation and model forecast cycle: The Rapid Refresh. *Mon. Wea. Rev.*, **144,** 1669–1694, doi:10.1175/MWR-D-15-0242.1.

Bentley, M. L., and J. A. Stallins, 2005: Climatology of cloud-to-ground lightning in Georgia, USA, 1992–2003. *Int. J. Climatol.*, **25,** 1979–1996, doi:10.1002/joc.1227.

Bentley, M. L., W. S. Ashley, and J. A. Stallins, 2010: Climatological radar delineation of urban convection for Atlanta, Georgia. *Int. J. Climatol.*, **30,** 1589–1594.

Bentley, M. L., J. A. Stallins, and W. S. Ashley, 2012a: Synoptic environments favourable for urban convection in Atlanta, Georgia. *Int. J. Climatol.*, **32,** 1287-1294, doi:10.1002/joc.2344.

——, 2012b: Synoptic environments favourable for urban convection in Atlanta, Georgia. *Int. J. Climatol.*, **32,** 1287–1294, doi:10.1002/joc.2344.

Bird, S., E. Loper, and E. Klein, 2009: *Natural Language Processing with Python.* O'Reilly Media Inc.

Black, A. W., and T. L. Mote, 2015: Characteristics of Winter-Precipitation-Related Transportation Fatalities in the United States. *Wea. Climate Soc.*, **7,** 133–145, doi:10.1175/WCAS-D-14-00011.1.

Black, A. W., G. Villarini, and T. L. Mote, 2017: Effects of Rainfall on Vehicle Crashes in Six U.S. States. *Wea. Climate Soc.*, **9,** 53–70, doi:10.1175/WCAS-D-16-0035.1.

Blair, S. F., and Coauthors, 2017: High-resolution hail observations: Implications for NWS warning operations. *Wea. Forecasting*, **32,** 1101–1119.

Bland, J. M., and D. G. Altman, 2000: The odds ratio. *BMJ,* **320,** 1468.

Bluestein, H. B., 2013: *Severe Convective Storms and Tornadoes: Observations and Dynamics.* Springer, 456 pp.

Blumberg, W. G., K. T. Halbert, T. A. Supinie, P. T. Marsh, R. L. Thompson, and J. A. Hart, 2017: SHARPpy: An open source sounding analysis toolkit for the atmospheric sciences. *Bull. Amer. Meteor. Soc.*, **98,** 1625–1636, doi:10.1175/BAMS-D-15-00309.1.

Breiman, L., 2001a: Random Forests. *Machine Learning,* **45,** 5–32, doi:10.1023/A:1010933404324.

——, 2001b: Statistical modeling: The two cultures (with comments and a rejoinder by the author). *Statistical science,* **16,** 199–231.

Brooks, H. E., 2013: Severe thunderstorms and climate change. *Atmos. Res.*, **123,** 129-138.

Brotak, E., 2009: Nasty surprise. *AeroSafety world*, **4**.

Browning, K., T. Harrold, A. Whyman, and J. Beimers, 1968: Horizontal and vertical air motion and precipitation growth, within a shower. *Quart. J. Roy. Meteorol. Soc.*, **94,** 498-509.

Bruick, Z. S., and C. D. Karstens, 2017: An investigation of local and national NWS warning outbreaks for severe convective events. *J. Operational Meteor.*, **5,** 14-25, doi:http://dx.doi.org/10.15191/nwajom.2017.0502.

Burgess, D. W., and L. R. Lemon, 1990: Severe thunderstorm detection by radar. *Radar in Meteorology*, D. Atlas, Ed., Springer, 619–647.

Burghardt, B. J., C. Evans, and P. J. Roebber, 2014: Assessing the predictability of convection initiation in the High Plains using an object-based approach. *Wea. Forecasting*, **29,** 403–418, doi:10.1175/WAF-D-13-00089.1.

Byers, H. R., 1949: Structure and dynamics of the thunderstorm. *Science*, **110,** 291-294, doi:10.1126/science.110.2856.291.

Byers, H. R., and R. R. Braham, 1948: Thunderstorm structure and circulation. *J. Meteor.*, **5,** 71-86.

Byers, H. R., and R. R. Braham, 1949: *The Thunderstorm: Report of the Thunderstorm Project.* US Government Printing Office, 287 pp.

Center for International Earth Science Information Network, 2016: Documentation for the Gridded Population of the World, Version 4. http://dx.doi.org/10.7927/H4D50JX4.

Cerniglia, C. S., and W. R. Snyder, 2002: Development of warning criteria for severe pulse thunderstorms in the Northeastern United States using the WSR-88D. National Weather Service. Eastern Region Technical Attachment No. 2002-03, 14 pp. [Available online at http://docs.lib.noaa.gov/noaa_documents/NWS/NWS_ER/Eastern_Region_Tech_Attachment/TA_2002-03.pdf.]

Changnon, S. A., 2001: Development and analysis of data bases for assessing long-term fluctuations in thunderstorms in the United States. National Oceanic and Atmospheric Administration. CRR-49.]

Corfidi, S. F., M. C. Coniglio, A. E. Cohen, and C. M. Mead, 2016: A proposed revision to the definition of “Derecho”. *Bull. Amer. Meteor. Soc.*, **97,** 935–949, doi:10.1175/bams-d-14-00254.1.

Cover, T. M., and J. A. Thomas, 1991: Information theory and statistics. *Elements of Information Theory*, 1 ed., John Wiley & Sons, 279–335.

Craven, J. P., and H. E. Brooks, 2004: Baseline climatology of sounding derived parameters associated with deep, moist convection. *Natl. Wea. Dig*, **28,** 13-24.

Cummins, K. L., and M. J. Murphy, 2009: An overview of lightning locating systems: history, techniques, and data uses, with an in-depth look at the US NLDN. *IEEE Trans. Electromagn. Compat.*, **51,** 499–518, doi:10.1109/temc.2009.2023450.

Cunning, J. B., H. W. Poor, and M. Demaria, 1986: An investigation of the development of cumulonimbus systems over south Florida. Part II: In-cloud structure. *Mon. Wea. Rev.*, **114,** 25-39.

de Szoeke, S. P., J. B. Edson, J. R. Marion, C. W. Fairall, and L. Bariteau, 2014: The MJO and air–sea interaction in TOGA COARE and DYNAMO. *J. Climate*, **28,** 597-622, doi:10.1175/JCLI-D-14-00477.1.

Diem, J. E., 2013: Influences of the Bermuda High and atmospheric moistening on changes in summer rainfall in the Atlanta, Georgia region, USA. *Int. J. Climatol.*, **33,** 160–172, doi:10.1002/joc.3421.

Diffenbaugh, N. S., M. Scherer, and R. J. Trapp, 2013: Robust increases in severe thunderstorm environments in response to greenhouse forcing. *Proc. Natl. Acad. Sci.*, **110,** 16361–16366, doi:10.1073/pnas.1307758110.

Donavon, R. A., and K. A. Jungbluth, 2007: Evaluation of a technique for radar identification of large hail across the Upper Midwest and Central Plains of the United States. *Wea. Forecasting*, **22,** 244-254.

Doswell, C. A., R. Davies-Jones, and D. L. Keller, 1990: On summary measures of skill in rare event forecasting based on contingency tables. *Wea. Forecasting*, **5,** 576–585, doi:10.1175/1520-0434(1990)005<0576:OSMOSI>2.0.CO;2.

Doswell, C. A. I., 1985: The operational meteorology of convective weather. Volume II: Storm scale analysis. NOAA. Technical Memorandum ERL ESG-15, 240 pp. [Available online at http://docs.lib.noaa.gov/noaa_documents/OAR/ERL_ESG/TM_ERL_ESG_15.pdf.]

Doswell, C. A. I., H. E. Brooks, and R. A. Maddox, 1996: Flash flood forecasting: an ingredients-based methodology. *Wea. Forecasting*, **11,** 560-581, doi:10.1175/1520-0434(1996)011<0560:fffaib>2.0.co;2.

Duda, J. D., and W. A. Gallus, 2010: Spring and summer midwestern severe weather reports in supercells compared to other morphologies. *Wea. Forecasting*, **25,** 190-206, doi:10.1175/2009waf2222338.1.

Eilts, M., J. Johnson, E. Mitchell, R. Lynn, P. Spencer, S. Cobb, and T. Smith, 1996: Damaging downburst prediction and detection algorithm for the WSR-88D.

Preprints, 18th Conf. on Severe Local Storms, San Francisco, CA, Amer. Meteor. Soc, 541-545

Ellrod, G. P., J. P. Nelson III, M. R. Witiw, L. Bottos, and W. P. Roeder, 2000: Experimental GOES sounder products for the assessment of downburst potential. *Wea. Forecasting*, **15,** 527-542.

Fabry, F., 2006: The spatial variability of moisture in the boundary layer and its effect on convection initiation: Project-long characterization. *Mon. Wea. Rev.*, **134,** 79–91, doi:10.1175/MWR3055.1.

Fabry, F., V. Meunier, B. Puigdomènech Treserras, A. Cournoyer, and B. Nelson, 2017: On the climatological use of radar data mosaics: Possibilities and challenges. *Bull. Amer. Meteor. Soc.*, **In press**, doi:10.1175/BAMS-D-15-00256.1.

Falk, K., L. Harrison, and J. Elmore, 1998: Preliminary downburst climatology and warning guidelines from a single cell thunderstorm database. National Weather Service. Technical Attachment SR/SSD 98-31 pp. [Available online at http://www.srh.noaa.gov/topics/attach/html/ssd98-31.htm.]

Fleiss, J. L., B. Levin, and M. C. Paik, 2003: *Statistical Methods for Rates and Proportions.* 3rd ed. Wiley, 800 pp.

Ford, T. W., S. M. Quiring, O. W. Frauenfeld, and A. D. Rapp, 2015: Synoptic conditions related to soil moisture-atmosphere interactions and unorganized convection in Oklahoma. *J. Geophys. Res.: Atmos.*, **120,** 11519–11535, doi:10.1002/2015JD023975.

Fowle, M. A., and P. J. Roebber, 2003: Short-range (0–48 h) numerical prediction of convective occurrence, mode, and location. *Wea. Forecasting*, **18,** 782–794, doi:10.1175/1520-0434(2003)018<0782:SHNPOC>2.0.CO;2.

Frank, N. L., P. L. Moore, and G. E. Fisher, 1967: Summer shower distribution over the Florida Peninsula as deduced from digitized radar data. *J. Appl. Meteor.*, **6,** 309–316, doi:10.1175/1520-0450(1967)006<0309:SSDOTF>2.0.CO;2.

Frugis, B., and T. Wasula, 2011: Development of warning thresholds for one inch or greater hail in the Albany, New York, county warning area. National Weather Service. Eastern Region Technical Attachment No. 2011-05, 24 pp. [Available online at http://docs.lib.noaa.gov/noaa_documents/NWS/NWS_ER/Eastern_Region_Tech_Attachment/TA_2011-05.pdf.]

Frye, J. D., and T. L. Mote, 2009: Convection initiation along soil moisture boundaries in the southern Great Plains. *Mon. Wea. Rev.*, **138,** 1140–1151, doi:10.1175/2009MWR2865.1.

Fujita, T. T., 1981: Tornadoes and downbursts in the context of generalized planetary scales. *J. Atmos. Sci.*, **38,** 1511–1534.

Funk, T., 2006: Flow chart to evaluate wet microburst and large hail potential from pulse or multicellular thunderstorms. [Available online at http://www.weather.gov/media/lmk/soo/pulse_svr_flowchart.pdf.]

Gagne, D. J., A. McGovern, and J. Brotzge, 2009: Classification of convective areas using decision trees. *J. Atmos. Oceanic Technol.*, **26,** 1341-1353, doi:10.1175/2008JTECHA1205.1.

Gagne, D. J., A. McGovern, and M. Xue, 2014: Machine learning enhancement of storm-scale ensemble probabilistic quantitative precipitation forecasts. *Wea. Forecasting*, **29,** 1024–1043, doi:10.1175/WAF-D-13-00108.1.

Gallus, W. A., N. A. Snook, and E. V. Johnson, 2008: Spring and summer severe weather reports over the midwest as a function of convective mode: a preliminary study. *Wea. Forecasting*, **23,** 101-113.

Gambill, L. D., and J. R. Mecikalski, 2011: A satellite-based summer convective cloud frequency analysis over the southeastern United States. *J. Appl. Meteor. Climatol.*, **50,** 1756–1769.

Gensini, V. A., and T. L. Mote, 2015: Downscaled estimates of late 21st century severe weather from CCSM3. *Climatic Change*, **129,** 307–321, doi:10.1007/s10584-014-1320-z.

Gensini, V. A., C. Ramseyer, and T. L. Mote, 2014a: Future convective environments using NARCCAP. *Int. J. Climatol.*, **34,** 1699-1705.

Gensini, V. A., T. L. Mote, and H. E. Brooks, 2014b: Severe-thunderstorm reanalysis environments and collocated radiosonde observations. *J. Appl. Meteor. Climatol.*, **53,** 742–751, doi:10.1175/JAMC-D-13-0263.1.

Gibson, H. M., and T. H. Vonder Haar, 1990: Cloud and convection frequencies over the southeast United States as related to small-scale geographic features. *Mon. Wea. Rev.*, **118,** 2215–2227.

Glickman, T., Ed., 2000: *Glossary of Meteorology*. 2nd ed. Amer. Meteor. Soc., 855 pp.

Gong, X., and M. B. Richman, 1995: On the application of cluster analysis to growing season precipitation data in North America east of the Rockies. *J. Climate*, **8,** 897–931.

Goodman, S. J., and Coauthors, 2013: The GOES-R Geostationary Lightning Mapper (GLM). *Atmos. Res.*, **125–126,** 34-49, doi:http://dx.doi.org/10.1016/j.atmosres.2013.01.006.

Grice, H. P., 1975: Logic and conversation. *Syntax and Semantics III - Speech Acts*, P. Cole, and J. L. Morgan, Eds., Academic Press, 41–58.

Guillot, E. M., T. M. Smith, V. Lakshmanan, K. L. Elmore, D. W. Burgess, and G. J. Stumpf, 2008: Tornado and severe thunderstorm warning forecast skill and its relationship to storm type. *24th Int. Conf. Interactive Information Processing Systems for Meteor., Oceanogr., and Hydrol.*, New Orleans, LA, American Meteorological Society. [Available online at http://ams.confex.com/ams/pdfpapers/132244.pdf.]

Haberlie, A. M., W. S. Ashley, and T. J. Pingel, 2015: The effect of urbanisation on the climatology of thunderstorm initiation. *Quart. J. Roy. Meteorol. Soc.*, **141,** 663–675.

Hallenbeck, C., 1922: The topographic thunderstorm. *Mon. Wea. Rev.*, **50,** 284–287.

Harrison, D. R., and C. D. Karstens, 2016: A climatology of operational storm-based warnings: A geospatial analysis. *Wea. Forecasting*, **32,** 47–60, doi:10.1175/WAF-D-15-0146.1.

Harrison, M. R., 1982: The media and public perceptions of climatic change. *Bull. Amer. Meteor. Soc.*, **63,** 730–730, doi:10.1175/1520-0477(1982)063<0730:TMAPPO>2.0.CO;2.

Hobson, A. G. K., V. Lakshmanan, T. M. Smith, and M. Richman, 2012: An automated technique to categorize storm type from radar and near-storm environment data. *Atmos. Res.*, **111,** 104-113.

Holsti, O. R., 1969: *Content Analysis for the Social Sciences and Humanities.* Addison-Wesley, 235 pp.

Howard, K. W., J. J. Gourley, and R. A. Maddox, 1997: Uncertainties in WSR-88D measurements and their impacts on monitoring life cycles. *Wea. Forecasting*, **12,** 166–174, doi:10.1175/1520-0434(1997)012<0166:uiwmat>2.0.co;2.

Hurlbut, M. M., and A. E. Cohen, 2013: Environments of Northeast U.S. severe thunderstorm events from 1999 to 2009. *Wea. Forecasting*, **29,** 3-22, doi:10.1175/WAF-D-12-00042.1.

Huschke, R. E., Ed., 1959: *Glossary of Meteorology*. 1st ed. Amer. Meteor. Soc., 638 pp.

Ingram, K. T., K. Dow, L. Carter, and J. Anderson, Eds., 2013: *Climate of the Southeast United States: Variability, Change, Impacts, and Vulnerability*. Island Press.

James, R. P., and P. M. Markowski, 2010: A numerical investigation of the effects of dry air aloft on deep convection. *Mon. Wea. Rev.*, **138,** 140–161, doi:10.1175/2009MWR3018.1.

JMP, 2017: JMP 12 Online Documentation. Accessed 20 July 2017. [Available online at http://www.jmp.com/support/help/Statistical_Details_8.shtml#1277120.]

Johns, R. H., and C. A. I. Doswell, 1992: Severe local storms forecasting. *Wea. Forecasting*, **7,** 588–612, doi:10.1175/1520-0434(1992)007<0588:SLSF>2.0.CO;2.

Johnson, R. H., T. M. Rickenbach, S. A. Rutledge, P. E. Ciesielski, and W. H. Schubert, 1999: Trimodal characteristics of tropical convection. *J. Climate*, **12,** 2397–2418, doi:10.1175/1520-0442(1999)012<2397:TCOTC>2.0.CO;2.

Jorgensen, D. P., and M. A. LeMone, 1988: Vertical velocity characteristics of oceanic convection. *J. Atmos. Sci.*, **46,** 621–640, doi:10.1175/1520-0469(1989)046<0621:VVCOOC>2.0.CO;2.

Kingsmill, D. E., and R. M. Wakimoto, 1991: Kinematic, dynamic, and thermodynamic analysis of a weakly sheared severe thunderstorm over northern Alabama. *Mon. Wea. Rev.*, **119,** 262–297, doi:10.1175/1520-0493(1991)119<0262:KDATAO>2.0.CO;2.

Kirshbaum, D. J., F. Fabry, and Q. Cazenave, 2015: The Mississippi Valley convection minimum on summer afternoons: Observations and numerical simulations. *Mon. Wea. Rev.*, **144,** 263–272, doi:10.1175/MWR-D-15-0238.1.

Krippendorff, K., 2012: *Content Analysis: An Introduction to Its Methodology.* Sage, 456 pp.

Kropfli, R., and L. Miller, 1976: Kinematic structure and flux quantities in a convective storm from dual-Doppler radar observations. *J. Atmos. Sci.*, **33,** 520–529.

Kuchera, E. L., and M. D. Parker, 2006: Severe convective wind environments. *Wea. Forecasting*, **21,** 595-612.

Kuster, C. M., P. L. Heinselman, and T. J. Schuur, 2016: Rapid-update radar observations of downbursts occurring within an intense multicell thunderstorm on 14 June 2011. *Wea. Forecasting*, **31,** 827–851, doi:10.1175/WAF-D-15-0081.1.

Lack, S. A., and N. I. Fox, 2012: Development of an automated approach for identifying convective storm type using reflectivity-derived and near-storm environment data. *Atmos. Res.*, **116,** 67–81, doi:10.1016/j.atmosres.2012.02.009.

Lackmann, G., 2011: *Midlatitude Synoptic Meteorology*. 1 ed. American Meteorological Society, 345 pp.

Lakshmanan, V., and T. Smith, 2009: Data mining storm attributes from spatial grids. *J. Atmos. Oceanic Technol.*, **26,** 2353–2365, doi:10.1175/2009jtecha1257.1.

Lee, J. W., 2002: Tornado proximity soundings from the NCEP/NCAR reanalysis data. Thesis. Dept. of Meteorology, University of Oklahoma, 61 pp.

Lee, T., and Coauthors, 2016: An observational Study of convection initiation under quiescent conditions in the Southeastern United States. Preprints. *Annual Meeting of the American Meteorological Society*, New Orleans, LA, American Meteorological Society, 6A3. [Available online at https://ams.confex.com/ams/96Annual/webprogram/Paper282669.html.]

Lehmann, C., 2005: Pleonasm and hypercharacterisation. *Yearbook of Morphology 2005*, G. Booij, and J. Van Marle, Eds., Springer Netherlands, 119–154.

LeMone, M. A., and E. J. Zipser, 1980: Cumulonimbus vertical velocity events in GATE. Part I: Diameter, intensity and mass flux. *J. Atmos. Sci.*, **37,** 2444–2457.

Lenning, E., H. E. Fuelberg, and A. I. Watson, 1998: An evaluation of WSR-88D severe hail algorithms along the Northeastern Gulf Coast. *Wea. Forecasting*, **13,** 1029–1045, doi:10.1175/1520-0434(1998)013<1029:AEOWSH>2.0.CO;2.

Lhermitte, R. M., and M. Gilet, 1975: Dual-Doppler radar observation and study of sea breeze convective storm development. *J. Appl. Meteor.*, **14,** 1346–1361.

Liu, C., and S. Heckman, 2011: The application of total lightning detection and cell tracking for severe weather prediction. *5th Conf. on the Meteor. Appl. Lightning Data*, Seattle, WA, American Meteorological Society, 1–10

Lock, N. A., and A. L. Houston, 2013: Empirical examination of the factors regulating thunderstorm initiation. *Mon. Wea. Rev.*, **142,** 240–258, doi:10.1175/MWR-D-13-00082.1.

Mahale, V. N., G. Zhang, and M. Xue, 2016: Characterization of the 14 June 2011 Norman, Oklahoma, downburst through dual-polarization radar observations and hydrometeor classification. *J. Appl. Meteor. Climatol.*, **55,** 2635–2655, doi:10.1175/JAMC-D-16-0062.1.

Markowski, P., and Y. Richardson, 2010: *Mesoscale Meteorology in Midlatitudes.* 1 ed. Wiley-Blackwell, 407 pp.

Mazur, R. J., J. F. Weaver, and T. H. Vonder Haar, 2009: A preliminary statistical study of correlations between inflow feeder clouds, supercell or multicell thunderstorms, and severe weather. *Wea. Forecasting*, **24,** 921-934, doi:10.1175/2009waf2222149.1.

McCann, D. W., 1994: WINDEX - a new index for forecasting microburst potential. *Wea. Forecasting*, **9,** 532–541, doi:10.1175/1520-0434(1994)009<0532:WNIFFM>2.0.CO;2.

McKenny, A. F., J. C. Short, and S. M. Newman, 2012: CAT Scanner. Version 1.0. [Available online at http://www.amckenny.com/CATScanner/.]

McLeod, J., M. Shepherd, and C. E. Konrad, 2017: Spatio-temporal rainfall patterns around Atlanta, Georgia and possible relationships to urban land cover. *Urban Climate*, **21,** 27–42, doi:https://doi.org/10.1016/j.uclim.2017.03.004.

Mesinger, F., and Coauthors, 2006: North American regional reanalysis. *Bull. Amer. Meteor. Soc.*, **87,** 343–360, doi:10.1175/bams-87-3-343.

Miller, D., and A. Petrolito, 2008: Anticipating pulse severe thunderstorms using the WSR-88D all-tilts display. National Weather Service. Eastern Region Technical Attachment No. 2008-02, 11 pp. [Available online at http://docs.lib.noaa.gov/noaa_documents/NWS/NWS_ER/Eastern_Region_Tech_Attachment/TA_2008-02.pdf.]

Miller, L. J., J. E. Dye, and B. E. Martner, 1983: Dynamical-microphysical evolution of a convective storm in a weakly-sheared environment. Part II: Airflow and precipitation trajectories from Doppler radar observations. *J. Atmos. Sci.*, **40,** 2097–2109.

Miller, P., and T. Mote, 2017a: A climatology of weakly forced and pulse thunderstorms in the Southeast United States. *J. Appl. Meteor. Climatol.*, **In press**.

——, 2018: Detecting severe weather potential in low signal-to-noise ratio regimes: weakly forced thunderstorm environments in the Southeast United States. *Natural Hazards and Earth System Sciences*, **In review**.

Miller, P. W., and T. L. Mote, 2017b: Standardizing the definition of a "pulse" thunderstorm. *Bull. Amer. Meteor. Soc.*, **98,** 905–913, doi:http://dx.doi.org/10.1175/BAMS-D-16-0064.1.

Miller, P. W., A. Ellis, and S. Keighton, 2015a: The utility of total lightning trends in diagnosing single-cell thunderstorm severity: Examples from the central Appalachians region *J. Operational Meteor.*, **3,** 82–98, doi:10.15191/nwajom.2015.0308.

——, 2015b: Spatial distribution of lightning associated with low-shear thunderstorm environments in the central Appalachians region. *Phys. Geography*, **36,** 127–141, doi:http://dx.doi.org/10.1080/02723646.2015.1011257.

——, 2015c: A preliminary assessment of using spatiotemporal lightning patterns for a binary classification of thunderstorm mode. *Wea. Forecasting*, **30,** 38–56, doi:10.1175/WAF-D-14-00024.1.

Miller, P. W., A. W. Black, C. A. Williams, and J. A. Knox, 2016: Quantitative assessment of human wind speed overestimation. *J. Appl. Meteor. Climatol.*, **55,** 1009–1020, doi:10.1175/JAMC-D-15-0259.1.

Moore, J. T., and J. P. Pino, 1990: An interactive method for estimating maximum hailstone size from forecast soundings. *Wea. Forecasting*, **5,** 508–525, doi:10.1175/1520-0434(1990)005<0508:AIMFEM>2.0.CO;2.

Mote, T. L., M. C. Lacke, and J. M. Shepherd, 2007: Radar signatures of the urban effect on precipitation distribution: a case study for Atlanta, Georgia. *Geophys. Res. Lett.*, **34,** 1–4, doi:10.1029/2007GL031903.

Murphy, M., 2017: Preliminary results from the inclusion of lightning type and polarity in the identification of severe storms. Preprints. *8th Conf. on the Meteor. Appl. of Lightning Data*, Seattle, WA, American Meteorological Society, 7.3. [Available online at https://ams.confex.com/ams/97Annual/webprogram/Manuscript/Paper308037/murphy_8mald_paper7.3.pdf.]

Murphy, M. S., and C. E. Konrad, 2005: Spatial and temporal patterns of thunderstorm events that produce cloud-to-ground lightning in the interior southeastern United States. *Mon. Wea. Rev.*, **133,** 1417–1430.

Niyogi, D., and Coauthors, 2010: Urban modification of thunderstorms: An observational storm climatology and model sase study for the Indianapolis urban region. *J. Appl. Meteor. Climatol.*, **50,** 1129–1144, doi:10.1175/2010JAMC1836.1.

NOAA, 2006: Doppler radar meteorological observations. Part C. WSR-88D products and algoritms. NOAA. FCM-H11C-2006, 390 pp. [Available online at http://www.ofcm.gov/fmh11/fmh11partc/pdf/FMH-11-PartC-April2006.pdf.]

Noel, J., and J. C. Dobur, 2002: A pilot study examining model-derived precipitation efficiency for use in precipitation forecasting in the eastern United States. *Natl. Wea. Dig.*, **26,** 3–8.

NTSB, 1986: Aircraft Accident Report: Delta Air Lines Inc., Lockheed L-1011-385-1, N726DA. Dallas/Fort Worth - International Airport, Texas, August 2,1985. NTSB/AAR-86/05, 164 pp. [Available online at http://www.ntsb.gov/investigations/AccidentReports/Reports/AAR8605.pdf.]

NWS, 2016a: National Weather Service Glossary. Accessed 21 January 2016. [Available online at http://w1.weather.gov/glossary/.]

——, 2016b: JetStream - Online school for weather. Accessed 21 January 2016. [Available online at http://www.srh.noaa.gov/jetstream/tstorms/tstrmtypes.html.]

Ortega, K. L., T. M. Smith, K. L. Manross, A. G. Kolodziej, K. A. Scharfenberg, A. Witt, and J. J. Gourley, 2009: The severe hazards analysis and verification experiment. *Bull. Amer. Meteor. Soc.*, **90,** 1519–1530, doi:10.1175/2009bams2815.1.

Outlaw, D. E., and M. P. Murphy, 2000: A radar-based climatology of July convective initiation in Georgia and surrounding area. NWS. Eastern Region Technical

Attachment No. 2000-04, 24 pp. [Available online at http://www.weather.gov/media/erh/ta2000-04.pdf.]

Patel, N., and R. W. Macemon, 2004: NEXRAD Open Radar Data Acquisition (ORDA) signal processing & signal path. Preprints. *20th International Conference on Interactive Information and Processing Systems (IIPS) for Meteorology, Oceanography, and Hydrology*, Seattle, WA, Amer. Meteor. Soc., 5.4. [Available online at https://ams.confex.com/ams/pdfpapers/70926.pdf.]

Paxton, C. H., and J. M. Shepherd, 1993: Radar diagnostic parameters as indicators of severe weather in central Florida. NOAA. Technical Memorandum NWS SR-149, 13 pp. [Available online at https://repository.library.noaa.gov/view/noaa/7316/Share.]

Pielke, R. A., 1974: A three-dimensional numerical model of the sea breezes over South Florida. *Mon. Wea. Rev.*, **102,** 115–139, doi:10.1175/1520-0493(1974)102<0115:ATDNMO>2.0.CO;2.

Púčik, T., P. Groenemeijer, D. Rýva, and M. Kolář, 2015: Proximity soundings of severe and nonsevere thunderstorms in Central Europe. *Mon. Wea. Rev.*, **143,** 4805–4821, doi:10.1175/MWR-D-15-0104.1.

Rickenbach, T. M., R. Nieto-Ferreira, C. Zarzar, and B. Nelson, 2015: A seasonal and diurnal climatology of precipitation organization in the southeastern United States. *Quart. J. Roy. Meteorol. Soc.*, **141,** 1938–1956, doi:10.1002/qj.2500.

Roberts, R. D., and J. W. Wilson, 1989: A proposed microburst nowcasting procedure using single-Doppler radar. *J. Appl. Meteor.*, **28,** 285–303, doi:10.1175/1520-0450(1989)028<0285:APMNPU>2.0.CO;2.

Rose, L. S., J. A. Stallins, and M. L. Bentley, 2008: Concurrent Cloud-to-Ground Lightning and Precipitation Enhancement in the Atlanta, Georgia (United States), Urban Region. *Earth Interact.*, **12,** 1–30, doi:10.1175/2008EI265.1.

Rudlosky, S. D., and H. E. Fuelberg, 2013: Documenting storm severity in the Mid-Atlantic Region using lightning and radar information. *Mon. Wea. Rev.*, **141,** 3186-3202, doi:10.1175/mwr-d-12-00287.1.

Sall, J., 2002: Monte Carlo Calibration of Distributions of Partition Statistics, 15 pp. [Available online at https://www.jmp.com/content/dam/jmp/documents/en/white-papers/montecarlocal.pdf.]

Sanger, N. T., 1999: A four-year summertime microburst climatology and relationship between microbursts and cloud-to-ground lightning flash rate for the NASA Kennedy Space Center, Florida: 1995-1998. Thesis. Meteorology, Texas A&M.

Schultz, C. J., W. A. Petersen, and L. D. Carey, 2009: Preliminary development and evaluation of lightning jump algorithms for the real-time detection of severe weather. *J. Appl. Meteor. Climatol.*, **48,** 2543-2563, doi:10.1175/2009jamc2237.1.

——, 2011: Lightning and severe weather: A comparison between total and cloud-to-ground lightning trends. *Wea. Forecasting*, **26,** 744–755, doi:10.1175/waf-d-10-05026.1.

Schultz, D., 2013: *Eloquent Science: A Practical Guide to Becoming a Better Writer, Speaker, and Atmospheric Scientist.* Springer Science & Business Media, 412 pp.

Schumacher, C., and R. A. Houze, 2003: The TRMM precipitation radar's view of shallow, isolated rain. *J. Appl. Meteor.*, **42,** 1519–1524, doi:10.1175/1520-0450(2003)042<1519:TTPRVO>2.0.CO;2.

Senkbeil, J. C., M. E. Saunders, and B. Taylor, 2017: Changes in summer weather type frequency in Eastern North America. *Annals of the American Association of Geographers***,** 1–17, doi:10.1080/24694452.2017.1295839.

Shepherd, J. M., 2005: A review of current investigations of urban-induced rainfall and recommendations for the future. *Earth Interact.*, **9,** 1–27, doi:10.1175/EI156.1.

Sherwood, S. C., P. Minnis, and M. McGill, 2004: Deep convective cloud-top heights and their thermodynamic control during CRYSTAL-FACE. *Journal of Geophysical Research: Atmospheres (1984–2012)*, **109,** 1–11, doi:10.1029/2004JD004811.

Sherwood, S. C., R. Roca, T. M. Weckwerth, and N. G. Andronova, 2010: Tropospheric water vapor, convection, and climate. *Reviews of Geophysics*, **48,** 1–29, doi:10.1029/2009RG000301.

Short, J. C., J. C. Broberg, C. C. Cogliser, and K. C. Brigham, 2009: Construct validation using computer-aided text analysis (CATA): An illustration using entrepreneurial orientation. *Organizational Research Methods***,** 1–28, doi:10.1177/1094428109335949.

Sims, A. P., and S. Raman, 2016: Interaction between two distinct mesoscale circulations during summer in the coastal region of eastern USA. *Boundary-Layer Meteorology*, **160,** 113–132, doi:10.1007/s10546-015-0125-6.

Smith, B. T., R. L. Thompson, J. S. Grams, C. Broyles, and H. E. Brooks, 2012: Convective modes for significant severe thunderstorms in the contiguous United States. Part I: storm classification and climatology. *Wea. Forecasting*, **27,** 1114-1135.

Smith, J. A., M. L. Baeck, A. A. Ntelekos, G. Villarini, and M. Steiner, 2011: Extreme rainfall and flooding from orographic thunderstorms in the central Appalachians. *Water Resour. Res.*, **47**.

Smith, T. M., K. L. Elmore, and S. A. Dulin, 2004: A damaging downburst prediction and detection algorithm for the WSR-88D. *Wea. Forecasting*, **19,** 240–250, doi:10.1175/1520-0434(2004)019<0240:ADDPAD>2.0.CO;2.

SPC, 2015: SPC product descriptions. Accessed 11 November 2015. [Available online at http://www.spc.noaa.gov/misc/about.html.]

Stahle, D. W., and M. K. Cleaveland, 1992: Reconstruction and analysis of spring rainfall over the Southeastern U.S. for the past 1000 years. *Bull. Amer. Meteor. Soc.*, **73,** 1947-1961, doi:10.1175/1520-0477(1992)073<1947:RAAOSR>2.0.CO;2.

Stewart, A. E., C. A. Williams, M. D. Phan, A. L. Horst, E. D. Knox, and J. A. Knox, 2016: Through the eyes of the experts: Meteorologists' perceptions of the probability of precipitation. *Wea. Forecasting*, **31,** 5–17, doi:10.1175/WAF-D-15-0058.1.

Stewart, S. R., 1991: The prediction of pulse-type thunderstorm gusts using vertically integrated liquid water content (VIL) and the cloud top penetrative downdraft mechanism. NOAA. Technical Memorandum NWS SR-136, 20 pp. [Available online at http://docs.lib.noaa.gov/noaa_documents/NWS/NWS_SR/TM_NWS_SR_136.pdf.]

Stull, R., 2015: *Practical Meteorology: An Algebra-based Survey of Atmospheric Science* University of British Columbia, 938 pp.

Taszarek, M., H. E. Brooks, and B. Czernecki, 2017: Sounding-derived parameters associated with convective hazards in Europe. *Mon. Wea. Rev.*, **145,** 1511-1528, doi:10.1175/MWR-D-16-0384.1.

Thompson, R. L., C. M. Mead, and R. Edwards, 2007: Effective storm-relative helicity and bulk shear in supercell thunderstorm environments. *Wea. Forecasting*, **22,** 102–115, doi:10.1175/WAF969.1.

Thompson, R. L., B. T. Smith, A. R. Dean, and P. T. Marsh, 2014: Spatial Distributions of Tornadic Near-Storm Environments by Convective Mode. *Electronic J. Severe Storms Meteor.*, **8,** 1–22.

Thompson, R. L., R. Edwards, J. A. Hart, K. L. Elmore, and P. Markowski, 2003: Close proximity soundings within supercell environments obtained from the Rapid Update Cycle. *Wea. Forecasting*, **18,** 1243–1261, doi:10.1175/1520-0434(2003)018<1243:CPSWSE>2.0.CO;2.

Trapp, R. J., D. M. Wheatley, N. T. Atkins, R. W. Przybylinski, and R. Wolf, 2006: Buyer beware: Some words of caution on the use of severe wind reports in postevent assessment and research. *Wea. Forecasting*, **21,** 408–415, doi:http://dx.doi.org/10.1175/WAF925.1.

Trapp, R. J., N. S. Diffenbaugh, H. E. Brooks, M. E. Baldwin, E. D. Robinson, and J. S. Pal, 2007: Changes in severe thunderstorm environment frequency during the 21st century caused by anthropogenically enhanced global radiative forcing. *Proc. Natl. Acad. Sci.*, **104,** 19719-19723.

UCAR, 2010: Radar signatures for severe convective weather. Accessed 21 January 2016. [Available online at http://www.meted.ucar.edu/radar/severe_signatures/.]

——, 2012: Tropical severe local storms. Accessed 21 January 2016. [Available online at http://www.meted.ucar.edu/tropical/synoptic/local_storms/.]

——, 2013: A convective storm matrix: Buoyancy/shear dependencies. Accessed 21 January 2016. [Available online at http://www.meted.ucar.edu/convectn/csmatrix/index.htm.]

Wakimoto, R. M., and V. Bringi, 1988: Dual-polarization observations of microbursts associated with intense convection: The 20 July storm during the MIST project. *Mon. Wea. Rev.*, **116,** 1521–1539, doi:10.1175/1520-0493(1988)116<1521:DPOOMA>2.0.CO;2.

Ward, J. H., 1963: Hierarchical grouping to optimize an objective function. *Journal of the American Statistical Association*, **58,** 236–244, doi:10.1080/01621459.1963.10500845.

Weisman, M. L., and J. B. Klemp, 1982: The dependence of numerically simulated convective storms on vertical wind shear and buoyancy. *Mon. Wea. Rev.*, **110,** 504–520, doi:10.1175/1520-0493(1982)110<0504:tdonsc>2.0.co;2.

Weiss, S. J., J. Hart, and P. Janish, 2002: An examination of severe thunderstorm wind report climatology: 1970–1999. Preprints. *21st Conf. Severe Local Storms*, San Antonio, TX, American Meteorological Society, 11B.2. [Available online at https://ams.confex.com/ams/SLS_WAF_NWP/techprogram/paper_47494.htm.]

Wheeler, M., and S. M. Spratt, 1995: Forecasting the potential for central Florida microbursts. NOAA. Technical Memorandum NWS SR-163, 9 pp. [Available online at www.weather.gov/media/mlb/research/SR_TechMemo163.pdf.]

Wilk, K. E., L. R. Lemon, and D. W. Burgess, 1979: Interpretation of radar echoes from severe thunderstorms: a series of illustrations with extended captions. National Severe Storms Laboratory. Prepared for FAA ARTCC coordinator training.]

Williams, E., and Coauthors, 1999: The behavior of total lightning activity in severe Florida thunderstorms. *Atmos. Res.*, **51,** 245–265, doi:10.1016/s0169-8095(99)00011-3.

Williams, E. R., 1988: The electrification of thunderstorms. *Sci. Amer.*, **259,** 88–99.

Wilson, J. W., and R. M. Wakimoto, 2001: The discovery of the downburst: TT Fujita's contribution. *Bull. Amer. Meteor. Soc.*, **82,** 49–62.

Wissmeier, U., and R. Goler, 2009: A comparison of tropical and midlatitude thunderstorm evolution in response to wind shear. *J. Atmos. Sci.*, **66,** 2385–2401, doi:10.1175/2009JAS2963.1.

Witt, A., M. D. Eilts, G. J. Stumpf, E. D. W. Mitchell, J. Johnson, and K. W. Thomas, 1998a: Evaluating the performance of WSR-88D severe storm detection algorithms. *Wea. Forecasting*, **13,** 513–518.

Witt, A., M. D. Eilts, G. J. Stumpf, J. T. Johnson, E. D. W. Mitchell, and K. W. Thomas, 1998b: An enhanced hail detection algorithm for the WSR-88D. *Wea. Forecasting*, **13,** 286–303, doi:10.1175/1520-0434(1998)013<0286:aehdaf>2.0.co;2.

Wolfson, M., 1988: Characteristics of microbursts in the continental United States. *Lincoln Lab Journal*, **1,** 49–74.

Ye, H., E. J. Fetzer, S. Wong, and B. H. Lambrigtsen, 2017: Rapid decadal convective precipitation increase over Eurasia during the last three decades of the 20th century. *Science Advances*, **3**, doi:10.1126/sciadv.1600944.

Zhu, Y., and Coauthors, 2017: Evaluation of ENTLN performance characteristics based on the ground-truth natural and rocket-triggered lightning data acquired in Florida. *J. Geophys. Res.: Atmos.*, **In press**, doi:10.1002/2017JD027270.

Zipser, E. J., C. Liu, D. J. Cecil, S. W. Nesbitt, and D. P. Yorty, 2006: Where are the most intense thunderstorms on Earth? *Bull. Amer. Meteor. Soc.*, **87,** 1057-1071.

APPENDICES

Appendix A

Table A1. Additional detail describing the convective parameters in Table 4.1.

Parameter	Comments
MLCAPE MLCIN MLLCL MLLFC MLEL	Mean-layer parcel mixed over the lowest 100 hPa
K_IND	$T_{850} – T_{500} + T_{d850} – (T_{700} – T_{d700})$
TT	CT + VT
CT	$T_{d850} – T_{500}$
VT	$T_{850} – T_{500}$
PW	Depth of liquid water if all water vapor were condensed from the sounding
HGT0	Pressure level of the 0°C isotherm
ApWBZ	Height above ground level of the RAP pressure level with the wet bulb temperature nearest to 0°C
W_LOW	Mean mixing ratio between 1000–850 hPa
W_MID	Mean mixing ratio between 850–500 hPa
RH_LOW	Mean RH between 1000–850 hPa
RH_MID	Mean RH between 850–500 hPa
ThE_LOW	Mean theta-e from 1000–850 hPa
ThE_MID	Mean theta-e from 850–500 hPa
ML_BRN	Bulk Richard Number of the mean-layer parcel
Tc	Temperature of parcel lowered dry adiabatically from the convective condensation level
PEFF	As defined by Noel and Dobur (2002). PEFF equals the product of PW and the mean 1000–700-hPa RH.
DCAPE	Downdraft CAPE with respect to parcel with the minimum 100 hPa layer-averaged theta-e found in the lowest 400 hPa
WNDG	(MLCAPE)/2000*(0–3-km lapse rate)/9*(1–3.5-km mean wind)/15*[(MLCIN + 50)/40)]. Values larger than 1 indicate an increased risk for strong outflow gusts.
TEI	Difference between the surface theta-e and the minimum theta-e value in the lowest 400 hPa AGL
MICROB	Weighted sum of the following individual parameters: surface theta-e, SBCAPE, surface-based lifted index, 0–3-km lapse rate, VT, DCAPE, TEI, and PW. Values exceeding 9 indicate that microbursts are likely.
SWEAT	$12(T_{d850}) + 20(TT – 49) + 2(U_{850}) + (U_{500}) + 125[\sin(U_{dir500} – U_{dir850}) + 0.2]$
0-3-km_SHR	Magnitude of vector shear between surface and 3 km AGL
0-6-km_SHR	Magnitude of vector shear between surface and 6 km AGL
0-8-km_SHR	Magnitude of vector shear between surface and 8 km AGL
EBWD	Magnitude of vector shear between effective inflow base and one half of the MU equilibrium level height

Appendix B. The height of the radar beam center is sensitive to several factors, such as transmission wavelength, lapse rate, etc. However, because of the limited role that beam height contributes to this work, the basic calculations shown below in Eq. (B1)-(B3) were selected. Equation (B1) uses the Haversine formula to calculate the great circle distance between the latitude (θ) and longitude (α) of the WFT grid cell (subscript 1) and radar site (subscript 2). Equation (2) uses the result of Eq. (B1) to calculate the distance, R, between the WFT and the nearest radar. Equation (B3) calculates the height of the beam, HGT, at the WFT using the tilt angle of the radar beam (φ), a typical refraction index (1.21), and the radius of the earth (6,371,000 m).

$$a = \sin\left(\frac{\theta_2 - \theta_1}{2}\right)^2 + cos(\theta_1) * cos(\theta_2) * \sin\left(\frac{\alpha_2 - \alpha_1}{2}\right)^2 \tag{B1}$$

$$R = 2 * \sin^{-1}\left(\sqrt{a}\right) * 6371000 \tag{B2}$$

$$HGT = R * \sin(\varphi) + \frac{R^2}{2 * \cos(\varphi)^2 * 1.21 * 6371000} \tag{B3}$$